

**MULTIDISCIPLINARY IMAGING OF ROCK PROPERTIES IN  
CARBONATE RESERVOIRS FOR FLOW-UNIT TARGETING**

**FINAL TECHNICAL REPORT**

Reporting Period Start Date: October 15, 2001

Reporting Period End Date: July 31, 2004

Author: Stephen C. Ruppel

Date Report Issued: February 2005

DOE Contract No. DE-FC26-01BC15351

Contractor Name and Address:

Bureau of Economic Geology  
John A. and Katherine G. Jackson School of Geosciences  
The University of Texas at Austin  
Box X, University Station, Austin, TX 78713-8924

## Disclaimer

This report was prepared as an account of work sponsored by an agency of the United States Government. Neither the United States Government nor any agency thereof, nor any of their employees, makes any warranty, express or implied, or assumes any legal liability or responsibility for the accuracy, completeness, or usefulness of any information, apparatus, product, or process disclosed, or represents that its use would not infringe privately owned rights. Reference herein to any specific commercial product, process, or service by trade name, trademark, manufacturer, or otherwise does not necessarily constitute or imply its endorsement, recommendation, or favoring by the United States Government or any agency thereof. The views and opinions of authors expressed herein do not necessarily state or reflect those of the United States Government or any agency thereof.



## Contents

<b>Disclaimer .....</b>	<b>ii</b>
 <b>Summary of Research Accomplishments</b>	
<i>Stephen C. Ruppel</i>	
INTRODUCTION .....	xix
OVERVIEW OF PROJECT .....	xix
SUMMARY OF PROJECT ACCOMPLISHMENTS AND FINDINGS .....	xxii
Accomplishments.....	xxii
Data Collection and Interpretation.....	xxii
Stratigraphic Architecture.....	xxii
Petrophysical Modeling .....	xxiii
Interpretation of 3D Seismic Data .....	xxiii
Reservoir Modeling .....	xxiii
Flow Simulation.....	xxiv
Definition of Opportunities for Drilling and Recompletion .....	xxiv
Definition of Resource Volumetrics .....	xxiv
Technology Transfer.....	xxiv
Major Findings.....	xxv
Stratigraphic Architecture.....	xxv
Petrophysics .....	xxv
Reservoir Simulation .....	xxv
3D Geophysics .....	xxvi
Porosity Characterization.....	xxvi
Architecture.....	xxvi
Reservoir Resources.....	xxvi
ACKNOWLEDGMENTS .....	xxvi

# **Facies, Sequence Stratigraphy and Porosity Development in the Fullerton Clear Fork Reservoir**

*Stephen C. Ruppel and Rebecca H. Jones*

ABSTRACT.....	9
INTRODUCTION .....	9
METHODS .....	10
PREVIOUS WORK.....	11
GEOLOGIC SETTING .....	12
OUTCROP ANALOGS.....	13
Abo Facies, Cyclicality, and Sequence Architecture .....	14
Lower Clear Fork Facies, Cyclicality, and Sequence Architecture .....	15
FULLERTON RESERVOIR FACIES AND STRATIGRAPHY .....	16
Facies and Depositional Setting.....	17
Peritidal Mudstone-Wackestone .....	18
Clay-rich Carbonate Mudstone .....	19
Exposed Tidal Flat .....	19
Peloid Wackestone.....	20
Peloid Packstone .....	21
Peloid Grain-dominated Packstone.....	21
Ooid-Peloid Grain-dominated Packstone-Grainstone.....	22
Fusulinid Wackestone-Packstone .....	22
Skeletal Wackestone-Packstone.....	23
Oncoid Wackestone-Packstone.....	23
Siltstone-Sandstone.....	24
Lithoclast Wackestone .....	25
Depositional Model.....	25
Sequence Stratigraphy .....	27
Abo Formation .....	27
Wichita Formation .....	29

Lower Clear Fork Formation .....	31
High-Frequency Sequence L 2.0.....	31
High-Frequency Sequence L 2.1.....	31
High-Frequency Sequence L 2.2.....	33
High-Frequency Sequence L 2.3.....	34
Tubb Formation .....	35
Cycle-Scale Stratigraphy .....	35
Wichita Cyclicity .....	36
Lower Clear Fork Cyclicity: HFS L 2.1 .....	36
Lower Clear Fork Cyclicity: HFS L 2.2 .....	38
Lower Clear Fork Cyclicity: HFS L 2.3 .....	38
MINERALOGY AND DIAGENESIS .....	39
Dolomite and Limestone Distribution .....	39
Stable Isotope Chemistry .....	40
Karst Development .....	42
Karst Fabrics .....	42
Causes and Timing of Karst.....	44
Impact of Karsting on Reservoir Quality.....	45
RESERVOIR IMAGING.....	46
Identifying Facies and Cyclicity from Borehole Image Logs.....	46
Imaging Stratigraphic Architecture and Reservoir Development from 3-D Seismic.....	51
Constraining Reservoir Architecture .....	52
Defining Reservoir Quality.....	52
RESERVOIR ARCHITECTURE.....	54
Cyclicity and Flow-Unit Definition.....	54
Lower Clear Fork Reservoir Architecture .....	56
Wichita Reservoir Architecture .....	58
Abo Reservoir Architecture .....	59

Reservoir Model.....	60
Porosity Distribution.....	60
Models for Porosity Development.....	63
SUMMARY .....	65
ACKNOWLEDGMENTS .....	67
REFERENCES .....	68

## Figures

1. Chart showing the Leonardian stratigraphic section in the Permian Basin including the Clear Fork Group and analogous units in New Mexico and in outcrop .....	73
2. Regional map of the Permian Basin showing location of Fullerton field and analogous outcrops in the Sierra Diablo mountains.....	73
3. Map of Fullerton Clear Fork field showing location of focused study areas, cores, and 3-D seismic data.....	74
4. Type log of producing reservoir section at Fullerton Clear Fork field showing cyclicity and general facies patterns .....	75
5. Structure of the Fullerton Clear Fork field .....	76
6. Outcrop photographs showing Abo–Lower Clear Fork section equivalent to producing reservoir interval at Fullerton field .....	77
7. Cross section depicting lateral changes in facies and cyclicity in Sierra Diablo outcrops partly equivalent to Lower Clear Fork (sequence L2) reservoir rocks at Fullerton field .....	77
8. Cross section (A-A') illustrating sequence stratigraphy and facies in the central part of the Clear Fork reservoir at Fullerton field based on cores .....	78
9. 3-D seismic section from southern part of Fullerton field showing seismic definition of the Clear Fork reservoir section.....	79
10. Core and thin-section photographs of typical Wichita tidal-flat facies .....	80
11. Core and thin-section photographs of typical tidal-flat facies and shallow subtidal facies in the Wichita and Lower Clear Fork .....	81
12. Core and thin-section photographs of typical peloid wackestone facies in the Lower Clear Fork.....	82
13. Core and thin-section photomicrographs of mud-rich peloid packstone-wackestone .....	83
14. Core and thin-section photomicrographs of peloid, grain-rich packstones and grainstones.....	84

15. Core and thin-section photomicrographs of Lower Clear Fork and Abo grainstones .....	85
16. Core and thin-section photomicrographs of the fusulinid wackestone-packstone facies .....	86
17. Core and thin-section photomicrographs of the oncoid, wackestone-packstone facies.....	87
18. Depositional model for Permian shallow-water carbonate platforms in the Permian Basin .....	88
19. Generalized sequence-stratigraphic model of the lower Leonardian succession at Fullerton field showing primary facies tracts and stratigraphic nomenclature.....	88
20. Map of limestone abundance in the Wichita Formation.....	89
21. Thickness of the Wichita Formation in the Fullerton field area .....	90
22. Northwest-southeast cross section (B-B') across the Fullerton field area showing the sequence architecture and general facies development based on cored well control .....	91
23. Map showing the distribution of limestone and dolostone in Lower Clear Fork HFS L 2.1 based on cores and wireline logs.....	92
24. Map of the thickness of the Lower Clear Fork L 2.1 sequence at Fullerton field .....	93
25. Map showing the distribution of limestone and dolostone in Lower Clear Fork HFS L 2.2 based on cores and wireline logs.....	94
26. Map of the thickness of the Lower Clear Fork L 2.2 sequence at Fullerton field .....	95
27. Facies stacking and cycle development in the fusulinid- and oncoid-rich, transgressive systems tract of Lower Clear Fork HFS L 2.1 .....	96
28. Facies stacking and cycle development in the grain-rich, highstand systems tract of Lower Clear Fork HFS L 2.1 .....	97
29. Facies stacking and cycle development in the grain-rich, late transgressive systems tract/early highstand systems tract of Lower Clear Fork HFS L 2.2 .....	98
30. Facies stacking and cycle development in the nonreservoir Lower Clear Fork HFS L 2.3 .....	98
31. Core slab photos of polymict conglomerate in the Wichita Formation of probable karst origin .....	99
32. Core slab box photo of breccias developed at the Abo/Wichita contact in FM-1 core .....	100
33. Core slab photos of contact zone of Abo/Wichita .....	101
34. Core slab photos of monomict breccias from the Wichita.....	102
35. Image log and core photo images of laminated tidal-flat facies .....	103
36. Image log and core photo images of fusulinid wackestone-packstone facies .....	104

37. Image log and core photo images of crossbedded grainstone.....	105
38. Image log and core photo images of peloid wackestone-packstone facies.....	106
39. Image log and core photo images of nodular peloid wackestone typical of the Lower Clear Fork HFS L 2.2 .....	107
40. Image log and core photo images of “vuggy” fabric .....	108
41. Image log and core photo images of polymict karst conglomerate .....	109
42. 3-D seismic section from Fullerton field showing general continuity and isopachous nature of Lower Clear Fork and Wichita reservoir intervals .....	110
43. Map of negative amplitude data extracted from Fullerton 3-D data.....	111
44. Porosity development in HFS 2.1 .....	112
45. Comparison of core-defined facies and cyclicity with porosity logs in tidal-flat-capped cycles of HFS L 2.3. FCU 6122.....	113
46. Comparison of core-defined facies and cyclicity with porosity logs in subtidal cycles of HFS L 2.2. FCU 6122 .....	114
47. Schematic depiction of reservoir framework used for model construction at the Fullerton Clear Fork reservoir .....	115
48. Map of total phi in the Wichita.....	116
49. Maps of porosity distribution in the lower and upper parts of the lower Wichita (Sequence L 1) .....	117
50. Maps of porosity distribution in the lower and upper parts of the upper Wichita (Sequence L 2.0) .....	118
51. Maps of porosity distribution in the Lower Clear Fork .....	119
52. Models of porosity formation in the upper Wichita and the Lower Clear Fork (L2 sequence).....	120

## **Integration of Rock Fabric, Petrophysical Class, and Stratigraphy for Petrophysical Quantification of Sequence-Stratigraphic Framework, Fullerton Clear Fork Field, Texas**

*Rebecca H. Jones and F. Jerry Lucia*

ABSTRACT.....	125
INTRODUCTION .....	126
METHODS .....	128
RESULTS .....	129

Abo Formation .....	130
Wichita Formation .....	130
Lower Clear Fork Formation .....	131
Lower Clear Fork L2.0 .....	131
Lower Clear Fork L2.1 .....	132
Lower Clear Fork L2.2 .....	133
Lower Clear Fork L2.3 .....	134
DISCUSSION .....	135
Limitations Due to Petrophysical Data Distribution.....	135
CONCLUSIONS.....	137
ACKNOWLEDGMENTS .....	138
REFERENCES .....	139
APPENDIX I: ROCK-FABRIC INSTRUCTIONS: Classifying Carbonate Pore Space from Thin Sections.....	157

## Figures

1. Diagram showing fabrics composing petrophysical classes 1, 2, and 3 and a cross plot showing interparticle porosity vs. permeability, petrophysical class fields, and associated transforms .....	141
2. Photomicrographs of class 1 fabrics observed in this study .....	142
3. Photomicrographs of class 2 fabrics observed in this study .....	143
4. Photomicrographs of class 3 fabrics observed in this study .....	144
5. Location and boundaries of Fullerton field, Andrews County, Texas.....	145
6. Type log showing nomenclature used in this study and general vertical stacking of petrophysical classes.....	146
7. Porosity-permeability plot of old Abo interval core analysis from wells throughout the field with core described in this study.....	147
8. Photomicrographs of tidal-flat, class 3 fabrics observed in this study .....	148

9. Distribution of limestone, dolostone, and petrophysical classes in the Wichita.....	149
10. Wichita facies core analysis porosity-permeability plot and petrophysical class 3 transform used to calculate permeability .....	150
11. Plot and histogram for Lower Clear Fork L2.1 subtidal unit high-resolution samples from wells FCU 5927 and 6429 .....	151
12. Porosity-permeability plot of core analysis from wells with core displaying dominantly class 1 fabrics in the subtidal portion of high-frequency sequence L2.1 .....	152
13. Regions of different petrophysical classes and mineralogy in the subtidal portion of HFS L2.1 .....	153
14. Regions of different petrophysical classes and mineralogy in HFS L2.2.....	154
15. Porosity-permeability plot of Lower Clear Fork L2.2 showing that most samples plot in the class 1 field and photomicrograph example of poikilotopic anhydrite in a class 2 medium-crystalline dolostone .....	155
16. Typical preexisting core analysis data vs. core analysis data resulting from unbiased sampling and careful cleaning of plugs .....	156

## **Development of the Wireline-Log Database and Determination of Porosity Using Wireline Logs**

*Jeffrey A. Kane and James W. Jennings, Jr.*

ABSTRACT.....	167
INTRODUCTION .....	167
OVERVIEW OF WIRELINE-LOG DATABASE.....	168
DATABASE ASSEMBLY PROCEDURES.....	170
QUALITY CONTROL .....	170
POROSITY-LOG NORMALIZATION.....	172
MOVING AVERAGE COMPUTATION.....	175
CORE CALIBRATION.....	175
CONCLUSIONS.....	177
REFERENCE.....	178



## Figures

1. Map showing 316 wells with Sidewall neutron logs (SNP) used to calculate porosity for Fullerton Clear Fork field.....	179
2. Map showing 437 wells with compensated neutron logs (NPHI) used to calculate porosity for Fullerton Clear Fork field .....	180
3. Map showing all 733 wells used in porosity calculation for Fullerton Clear Fork field ....	181
4. An example of the Gaussian weighting function using various scale factors .....	182
5. Examples of average SNP porosity areally averaged with different scale factors .....	183
6. Plot of layer averaged core porosity (y-axis) as a function of layer averaged normalized compensated neutron porosity (x-axis) showing the calibration line for dolomites.....	184
7. Plot of layer averaged core porosity (y-axis) as a function of layer averaged normalized sidewall neutron porosity (x-axis) showing the calibration line for dolomites .....	185
8. Plot of core porosity (y-axis) as a function of normalized compensated neutron porosity (x-axis) showing the calibration line for limestone .....	186
9. Plot of core porosity (y-axis) as a function of normalized sidewall neutron porosity (x-axis) showing the calibration line for limestone .....	187

## **Calculations of Permeability and Initial Water Saturations from Wireline Logs**

*F. Jerry Lucia and Jeffrey A. Kane*

ABSTRACT.....	193
PERMEABILITY CALCULATIONS FROM WIRELINE LOGS .....	194
ESTIMATION OF ORIGINAL WATER SATURATION.....	196
COMPARISON OF MODEL $S_w$ WITH ARCHIE $S_w$ .....	200
DISCUSSION .....	201
REFERENCES .....	202

## Tables

1. Thomeer and core analysis values for class 2 samples .....	203
2. Thomeer and core analysis values for class 3 samples.....	203
3. List of electrical measurements from the Lower Clear Fork.....	204

## Figures

1. Map showing location of calibration wells in the simulation area .....	205
2. Cross plots showing development of permeability transforms for dolostone in sequence L2.2 .....	206
3. Comparison of core and calculated permeability in sequence L2.2 .....	207
4. Porosity-permeability cross plot for moldic limestone in sequence L2.2.....	208
5. Comparison of core and calculated permeability in sequence L2.1 .....	208
6. Comparison of core and calculated permeability in the Wichita peritidal facies .....	209
7. An example of fitting Thomeer parameters to a class 2 medium crystalline dolostone .....	210
8. Cross plots of Thomeer G factor and porosity for class 3 fabrics and class 2 fabrics showing little relationship between porosity and G factor .....	211
9. Cross plots of extrapolated entry pressures and porosity for class 3 fabrics and class 2 fabrics showing statistical relationships between entry pressure and porosity.....	212
10. Comparison of class 3 curves with curves calculated using the Thomeer model.....	213
11. Comparison of Thomeer class 3 capillary pressure model with generic class 3 model .....	214
12. Comparison of class 2 curves with curves calculated using the Thomeer model.....	215
13. Comparison of Thomeer class 2 capillary pressure model with generic class 2 model .....	216
14. Capillary pressure curves from moldic limestone .....	217
15. Comparison of capillary pressure curves from class 1 anhydritic dolostones with curves using the generic class 1 model .....	217
16. Example of model and Archie $S_w$ from well FCU 5727.....	218

## **Reservoir Modeling and Simulation of Fullerton Clear Fork Field, Andrews County, Texas**

*Fred Wang and F. Jerry Lucia*

ABSTRACT .....	225
INTRODUCTION .....	226
3-D RESERVOIR MODELING.....	227
Stratigraphic Modeling .....	227

Upscaling .....	229
Petrophysical Modeling .....	230
Porosity Distribution.....	231
Permeability (k) and kh Distribution .....	232
$S_w$ and $S_o\phi h$ Distribution.....	234
VOLUMETRICS .....	235
Sensitivity Analysis .....	236
Search Radius in Mapping.....	236
Grid Resolution.....	237
Water-Oil Contact.....	237
Porosity Cutoffs .....	238
Water Saturation Cutoffs .....	239
Permeability Cutoffs .....	239
Compound Effects of Vertical Resolution and Cutoff Values.....	240
PRODUCTION-TREND ANALYSIS .....	242
FLOW-UNIT MODEL AND RESERVOIR SIMULATION .....	243
Flow-unit Model .....	243
Flow Simulation.....	249
Sensitivity Study .....	250
SUMMARY .....	253
REFERENCES .....	256
APPENDIX A: UPSCALING .....	295

## Tables

1. Geologic and reservoir parameters of Fullerton Clear Fork Unit.....	257
2. Geologic frameworks used in 3-D reservoir models.....	258
3. Dimensions of 3-D field models.....	259
4. Formation volume factor, oil-gas ratio, and WOC used in OOIP estimates.....	259
5. Effect of variable search radius on OOIP estimates of FCU.....	259
6. Effect of water-oil contact on OOIP estimates of FCU.....	260
7. Effect of cutoff values on OOIP.....	260
8. Effect of cutoff values on OOIP in FCU for WOC at -3940 ft summarized by ExxonMobil zonation.....	261
9. Effect of cutoff values on OOIP in Fullerton field for WOC at -3940 ft summarized by ExxonMobil zonation.....	261
10. Effect of cutoff values on OOIP in FCU for WOC at -3940 ft summarized by high frequency cycles.....	262
11. Effect of cutoff values on OOIP in Fullerton Clear Fork field for WOC at -3940 ft summarized by high frequency cycles.....	263
12. Effect of vertical resolution on OOIP.....	264
13. Summary of parameters affecting OOIP.....	264
14. Dimensions of 3-D Model of Initial 2,000 acre model (simulation area).....	264

## Figures

1. Production history of waterflooding in Fullerton Clear Fork Unit.....	265
2. Workflow of 3-D modeling.....	265
3. Geologic framework used to build 3-D models of Fullerton Clear Fork field.....	266
4. Effect of search radius of 2,500 ft and 5,000 ft on porosity mapping.....	266
5. Porosity distribution in fine-grid model.....	267
6. Average porosity distribution in Zone 1, Zone 2, Wichita, Zone 3, Zone 3B, and Zone 4.....	267

7. $\phi h$ distribution in reservoir Zone 1 (Lower Clear Fork HFS 2.2) by cycle .....	268
8. Porosity distribution in reservoir Zone 1 (Lower Clear Fork. HFS 2.2) by cycle.....	268
9. Porosity distribution in reservoir Zone 2 (Lower Clear Fork. HFS 2.1) by cycle.....	268
10. Porosity distribution in Zones Wichita, 3, 3B, and 4, in the Wichita Formation .....	269
11. Permeability distribution in 3-D model.....	269
12. Permeability distribution in reservoir zones 1, 2, Wichita, 3, 3B, and 4.....	270
13. Kh distributions in Zone 1, Zone 2, Wichita, Zone 3, Zone 3B, and Zone 4.....	270
14. Results of petrophysical analysis in FCU 5927, 1284, and 1435 .....	271
15. Water saturation distribution in 3-D model with oil-water contact at –3,940 ft .....	271
16. Water saturation distributions in Zone 1, Zone 2, Wichita, Zone 3, Zone 3B, and Zone 4 .....	272
17. Hydrocarbon volume distributions in Zone 1, Zone 2, Wichita, Zone 3, Zone 3B, and Zone 4 .....	272
18. Hydrocarbon volume distribution in six reservoir zones .....	273
19. Hydrocarbon volume (distribution in Zone 1 (Lower Clear Fork HFS L 2.2).....	273
20. Hydrocarbon volume distribution in Zone 2 (Lower Clear Fork HFS 2 L 2.1) .....	273
21. Hydrocarbon volume distribution in the Wichita Formation .....	274
22. Formation volume factor and oil-gas ratio of two types of crude in FCU .....	274
23. Effect of water-oil contact on vertical coverage in Zone 3B, Zone 4, and Zone 5 (Abo) .....	275
24. Effect of water-oil contact on areal coverage in Zone 3, Zone 3B, Zone 4, and Zone 5 (Abo) .....	275
25. Effect of water-oil contacts on OOIP estimate.....	276
26. Effects of porosity cutoffs of 3%, 5% and 10%, and permeability cutoffs of 0.1, 0.5, and 1 mD on volumetrics .....	276
27. Effects of cutoff values on OOIP estimate porosity, water saturation, and permeability .....	277

28. Relationship between permeability and porosity cutoff values. A specific permeability cutoff represents rock-fabric-dependent porosity cutoffs.....	277
29. Effects of porosity cutoffs and grid vertical resolution on volumetrics, 3%, 5%, and 10% on fine-grid model, and 3%, 5% and 10% on cycle-based model .....	278
30. Effects of porosity cutoffs and grid vertical resolution on volumetrics, 0.1, 0.5, and 1.0 mD on fine-grid model, and 0.1, 0.5, and 1.0 mD on cycle-based model.....	279
31. Changes in OOIP between high-resolution and cycle-based models with respect to porosity cutoff, water saturation cutoff, and permeability cutoff values .....	279
32. Production data and trends in primary and waterflooding .....	280
33. Initial 3:1 line-drive waterflooding pattern .....	280
34. Porosity and $S_{oph}$ in Zone 2, Wichita, and Zone 3, overlaid with production trends.....	281
35. Water-injection patterns in the initial reservoir model area in 2001 .....	281
36. Production data and trends in primary and waterflooding in simulation area.....	282
37. Lawyer Canyon cycle 1 flow-layer model .....	283
38. Average porosity for various rock fabrics in sequences L2.1 and L2.2 .....	284
39. Flow layers and cycles in sequence L2.1 .....	285
40. Flow layers in sequence L2.2 .....	286
41. Flow layers in the Wichita.....	287
42. Lower Clear Fork and Wichita flow layers in cored wells of simulation area illustrating the use of porosity to build a flow model .....	288
43. Porosity distribution in the simulation area.....	288
44. Permeability distribution in the simulation area.....	289
45. Water saturation distribution in the simulation area.....	289
46. Porosity and $S_{oph}$ trends in the simulation area.....	290
47. Porosity distribution in simulation model .....	290
48. Initial oil saturation in simulation model.....	291
49. Simulated oil saturation in 1960, 1970, 1980, and 2002, simulation area .....	291

50. Simulated oil saturation in 2002, in Zone 1 .....	292
51. Simulated oil saturation in 2002, in selected model layer slices of the Lower Clear Fork HFS L2.1 (reservoir Zone 2) .....	292
52. Simulated oil saturation in 2002, in upper model layers of the Wichita .....	293
53. Simulated oil saturation in 2002, in model layers of Wichita reservoir Zone 3B .....	293
54. Corey correlations for relative permeability.....	293
55. Effect of relative permeability on simulated oil rate, water rate, pressure, and oil recovery .....	294
56. Effect of permeability multiplication on simulated water production.....	294

## **Construction and Analysis of 3-D Seismic Porosity Inversion Models**

*Hongliu Zeng*

ABSTRACT.....	309
INTRODUCTION .....	309
METHODOLOGY .....	311
DATA AND TIE.....	313
IMPROVEMENT OF SEISMIC DATA INTERPRETABILITY.....	314
90°-phasing .....	314
High-frequency Signal Enhancement .....	315
WELL-BASED AI MODEL.....	316
MODEL-BASED SEISMIC INVERSION.....	317
Why Model-based? .....	317
How Well and Seismic Data Are Integrated .....	319
PROGRESSIVE INVERSION .....	320
Problems in Model-based Inversion .....	320
Solution .....	322
Blind Test.....	324
CONCLUSIONS.....	325
REFERENCES .....	326

## Figures

1. Location of well and seismic data in Fullerton field, Andrews County, Texas, and 3-D seismic inversion area around Phase 2 area.....	327
2. Synthetic seismogram of lower Clear Fork and Wichita and surrounding formation in well Cal/Mon 1 across 2-D seismic line 0123 .....	328
3. Linear relationship between AI and log porosity of carbonate rocks in the lower Clear Fork and Wichita, Fullerton field, Andrews County, Texas.....	328
4. A 0°-phase seismic section (trace 2382) in the 3-D survey area showing poor tie between high-porosity/low-AI units and amplitude/polarity and difficulty in picking high-frequency sequence boundaries.....	329
5. A 90°-phase seismic section (trace 2382) in the 3-D survey area showing improved tie between high-porosity/low-AI units and amplitude/polarity .....	330
6. A high-frequency-enhanced (spectral-balanced) version of Figure 5 showing improvement in seismic resolution.....	331
7. Wireline log-based AI models for reservoir characterization and seismic inversion.....	332
8. Procedure of a model-based inversion.....	333
9. Model based inversion from background model, blocky model, smoothed log model, and log model.....	334
10. Differences of AI inversion corresponding to different initial model inputs .....	335
11. Initial models for progressive inversion .....	336
12. Progressive inversion.....	337
13. Differences of stratigraphic framework used in initial model construction .....	338
14. Difference in AI estimation through progressive inversion.....	339
15. Blind test showing value and limit of progressive inversion (example 1).....	340
16. Blind test showing value and limit of progressive inversion (example 2).....	341
17. Blind test showing value and limit of progressive inversion (example 3).....	342



# Summary of Research Accomplishments

Stephen C. Ruppel

## INTRODUCTION

Despite declining production rates, existing reservoirs in the United States contain large quantities of remaining oil and gas that constitute a huge target for improved diagnosis and imaging of reservoir properties. The resource target is especially large in carbonate reservoirs, where conventional data and methodologies are normally insufficient to resolve critical scales of reservoir heterogeneity. The objectives of the research described in this report were to develop and test such methodologies for improved imaging, measurement, modeling, and prediction of reservoir properties in carbonate hydrocarbon reservoirs. The focus of the study is the Permian-age Fullerton Clear Fork reservoir of the Permian Basin of West Texas. This reservoir is an especially appropriate choice considering (a) the Permian Basin is the largest oil-bearing basin in the United States, and (b) as a play, Clear Fork reservoirs have exhibited the lowest recovery efficiencies of all carbonate reservoirs in the Permian Basin.

## OVERVIEW OF PROJECT

The elements of the research carried out on Fullerton field are presented in six chapters. In the first chapter, Ruppel and Jones describe the depositional facies and sequence stratigraphy of the reservoir based on integrated study of outcrops and subsurface data from Fullerton field. They also describe the key steps in using outcrop- and core-based facies-stacking patterns and wireline log response relationships to develop a robust reservoir framework having sufficient resolution and accuracy to form the basis for reservoir modeling and simulation. In addition, they document the products of diagenesis and using three-dimensional relationships of geochemical

and porosity distribution data suggest models for dolomitization and porosity development. Finally, they describe the use of two modern techniques for improved reservoir imaging: (1) borehole imaging logs for improved definition of facies distribution and cycles, and (2) 3D seismic data, to better define the distribution of reservoir porosity.

Jones and Lucia document the nature and distribution of reservoir rock fabrics in the field. A knowledge of rock fabrics, groupings of rock types with similar petrophysical relationships, is critical for accurate modeling of permeability and saturation. Jones and Lucia show that each of the three major stratigraphic units in the reservoir contains distinct rock-fabric types that belong to three petrophysical classes. These classes vary substantially in petrophysical character. For example, rocks from Petrophysical Class 3 exhibit two orders of magnitude lower permeability for a given porosity value than do rocks of Petrophysical Class 1. Rock-fabric types and petrophysical classes were mapped throughout the field, thus providing an improved basis for calculating permeability and original oil saturation in the reservoir.

Kane and Jennings describe the procedures and methods used to develop a robust calculation of well-log porosity for each well in the field. This work includes the process used to assemble and quality-check the original wireline log data to create a workable database and the methodology used to create a final calculated porosity. Because calculations of reservoir porosity and saturation are based on porosity, this process is fundamental to accurate reservoir characterization and modeling.

Lucia and Kane discuss the approaches used to calculate permeability from wireline logs. As the chapter documents, accurate permeability calculation depends on two primary factors: porosity and rock fabric. As such, their work is built on the procedures documented by Kane and Jennings for porosity determination and interpretation and distribution of rock-fabric properties

described by Jones and Lucia. Lucia and Kane also describe the approaches used to calculate initial water saturation using capillary pressure and rock-fabric data. This approach, which is commonly the best way to define original saturations in carbonates, is the key to calculating original oil in place and remaining oil resource.

Wang and Lucia present the methods and results of reservoir modeling and simulation activities undertaken during the project. The primary goal of these studies was to better define the distribution of original and remaining oil resource in the reservoir. Key parts of this effort were (1) the construction of a 2,000-acre flow-unit model and a flow simulation sensitivity study of the model, and (2) the construction of a 35,000-acre full-field, static reservoir model. The simulation study produced an excellent image of waterflood performance and provides fundamental guidelines to predicting the distribution of remaining oil resources across the entire reservoir. The full-field model, which is based on integration of research completed on stratigraphy, reservoir architecture, porosity distribution, rock fabrics, and petrophysics, provides an excellent modern image of the 3D distribution of reservoir properties that will serve as a future guide to model effective recovery operations in the field. Calculations of original resource volume based on this new model will also provide a needed economic incentive for these plans.

Finally, Zeng reports on research carried out to recondition 3D seismic data and to develop an integrated wireline log–3D seismic inversion model of porosity. The data reconditioning work demonstrates how relatively simple procedures can lead to greatly improved seismic resolution, in turn leading to better definition of reservoir architecture and porosity distribution. Zeng also describes procedures used to construct a robust wireline inversion model of porosity for the reservoir. The results of this work illustrate the tremendous untapped potential

that exists for utilizing 3D seismic data in improved imaging of reservoir properties in incompletely exploited carbonate reservoirs.

Collectively, the work carried out on this project represents one of the most comprehensive studies of a major carbonate reservoir ever published. As such it contains lessons of value for geoscientists, engineers, and managers—not just of Fullerton field, but of all carbonate platform reservoirs in the United States.

## SUMMARY OF PROJECT ACCOMPLISHMENTS AND FINDINGS

### Accomplishments

#### *Data Collection and Interpretation*

- Completed quality control procedures on 18,000 logs
- Assembled core, log, and interpretive data into integrated database (Landmark OpenWorks) including
  - 1,500 well files (23,000 log files)
  - 30 core analysis files
  - Core facies descriptions (27 wells)
  - Stratigraphic tops (~45,000)
  - Calculated porosity (733 wells)
  - Calculated permeability (733 wells)
  - Calculated saturation (733 wells)
  - Flow-unit tops (265 wells)

#### *Stratigraphic Architecture*

- Integrated subsurface data with outcrop models
- Defined facies and cyclicity in 27 cored wells (14,383 ft of core)
- Correlated cycles and tops in more than 850 wells (~ 45,000 tops)
- Described more than 1,700 thin sections (19 wells)
- Integrated core and log data with 3D and 2D seismic data

- Defined sequence and cycle stratigraphic framework for entire field
- Mapped structure and thickness of major sequences
- Demonstrated key architectural differences within reservoir
- Demonstrated presence of karst features
- Developed model for porosity development
- Utilized 3D seismic inversion for improved imaging of porosity distribution

### *Petrophysical Modeling*

- Obtained new conventional core analyses (705)
- Obtained new special core analyses (30)
- Obtained new thin sections for rock-fabric analysis (950)
- Analyzed core data from 63 cored wells
- Calculated log porosity for 733 wells
- Created and applied porosity log normalization procedures for entire field
- Defined and mapped petrophysical classes throughout field
- Defined porosity-permeability transforms for all petrophysical classes
- Constructed original saturation model from capillary pressure and petrophysical class data

### *Interpretation of 3D Seismic Data*

- Reprocessed 3D and 2D data for phase character and resolution
- Integrated 222 miles of 2D and 33,000 acres of 3D data with wireline and core data
- Mapped time structure and isochrons of major horizons
- Correlated major sequences in 3D and 2D data volumes
- Defined relationships between deep structure and reservoir quality
- Employed amplitude extractions for reservoir-quality mapping
- Demonstrated robust relationship between impedance and porosity
- Constructed wireline log/3D seismic inversion model

### *Reservoir Modeling*

- Constructed 2,000-acre flow model comprising 39 flow units, 85 wells, 265 layers, and 3.2 million cells (150 ft × 150 ft × 3–5 ft cell size)

- Constructed 35,000-acre, full-field reservoir model comprising 35 stratigraphic surfaces/cycles, 730 wells, 380 layers, and 42 million cells (150 ft × 150 ft × 10–15 ft cell size)

### *Flow Simulation*

- Performed history match and sensitivity study for 1,600-acre flow model
- Completed flow simulation in Eclipse
- Used simulation results to characterize sweep characteristics of field

### *Definition of Opportunities for Drilling and Recompletion*

- Completed 3D amplitude analysis and provided recommendations on eight proposed infill locations
- Completed production streamline analysis of 15 proposed infill wells and recommended alternatives
- Reservoir models and simulation results provide invaluable guides to additional drilling and recompletion opportunities
- Completed study is being used as basis for designing and implementing a tertiary, CO<sub>2</sub> flood program

### *Definition of Resource Volumetrics*

- Calculated volumetrics for entire reservoir using multiple petrophysical and stratigraphic scenarios:
  - Two oil-water contact cases
  - Four porosity-cutoff cases
  - Three permeability-cutoff cases
  - Four water saturation-cutoff cases

### *Technology Transfer*

- Met regularly with operator staff to maintain focus of research.
- Responded to interim operator requests for data and interpretations
- Provided analysis of infill drilling locations
- Delivered final digital data sets to operator
  - OpenWorks database
  - GoCad and RMS reservoir models

- Eclipse simulation
- Interpreted 2D seismic data set
- Delivered final report
  - Written report with illustrations
  - Digital data files
- Created computer animation of project for Web-site distribution
- Presented oral papers and posters on major aspects of the study
- Disseminated final report and other project products through Web site and CD's

## Major Findings

### *Stratigraphic Architecture*

- 3D seismic data can provide inaccurate images of reservoir architecture
- Porosity development is a function of early diagenesis
- Borehole image logs provide almost as much facies and cyclicity data as cores
- Cycle-scale architecture is not definable in peritidal facies tracts
- Karst features are widespread but discontinuous
- Porosity development is partially controlled by deep structure
- Permeability is a function of facies, but porosity is a function of diagenesis

### *Petrophysics*

- Peritidal successions (Wichita Formation) contain high-porosity, low-permeability rock fabrics
- Subtidal successions (Lower Clear Fork and Abo Formations) contain higher permeability rock fabrics than peritidal successions
- Peritidal limestones are flow baffles; subtidal limestones are high-flow zones
- Petrophysical classes and rock fabrics can be mapped throughout the field using stratigraphic framework
- A single porosity cutoff or permeability transform is inadequate
- Permeability models must consider rock-fabric distribution

### *Reservoir Simulation*

- Provides key insights to sweep and remaining oil distribution for *much* of the reservoir

- Dominant issues controlling sweep efficiency are rock fabric, continuity, and completion coverage

### *3D Geophysics*

#### Porosity Characterization

- Strong relationship between amplitude and porosity
- Progressive 3D inversion provides excellent constraints on interwell and extrawell porosity distribution
- Simple amplitude extractions provide robust qualitative guide to interwell and extrawell porosity distribution

#### Architecture

- Seismic response controlled by porosity (facies and diagenesis)
- Seismic architecture must be vetted by geological models
- Continuing and differential fault motion through Permian

### *Reservoir Resources*

- Total hydrocarbon pore volume is conservatively estimated at 1.58 billion barrels
- Peritidal facies (Wichita Formation) contains 55 percent of the total pore volume but only 43 percent of the original hydrocarbon pore volume
- Resource estimations provide critical data for developing economically sound plans for further exploitation of the reservoir

## ACKNOWLEDGMENTS

The research documented here was co-funded by the U.S. Department of Energy, The University of Texas System, ExxonMobil Corporation, and the Reservoir Characterization Research Laboratory of the Bureau of Economic Geology. I thank John Stout, Jeff Simmons, and Craig Kemp of Occidental Permian for providing important data for the study and for providing thoughtful insights into project planning. Steve Krohn and Amy Powell helped develop and promote the project within ExxonMobil. Terry Anthony and David Smith, also with ExxonMobil, provided ongoing operator liaison, data exchange, and input on project activities



and deliverables. Tim Hunt, University of Texas System West Texas Operations Office, helped with technology transfer activities and gathered new GPS location data for wells in the field. Dan Ferguson served as contract officer for DOE. The Bureau acknowledges support of this research by Landmark Graphics Corporation via the Landmark University Grant Program.

FACIES, SEQUENCE STRATIGRAPHY AND POROSITY DEVELOPMENT IN THE  
FULLERTON CLEAR FORK RESERVOIR

Stephen C. Ruppel and Rebecca H. Jones

Bureau of Economic Geology  
Scott W. Tinker, Director  
John A. and Katherine G. Jackson School of Geosciences  
The University of Texas at Austin  
Austin, Texas 78713-8924

ABSTRACT.....	9
INTRODUCTION .....	9
METHODS .....	10
PREVIOUS WORK.....	11
GEOLOGIC SETTING .....	12
OUTCROP ANALOGS.....	13
Abo Facies, Cyclicity, and Sequence Architecture .....	14
Lower Clear Fork Facies, Cyclicity, and Sequence Architecture .....	15
FULLERTON RESERVOIR FACIES AND STRATIGRAPHY .....	16
Facies and Depositional Setting.....	17
Peritidal Mudstone-Wackestone .....	18
Clay-rich Carbonate Mudstone .....	19
Exposed Tidal Flat .....	19
Peloid Wackestone.....	20
Peloid Packstone .....	21
Peloid Grain-dominated Packstone.....	21
Ooid-Peloid Grain-dominated Packstone-Grainstone.....	22
Fusulinid Wackestone-Packstone .....	22
Skeletal Wackestone-Packstone.....	23
Oncoid Wackestone-Packstone.....	23
Siltstone-Sandstone.....	24
Lithoclast Wackestone .....	25
Depositional Model.....	25
Sequence Stratigraphy .....	27
Abo Formation .....	27

Wichita Formation .....	29
Lower Clear Fork Formation .....	31
High-Frequency Sequence L 2.0.....	31
High-Frequency Sequence L 2.1.....	31
High-Frequency Sequence L 2.2.....	33
High-Frequency Sequence L 2.3.....	34
Tubb Formation .....	35
Cycle-Scale Stratigraphy .....	35
Wichita Cyclicity .....	36
Lower Clear Fork Cyclicity: HFS L 2.1 .....	36
Lower Clear Fork Cyclicity: HFS L 2.2 .....	38
Lower Clear Fork Cyclicity: HFS L 2.3 .....	38
MINERALOGY AND DIAGENESIS .....	39
Dolomite and Limestone Distribution .....	39
Stable Isotope Chemistry .....	40
Karst Development .....	42
Karst Fabrics .....	42
Causes and Timing of Karst.....	44
Impact of Karsting on Reservoir Quality.....	45
RESERVOIR IMAGING.....	46
Identifying Facies and Cyclicity from Borehole Image Logs.....	46
Imaging Stratigraphic Architecture and Reservoir Development from 3D Seismic .....	51
Constraining Reservoir Architecture .....	52
Defining Reservoir Quality.....	52

RESERVOIR ARCHITECTURE.....	54
Cyclicality and Flow-Unit Definition.....	54
Lower Clear Fork Reservoir Architecture .....	56
Wichita Reservoir Architecture .....	58
Abo Reservoir Architecture .....	59
Reservoir Model.....	60
Porosity Distribution.....	60
Models for Porosity Development.....	63
SUMMARY .....	65
ACKNOWLEDGMENTS .....	67
REFERENCES .....	68

### Figures

1. Chart showing the Leonardian stratigraphic section in the Permian Basin including the Clear Fork Group and analogous units in New Mexico and in outcrop .....	73
2. Regional map of the Permian Basin showing location of Fullerton field and analogous outcrops in the Sierra Diablo mountains.....	73
3. Map of Fullerton Clear Fork field showing location of focused study areas, cores, and 3-D seismic data.....	74
4. Type log of producing reservoir section at Fullerton Clear Fork field showing cyclicality and general facies patterns .....	75
5. Structure of the Fullerton Clear Fork field .....	76
6. Outcrop photographs showing Abo–Lower Clear Fork section equivalent to producing reservoir interval at Fullerton field .....	77
7. Cross section depicting lateral changes in facies and cyclicality in Sierra Diablo outcrops partly equivalent to Lower Clear Fork (sequence L2) reservoir rocks at Fullerton field .....	77
8. Cross section (A-A') illustrating sequence stratigraphy and facies in the central part of the Clear Fork reservoir at Fullerton field based on cores .....	78

9. 3-D seismic section from southern part of Fullerton field showing seismic definition of the Clear Fork reservoir section.....	79
10. Core and thin-section photographs of typical Wichita tidal-flat facies .....	80
11. Core and thin-section photographs of typical tidal-flat facies and shallow subtidal facies in the Wichita and Lower Clear Fork .....	81
12. Core and thin-section photographs of typical peloid wackestone facies in the Lower Clear Fork.....	82
13. Core and thin-section photomicrographs of mud-rich peloid packstone-wackestone .....	83
14. Core and thin-section photomicrographs of peloid, grain-rich packstones and grainstones.....	84
15. Core and thin-section photomicrographs of Lower Clear Fork and Abo grainstones .....	85
16. Core and thin-section photomicrographs of the fusulinid wackestone-packstone facies .....	86
17. Core and thin-section photomicrographs of the oncoid, wackestone-packstone facies.....	87
18. Depositional model for Permian shallow-water carbonate platforms in the Permian Basin .....	88
19. Generalized sequence-stratigraphic model of the lower Leonardian succession at Fullerton field showing primary facies tracts and stratigraphic nomenclature.....	88
20. Map of limestone abundance in the Wichita Formation.....	89
21. Thickness of the Wichita Formation in the Fullerton field area .....	90
22. Northwest-southeast cross section (B-B') across the Fullerton field area showing the sequence architecture and general facies development based on cored well control .....	91
23. Map showing the distribution of limestone and dolostone in Lower Clear Fork HFS L 2.1 based on cores and wireline logs.....	92
24. Map of the thickness of the Lower Clear Fork L 2.1 sequence at Fullerton field .....	93
25. Map showing the distribution of limestone and dolostone in Lower Clear Fork HFS L 2.2 based on cores and wireline logs.....	94
26. Map of the thickness of the Lower Clear Fork L 2.2 sequence at Fullerton field .....	95
27. Facies stacking and cycle development in the fusulinid- and oncoid-rich, transgressive systems tract of Lower Clear Fork HFS L 2.1 .....	96

28. Facies stacking and cycle development in the grain-rich, highstand systems tract of Lower Clear Fork HFS L 2.1 .....	97
29. Facies stacking and cycle development in the grain-rich, late transgressive systems tract/early highstand systems tract of Lower Clear Fork HFS L 2.2 .....	98
30. Facies stacking and cycle development in the nonreservoir Lower Clear Fork HFS L 2.3 .....	98
31. Core slab photos of polymict conglomerate in the Wichita Formation of probable karst origin .....	99
32. Core slab box photo of breccias developed at the Abo/Wichita contact in FM-1 core .....	100
33. Core slab photos of contact zone of Abo/Wichita .....	101
34. Core slab photos of monomict breccias from the Wichita .....	102
35. Image log and core photo images of laminated tidal-flat facies .....	103
36. Image log and core photo images of fusulinid wackestone-packstone facies .....	104
37. Image log and core photo images of crossbedded grainstone .....	105
38. Image log and core photo images of peloid wackestone-packstone facies .....	106
39. Image log and core photo images of nodular peloid wackestone typical of the Lower Clear Fork HFS L 2.2 .....	107
40. Image log and core photo images of “vuggy” fabric .....	108
41. Image log and core photo images of polymict karst conglomerate .....	109
42. 3-D seismic section from Fullerton field showing general continuity and isopachous nature of Lower Clear Fork and Wichita reservoir intervals .....	110
43. Map of negative amplitude data extracted from Fullerton 3-D data .....	111
44. Porosity development in HFS 2.1 .....	112
45. Comparison of core-defined facies and cyclicity with porosity logs in tidal-flat-capped cycles of HFS L 2.3. FCU 6122 .....	113
46. Comparison of core-defined facies and cyclicity with porosity logs in subtidal cycles of HFS L 2.2. FCU 6122 .....	114
47. Schematic depiction of reservoir framework used for model construction at the Fullerton Clear Fork reservoir .....	115

48. Map of total porosity in the Wichita .....	115
49. Maps of porosity distribution in the lower and upper parts of the lower Wichita (Sequence L 1) .....	116
50. Maps of porosity distribution in the lower and upper parts of the upper Wichita (Sequence L 2.0) .....	117
51. Maps of porosity distribution in the Lower Clear Fork .....	118
52. Models of porosity formation in the upper Wichita and the Lower Clear Fork (L2 sequence) .....	119



# Facies, Sequence Stratigraphy and Porosity Development in the Fullerton Clear Fork Reservoir

Stephen C. Ruppel and Rebecca H. Jones

## ABSTRACT

The analysis of reservoir sequence and cycle stratigraphy, of depositional and diagenetic facies, and of the interrelationships between these attributes and reservoir properties is key to the construction of an accurate reservoir framework needed for reservoir modeling and improved imaging of remaining hydrocarbons. In the Fullerton Clear Fork field, fundamental steps in the process included (1) creating and applying an analogous outcrop depositional model, (2) describing and interpreting subsurface core and log data in terms of this initial model, (3) defining the sequence-stratigraphic architecture of the reservoir section, and (4) developing a cycle-based reservoir framework. Key data in this analysis included 29 cores totaling 14,383 ft, more than 1,700 rock thin sections, nearly 800 wells, 3-D and 2-D seismic, a borehole image log, and applicable outcrop models.

## INTRODUCTION

The Clear Fork Group (fig. 1) in the Permian Basin comprises a thick (as much as 2,500 ft; 800 m) succession of dominantly shallow-water-platform carbonates that were deposited across West Texas and New Mexico during the Early Permian (Leonardian). Reservoirs developed in these carbonates (fig. 2) have accounted for more than 3.2 billion barrels of oil production (Dutton and others, 2004)—more than 10 percent of the total recovered from the Permian Basin to date. Despite this substantial production, estimates of original oil in place (OOIP) indicate that, overall, Leonardian reservoirs contained more than 14.5 billion barrels of

oil at discovery. Recovery efficiency is thus only about 22 percent, considerably below the 32-percent average for carbonate reservoirs in the Permian Basin (Tyler and Banta, 1989; Holtz and Garrett, 1990). Recovery from the shallow-water-platform reservoirs of the Clear Fork Group has been even less efficient. Holtz and others (1992) estimated a recovery efficiency of only 18 percent of OOIP for these reservoirs.

To recover the remaining oil in Clear Fork reservoirs, operators must turn to increasingly sophisticated recovery technologies: e.g., waterflooding, gas injection, horizontal wells, etc. To effectively deploy these technologies, however, it is critical that an accurate reservoir framework first be constructed to form the basis for modeling and interpreting past, present, and future recovery operations.

This report details the approaches used to develop such a framework in the Fullerton Clear Fork field in West Texas. Like many mature Clear Fork reservoirs in the Permian Basin, Fullerton field has undergone a major decline in oil production rate and a major increase in water production rates for several years. Current production from the field stands at about 310 million bbl, representing only about 25 percent of the calculated OOIP. An understanding of the depositional and diagenetic facies, the cycle and sequence stratigraphy, and the architecture of these stratigraphic elements is the crucial first step to determining the probable oil distribution at discovery and defining the best strategies for recovering the sizeable remaining oil volume.

## METHODS

The focus of this study of the Fullerton reservoir is the Fullerton Clear Fork Unit, a unitized production area in Fullerton field operated by ExxonMobil Corporation. Data and interpretations presented in this report were derived from investigation of 29 cores totaling 14,383 ft, the examination of more than 1,700 rock thin sections, and the correlation of

approximately 45,000 stratigraphic tops in nearly 800 wells. The basic procedure followed in this study to develop a full-field sequence-stratigraphic model and reservoir framework is as follows: (1) identify depositional facies and vertical facies-stacking patterns and cycles in cores, (2) calibrate facies and cycle patterns to wireline logs, (3) construct 2D cross sections of core/log data sections, (4) define 2D cycle and sequence stratigraphy from core/log sections, and (5) extrapolate 2D cycle and sequence correlations into 3-D space by correlating all available well logs. Stratigraphic sequences were tied into available 3-D seismic data to check their accuracy and geometry. Conventional core analysis data were available for all cores; these data were used to determine relationships between facies, cyclicity, and porosity and permeability development. Figure 3 depicts the distribution of cores and 3-D seismic data in the field.

## PREVIOUS WORK

Mazzullo (1982) and Mazzullo and Reid (1989) presented overviews of lower Leonardian stratigraphy and depositional systems in the Midland Basin. Presley and McGillis (1982; see also Presley, 1987) documented the highly cyclic, predominantly evaporitic facies of the upper Leonardian Glorieta and Upper Clear Fork units in the Texas Panhandle. Ruppel (1992; 2002) described the facies, cyclicity, and diagenesis in the Glorieta and Upper Clear Fork at Monahans Clear Fork field on the Central Basin Platform and postulated that reservoir development was caused by cyclic deposition and diagenesis driven by episodic sea-level rise and fall. Atchley and others (1999) described Clear Fork facies at Robertson field at the north end of the Central Basin Platform and proposed a similar model for structural control over facies deposition and reservoir development. Ruppel and others (2000) described outcrop equivalents of the producing subsurface Clear Fork reservoirs from outcrops in the Sierra Diablo mountains of West Texas. Kerans and others (2000) documented the depositional setting, facies, and

architecture of the Abo from outcrops in the Sierra Diablo (fig. 2) and showed that karsting has had a major effect on both the Abo and the overlying Lower Clear Fork succession.

## GEOLOGIC SETTING

The Fullerton Clear Fork field is the largest of a large number of fields developed in the Leonardian Series on the Central Basin Platform of the Permian Basin (fig. 2). In some parts of the Basin, the Leonardian is productive from all of its component stratigraphic units (fig. 1). The productive reservoir section at Fullerton, however, is essentially restricted to the Lower Clear Fork, Wichita, and Abo stratigraphic units (fig. 4); very minor production has also been reported from the Upper Clear Fork section. By far the bulk of the oil production has come from the lower two-thirds of the Lower Clear Fork and the Wichita sections of the reservoir. Even where oil saturated, the Abo has proven difficult to exploit in part owing to its active water drive (as opposed to the pressure depletion drive that characterizes the overlying parts of the reservoir) and the fact that it is at or near the oil-water contact throughout most of the field.

Regionally, the Leonardian is dominated by shallow-water-platform carbonates. Each of the component stratigraphic units contains updip peritidal tidal-flat carbonates and downdip subtidal carbonates. Mineralogy in each is dominated by dolomite and anhydrite. Calcite, in the form of limestone, is relatively uncommon; however, where present it is most common in the lower part of the Leonardian and in the distal, downdip sections (Ruppel, 2002). The reservoir section at Fullerton is generally consistent with this regional pattern, but it does contain a higher volume of limestone than most other Leonardian platform reservoir successions in the Basin.

Structurally, Fullerton field is developed over a large compound structural high (fig. 5) that reflects deep-seated faulting and differential uplift of the area that began in the Pennsylvanian (Jones and Ruppel, 2004). Deeper oil production comes from block-faulted

Silurian (Wristen Group) carbonates in the southern and central parts of the fields. The Clear Fork reservoir seal is provided by evaporite-rich carbonates in the Lower Clear Fork, Tubb, Upper Clear Fork, and Glorieta.

The reservoir is currently drilled to well spacings of 40 to 10 acres and is under active waterflood. The greatest well density is in the northern part of the field (mostly 20- and 10-acre well spacings); poorer well control exists in the southern half of the field. In general, these closely spaced wells provide good control for definition of stratigraphic horizons and reservoir attributes. In many parts of the field, especially along the western edge of the field and in the southern half of the field wells are represented only by poor-quality (old gamma-ray/neutron) logs and cannot be correlated or interpreted with any precision.

## OUTCROP ANALOGS

Studies of analogous reservoir outcrops in the Sierra Diablo in Hudspeth and Culberson Counties (fig. 2), Texas, provide important insights into the geological controls on reservoir development in the Fullerton reservoir and on the reservoir architecture. The Leonardian of the Sierra Diablo contains direct analogs of all major reservoir intervals at Fullerton field, including the shallow-water-platform carbonates of the Lower Clear Fork Group (Fitchen and others, 1995; Ruppel and others, 2000) and Wichita units, and the karsted, platform-margin subtidal carbonates of the Abo (Fitchen and others, 1995; Kerans and others, 2000). The overall Leonardian stratigraphic section and its component sequences are thinner in the Sierra Diablos than in the subsurface of the Permian Basin. This seems most likely due to a more dominant control of local tectonics in the outcrop area during the Leonardian (e.g., King, 1942). However, styles of depositional architecture and facies development are very representative of subsurface

succession and thus form excellent, if not essential, models for interpreting sparser subsurface data sets. Key observations established from these outcrops are described below.

### Abo Facies, Cyclicity, and Sequence Architecture

Integrated studies of outcrops and subsurface data sets indicate that the Abo represents the basal depositional sequence (sequence L1) of the Leonardian (Fitchen and others, 1995). Studies of Abo outcrops in the Sierra Diablo (Fitchen and others, 1995 ; Kerans and others, 2000) demonstrate three important aspects of this succession in the Permian Basin: (1) it consists of dominantly open-marine, outer platform facies, (2) it displays clinoformal architecture, and (3) it is overprinted by karst features (sinkholes, caves, cave fill, and collapse features). The dominance of clinoformal, outer ramp, fusulinid-crinoid packstones and wackestones and less common ramp-crest, ooid-peloid, grain-rich packstones and grainstones in the Abo contrasts with the flat-lying, alternating tidal-flat and shallow subtidal wackestone-packstone successions of the Wichita and Lower Clear Fork. The top-lapping clinoforms of the Abo document rapid basinward progradation, a forced regression probably caused by a rapid fall in sea level. Karsting in the Abo, although initiated at the exposed top of the Abo during sea-level fall, is manifested downsection in the Abo by caves and sinkholes and upsection in the overlying Lower Clear Fork as collapse features. Where karsting and associated thickness variations are developed, largely in platform-marginal settings, the contact between the Abo and Lower Clear Fork is a relatively sharp and undulating, unconformable surface. Updip, karsting is less apparent and the contact less pronounced.

## Lower Clear Fork Facies, Cyclicity, and Sequence Architecture

The outcropping Lower Clear Fork succession in the Sierra Diablo represents a single depositional sequence (L2). Key elements of this succession are (1) basal backstepping tidal-flat deposits that locally fill relief on the underlying, karsted Abo surface (fig. 6), (2) an updip succession of amalgamated tidal-flat facies, (3) a cyclic, downdip succession of alternating tidal-flat and midramp, subtidal facies, and (4) an overall backstepping (upward-deepening) trend (fig. 7).

The Lower Clear Fork outcrop succession records the gradual flooding of the previously exposed Abo platform and a continued, although punctuated, increase in accommodation and water depth. Downdip Lower Clear Fork deposits are characterized by alternating peritidal, tidal-flat deposits and subtidal, skeletal wackestones and packstones that document cyclic rise and fall of sea level at the high-frequency sequence and cycle scale. These cycles, which average about 20 ft in thickness, display consistent patterns of facies stacking (cycle-base skeletal wackestones and overlying peloidal grain-rich packstones) and appear to be widely continuous (Ruppel and others, 2000). Recent studies undertaken in the course of this project reveal that these shallow subtidal platform rocks pass downdip into clinoformal fusulinid-crinoid wackestones and packstones of the outer ramp/slope within less than 2 mi basinward. Updip, in the platform interior (landward), the Lower Clear Fork is characterized by amalgamated, peritidal tidal-flat deposits (fig. 7). These updip tidal flats are analogous to the Wichita of the subsurface. The absence of shallow-water highstand deposits at the top of the Lower Clear Fork suggests a rapid, perhaps forced, regression followed by exposure and possible erosion at the top of the L2 sequence.

Lower Clear Fork outcrops in the Sierra Diablo also provide important insights into the cycle architecture of analogous subsurface reservoir sections like that at Fullerton. In tidal-flat-capped successions, and less commonly in subtidal successions, 3- to 6-ft-thick (1- to 2-m-thick) cycles are definable in vertical sections but, because of poor outcrop continuity, are not readily correlatable. However, subtidal cycle bundles, which average 15 to 30 ft (5 to 9 m) in thickness, can be correlated at typical interwell distances. These bundles typically consist of upward-shallowing successions that have skeletal wackestones at their bases and peloid-oid packstones at their tops (fig. 7).

## FULLERTON RESERVOIR FACIES AND STRATIGRAPHY

The productive reservoir section at Fullerton field includes parts of the Abo, Wichita, and Lower Clear Fork Formations (fig. 4). Like many stratigraphic names used in the subsurface, each of these units is commonly considered to display both regional time equivalency and facies constancy across the region. In other words, each is considered to be both a rock-stratigraphic and a time-stratigraphic unit. In fact, these names are best considered rock-stratigraphic terms (essentially facies) at the formation level of nomenclature. To place these units in their proper perspective, however, it is best to consider both facies and time interrelationships. In this report we treat these named stratigraphic units (i.e., formations) as facies or rock-stratigraphic units but place them in an interpreted sequence-stratigraphic (i.e., time-stratigraphic) framework that has been developed from previous studies (e.g., Fitchen and others, 1995; Kerans and others, 2000; Ruppel and others, 2000). In this framework, the Abo and part of the Wichita Formation are time-equivalent facies of the earliest composite (third-order) depositional sequence of the Leonardian (sequence L1). Sequence L 2 comprises part of the Wichita Formation (updip peritidal deposits) and the Lower Clear Fork Formation (downdip, dominantly subtidal deposits).



The L 3 sequence contains siliciclastics of the Tubb Formation and carbonates of the part of the overlying Upper Clear Fork (fig. 4). Stratigraphic data at Fullerton field are consistent with this interpretation of time and rock interrelationships.

Correlations of usable wireline log suites (about 750) show that across most of the area of the Fullerton Clear Fork Unit (figs. 3, 5), stratigraphic units are relatively isopachous (fig. 8). This is consistent with the depositional setting of the field area on the Central Basin Platform, a broad, flat carbonate platform not unlike the modern-day Bahamas platform.

The same generally isopachous nature of the Wichita and Lower Clear Fork shows up in 3-D and 2-D seismic data. These data, however, show that the Wichita and Abo vary considerably in thickness across the field. Wichita deposits thin and Abo deposits thicken to the east and southeast (fig. 9). Synthesis of core, wireline, and seismic data indicates that this reciprocal thickness relationship is the result of facies change, i.e., the Wichita represents the updip, shallower water (inner platform) equivalent of the distal, deeper water (outer platform to slope) Abo. Support for this conclusion will be presented in subsequent sections.

### Facies and Depositional Setting

The facies encountered at Fullerton field are typical of those observed throughout most carbonate platform successions of Leonardian and early Guadalupian age in the Permian Basin. The characteristics of these and similar facies have been documented by many authors, including Bebout and others (1987), Ruppel and Cander (1988a, 1988b), Garber and Harris (1990), Longacre (1990), Kerans and others (1994; see also Kerans and Fitchen, 1995; Kerans and Kempter, 2002), and Ruppel and Bebout (2001). Leonardian facies successions have been documented both in outcrop (Ruppel and others, 2000) and in the subsurface (Ruppel (2002).

The facies groupings defined in this study and presented below were defined with three goals in mind: (1) to document the characteristics of distinct depositional settings, (2) to document widespread and potentially correlatable sediment packages, and (3) to create a sound geological basis for assessing relationships between rock textures and fabrics and petrophysics. In many ways, it is the last of these goals that is most important, for it provides the foundation for reservoir modeling. However, as a result of this, facies characteristics used for subdivision are dominantly small-scale matrix properties, e.g., grain size and shape, grain type. Larger scale features such as fractures, anhydrite nodules, and evidence of burrowing, although noted, are not used for facies subdivision.

Twelve facies can be at least locally identified in the Fullerton reservoir succession. Most of these are intergradational with one or more others. In many cases, their distinction is somewhat subjective, based on differences in grain preservation, diagenesis, grain size, etc. Most can be found in any part of the reservoir succession.

#### *Peritidal Mudstone-Wackestone*

These rocks are most abundant in the Wichita but are also locally common in the Lower Clear Fork. They are massive to parallel-laminated mud-rich rocks that only rarely contain any grains other than a few peloids (fig. 10. a, b). They are most typically associated with the exposed tidal-flat facies and the clay-rich carbonate mudstone facies and are assumed to represent peritidal deposition on a very low energy tidal flat. They are dominantly dolomitized. Where dolomite, they may display very high porosities (as much as 15 percent). Because this porosity is due to intercrystalline pores within fine crystalline dolomite, however, the permeability is generally low. Where limestone, they invariably exhibit very low porosity

(typically less than 2 percent) and permeability. Gamma-ray signature is medium to high and highly variable in these rocks owing to the local presence of clay minerals.

### *Clay-rich Carbonate Mudstone*

These rocks are found intimately associated with rocks of the Peritidal mudstone-wackestone facies in the Wichita. They are typically dark gray to nearly black and 1 to 8 cm in thickness (fig. 10, c). Where cyclic upward-shallowing successions can be identified, these deposits are found at or near cycle tops in both the Lower Clear Fork and the Wichita. Although they are probably contributors to the high gamma-ray response observed in the Wichita and in Lower Clear Fork peritidal intervals, because of their thinness, they cannot be discretely defined by logs and therefore are not correlatable. Their color and clay content and lack of apparent lateral continuity suggest that they were formed as local organic-rich ponds or stagnant pools on the tidal flat. They may act as local baffles to reservoir fluid flow but are probably very discontinuous laterally.

### *Exposed Tidal Flat*

These deposits show obvious evidence of exposure such as fenestral pores, pisolites, mudcracks, insect burrows, sheet cracks, tepee structures, and cyanobacterial or microbial laminations (fig. 11). They are locally common in both the Lower Clear Fork and the Wichita. In the Lower Clear Fork, they define cycle tops; in the Wichita, their relative sea-level significance is less apparent. Their sedimentary structures demonstrate, however, that they were formed during at least local sea-level fall and exposure. Porosity is locally very high (at least 30 percent) and is associated with a combination of fenestral pores and intercrystalline and interparticle pores. Permeability is lower than in grain-dominated subtidal rocks but can be significant where high porosities are present. Like the peritidal mudstone-wackestone facies, these rocks typically

display somewhat elevated and variable gamma-ray response. This can sometimes be used to distinguish these rocks from overlying and underlying subtidal facies.

### *Peloid Wackestone*

This grain-poor facies differs from the rocks of the Peritidal mudstone-wackestone facies in its association and sedimentary structures. The rocks are invariably associated with other, demonstrably subtidal, facies; they are burrowed; and they locally contain skeletal debris (fig. 11 c). These features suggest they were deposited in low-energy subtidal settings. Dominant grains (usually 80 to 150  $\mu\text{m}$  in diameter) are probably fecal pellets created by infaunal burrowers. The absence of skeletal allochems supports a low-energy, perhaps restricted, setting.

Anhydrite nodules are locally common in these rocks, probably reflecting the postdepositional entry of sulfate-bearing diagenetic fluids into permeability pathways created by burrowers. In many cases, anhydrite nodules occupy solution-widened vertical burrow pathways that are surrounded by alteration halos (fig. 12). These halos (which have been reported from most Permian platform carbonate successions) commonly display a more grain-rich texture, higher porosity and permeability, and a depleted oxygen isotope signature (Major and others, 1990; Ruppel and Bebout, 2002). At Fullerton, they are most commonly developed in HFS L 2.2. This stratigraphic position (in the late highstand of the L2 composite sequence) is analogous in terms of accommodation to similar features documented from the younger Grayburg Formation at (Ruppel and Bebout, 2001), suggesting that these features are an expected and perhaps predictable feature of late highstand sedimentation on Permian shallow-water-carbonate platforms.

### *Peloid Packstone*

The distinction between these rocks and those assigned to the Peloid wackestone facies is usually based on apparent peloid abundance and can be subjective. As with the Peloid wackestone facies, peloids are mostly fecal pellets created by burrowing infauna, although skeletal debris (chiefly mollusk fragments) are locally common. It should be noted that the preservation of these pellets is largely a function of diagenesis, both early and late. Nearly all of the low-energy mud-dominated facies in the Permian contain obvious pellets indicating that burrowers were ubiquitous in these deposits. There is a complete gradation in texture between pelleted mudstones and peloid packstones. Differences in texture are probably most commonly due to differences in early diagenesis. Pellets that were early lithified and stabilized are more likely to be preserved. Thus, peloid (i.e., pellet) packstones are sediments that underwent significant amounts of early diagenesis, whereas peloid wackestones and pelleted mudstones underwent relatively little. The textural significance of these pelleted facies is thus more diagenetic than depositional. Accordingly, apparent variations in peloid abundance in these mud-dominated facies packstones, wackestones, and mudstones is not necessarily an indication of differing depositional environment or fluctuations in wave energy. Rather, they may be predominantly due to local changes in rates and effects of early diagenesis. Porosity in these rocks is usually associated with intercrystalline pores and rare skeletal moldic pores (fig. 13).

### *Peloid Grain-dominated Packstone*

Unlike mud-rich peloid facies discussed above, grain-dominated (or grain-rich) peloid packstones commonly display evidence of possible wave-related transport. These rocks are typically well sorted and contain interparticle pores that are either open or filled with cements (fig. 14). The interparticle pores indicate that these peloids acted as true grains rather than

pelleted mud, in contrast with the intercrystalline and moldic pores that typify mud-dominated facies. It should be noted, however, that in some instances the grain-dominated texture is associated with vertical burrows and probably owes its origin to burrow-related diagenesis. For the most part, this facies is restricted to the subtidal legs of Lower Clear Fork depositional sequences. These rocks are among the highest quality reservoir facies in the field. Highest porosity and permeability are encountered in peloid grain-dominated packstone limestones (as much as 20 percent porosity), although dolostones also exhibit good porosity and permeability.

#### *Ooid-Peloid Grain-dominated Packstone-Grainstone*

These rocks differ from the peloid grain-dominated packstone facies, with which they are often closely associated, in having recognizable ooids (as much as 250  $\mu$ m in diameter) in addition to pervasive pellets (fig. 15). Skeletal grains in the form of fusulinids, mollusks, and crinoids are also common. In most cases, these deposits, which are restricted to subtidal sections of the Lower Clear Fork, are also well sorted, possibly due to wave action. Grainstones, although relatively rare, display excellent size sorting and in some cases possess inclined or cross laminations (fig. 15a). These rocks, which occur as both dolostone and limestone, represent the highest energy facies in the reservoir succession and in many cases display the best porosity and permeability. Pores are dominantly interparticle, but moldic pores are very abundant, especially in limestone-dominated intervals.

#### *Fusulinid Wackestone-Packstone*

Fusulinid-bearing rocks are found in all three formations (Abo, Wichita, and Lower Clear Fork), although they are very limited in the Wichita. In all occurrences they are most commonly dolomitized. The fusulinids that dominate this facies can constitute as much as 40 percent of the rock (fig. 16). Fusulinids are preserved either as open or anhydrite-filled molds or as well-

preserved fossil tests. In the Lower Clear Fork and Wichita, they are associated with abundant peloids (probably pellets). In the Abo, they commonly co-occur with crinoids, and less commonly with brachiopods. Fusulinids are thought to have occupied water depths of 30 m or more and here represent the deepest water facies observed at Fullerton field. Accordingly, their presence is an indicator of platform flooding and relative sea-level rise, making them key indicator facies of cycle and sequence boundaries.

#### *Skeletal Wackestone-Packstone*

Typically these rocks contain small volumes of skeletal debris (most commonly mollusks fragments but also including crinoids and less common ostracodes) and the ubiquitous peloids. They are gradational into peloid wackestones and packstones. Evidence of burrowing is common. The dominance of mollusks and the essential absence of more normal marine organisms in these rocks suggests they were deposited in an inner platform setting. Typically they exhibit low porosity; pore space is created by skeletal molds and intercrystalline pores.

#### *Oncoid Wackestone-Packstone*

Oncoids (or oncolites) are large microbial-coated grains (fig. 17) formed under conditions of continuous wave agitation in shallow water. They are abundant at the base of the Lower Clear Fork throughout the entire field area. Invariably they are associated with fusulinids and other faunas indicative of open-marine deposition. This association and their stratigraphic position immediately above the top of the tidal-flat-dominated Wichita indicates that they represent marine flooding of the platform during sea-level rise (transgression). In some downdip some wells (e.g., the Amoco FM-1 well; fig. 3), they are present at many intervals in the Lower Clear Fork. Overall, they are most abundant at cycle bases. Their distribution suggests that they document relatively high energy conditions developed during platform flooding. Like the

fusulinid facies, the oncoid wackestone-packstone facies is a marker facies indicative of transgression or platform deepening (i.e., sea-level rise).

### *Siltstone-Sandstone*

Quartz silt- and sand-bearing rocks are common only at the top of the Lower Clear Fork and in the overlying Tubb Formation. Because the quartz is associated with potassium- and thorium-rich clay minerals, its presence in the Lower Clear Fork and Tubb is well defined by high CGR (corrected gamma ray) wireline log response (figs. 4 and 8). Their size (fine sand to coarse silt ) and shape (generally subangular) suggests these sediments were originally windblown. This indicates that most of the quartz in the section was delivered to the area during sea-level lowstands when the platform was emergent. Quartz silt/sand occurs in two scenarios: (1) in peritidal tidal-flat facies and (2) in reworked subtidal facies. The former are probably formed as small volumes of silt, sand, and clay are blown onto intermittently exposed, slowly accumulating tidal flats and admixed with peritidal carbonate sediment. The presence of potassium and thorium in these clastics produces the increased gamma-ray response that is associated with many tidal-flat deposits in the Clear Fork and facilitates recognition of these cycle-capping deposits in these sediments (Ruppel, 2002). Most of the occurrences of silt, sand, and clay in the Lower Clear Fork at Fullerton are of this type.

Subtidal silt, sand, and clay deposits are most common in the Tubb. These rocks were formed first by large-volume eolian deposition during extended sea-level lowstand and carbonate nondeposition, then reworked during the ensuing sea-level rise and marine flooding of the platform. These deposits are generally richer in clastic content, are intermixed with carbonate mud, and show evidence of subtidal conditions (e.g., burrows, stratification). Although these



rocks may locally exhibit some minor porosity, they do not appear to display any significant reservoir permeability.

### *Lithoclast Wackestone*

Thin intervals (usually less than 1 ft) containing scattered lithoclasts are locally encountered at the contacts between transgressive marine facies and underlying tidal-flat deposits or other facies showing evidence of subaerial exposure (fig. 11c). Clasts are variable in composition but most commonly consist of fragments or intraclasts derived from the underlying bed. Clasts typically are 1 cm in width or less. Although volumetrically minor, these rocks are an important indicator facies of lithification due to exposure or nondeposition and subsequent sea-level rise and thus of cycle boundaries.

### Depositional Model

The relative distribution of the facies described above can best be understood when considered in light of a conceptual geological model. Figure 10 portrays idealized three-dimensional relationships among major facies types and depositional environments typical of most middle Permian (Leonardian and Guadalupian) platform carbonate successions in the Permian Basin. It should be understood that this model reflects only the relative interrelationships among facies tracts. The actual position of individual facies tracts at a given point in time is a function of many factors, including accommodation, rates and magnitude of sea-level rise, rising versus falling sea-level trends, climate, tectonics, etc. However, during normal relative rises in sea level facies tracts normally step landward, whereas during falls they step basinward. Exceptions to this general pattern are common. For example, ramp-crest facies may be much better developed during sea-level highstand and fall than during transgression and rise. The basal Leonardian (L1) depositional sequence at Fullerton, for example, appears to be

dominated by an updip inner ramp succession (Wichita) and a downdip outer platform succession (Abo) with a very poorly developed middle-ramp to ramp-crest facies tract. Nevertheless, the vertical successions (facies stacking patterns) formed by sea-level-driven migrations of these facies tract are the key to identifying depositional cycles in cycles from cores and logs.

Among the identified facies at Fullerton, the peritidal mudstone-wackestone facies, the clay-rich carbonate mudstone facies, and the exposed tidal-flat facies for the most part represent deposition on the inner ramp in sabkha-tidal flat setting as low-exposure index (cf. Hardie and Garrett, 1977) peritidal deposits, tidal-flat ponds, and high-exposure tidal-flat deposits, respectively (fig. 18). It should be noted, however, that exposure fabrics like those developed in the inner platform can also form on the ramp crest following complete aggradation and exposure at any time.

The peloid/pellet-rich facies at Fullerton (peloid wackestone facies, peloid packstone facies, peloid grain-dominated packstone facies, and skeletal wackestone-packstone facies) are also dominantly associated with the inner ramp but occupy a somewhat more distal, lagoonal to restricted subtidal setting where sediment formation is dominated by infaunal and epifaunal burrowing activities (fig. 18).

The ooid-peloid grain-dominated packstone – grainstone facies in the Lower Clear Fork at Fullerton is typical of facies deposited in a platform ramp crest at the platform-margin setting where relatively high wave energies are developed (fig. 18). However, none of the cored wells in the field reveal the kind of vertically stacked succession of these deposits that typically defines a well-developed ramp crest (see, for example, Ruppel and others, 2000). This may reflect

insufficient core control or the absence of a true ramp crest on the Lower Clear Fork platform. As previously stated, the Abo appears to lack a ramp-crest facies succession.

As in most middle Permian carbonate-platform successions, the fusulinid wackestone-packstone facies documents outer platform deposition. These rocks are well developed in both the Lower Clear Fork and the Abo. In the Abo, these rocks display classic clinoformal bedding and the general lack of cyclicity that typifies a distal outer platform setting (fig. 18). By contrast, fusulinid wackestone-packstone facies rocks in the Lower Clear Fork are horizontally bedded and interbedded with middle and inner platform facies. This suggests that these fusulinid-rich rocks were deposited in a much more proximal outer ramp position.

The oncolid wackestone-packstone facies is closely associated with the fusulinid wackestone-packstone facies in the Lower Clear Fork at Fullerton, indicating that the former was deposited during platform deepening. This facies has not previously been reported from middle Permian rocks in the Permian Basin. Its occurrence at Fullerton field may indicate the development of relatively higher energy conditions on the outer platform in the Fullerton area than is generally developed in other regions in the Basin.

## Sequence Stratigraphy

Figure 11 illustrates diagrammatically the sequence architecture, basic facies tracts interrelationships, and rock and time terminology of the lower Leonardian at Fullerton field. In this section, we describe the sequence-stratigraphic characteristics of each of the major Leonardian units at Fullerton.

### *Abo Formation*

As already discussed, the Abo represents the distal facies or systems tract of the earliest (oldest) Leonardian sequence in the Permian Basin: the L 1 sequence (fig. 11). Regionally, the

Abo consists of outer ramp to slope, skeletal crinoid-fusulinid-dominated subtidal facies and less common ramp-crest ooid-peloidal grainstones (Kerans and others, 2000). In both outcrop and in the subsurface, the Abo is dominantly characterized by clinoformal, top-lapping geometries (Kerans and others, 2000; Zeng and Kerans, 2003; figs. 6 and 9). This typical Abo architecture is very apparent in 3-D and 2D data from Fullerton field. The Abo is readily defined by its clinoformal reflectors and its top by a prominent toplap surface that is apparent throughout the field (fig. 9).

Although the Abo at Fullerton field is penetrated by relatively few wells and has been cored in even fewer, existing cores display facies and bedding characteristics typical of sediments deposited in an outer ramp/slope setting. Facies consists of alternating beds of fusulinid-crinoid packstones and wackestones, and peloidal packstones. No true cyclicity is apparent in the Abo, although there are alternations between skeletal-rich and skeletal-poor intervals. Inclined beds are locally common. Additionally, correlations within the Abo are not apparent either from core sections or from wireline logs. In part this is the result of limited core and well-log control through the Abo section. But poor correlatability is typical of outer platform depositional successions that display clinoformal architectures because of the associated dipping bedding surfaces, discontinuous facies packages, and poor vertical facies contrasts.

Abo rocks are almost entirely composed of dolomite at Fullerton field. Porosity is locally very high, reaching values of as much as 25 percent. Pore types vary among fusumolds, intercrystalline pores within coarse crystalline dolostones, and interparticle pores in skeletal/peloidal packstones.

The thickness of the Abo is indeterminate largely for two reasons. First, few wells and no cores penetrate the complete Abo to Wolfcamp section. Second, outcrop studies reveal that the

Abo–Wolfcamp contact may be lithologically indistinct in many areas: in outcrop both the uppermost Wolfcamp and the Abo are composed of clinoformal, outer platform fusulinid/crinoid wackestones. A minimum thickness of 300 ft is established by the Amoco FM-1 cored well in the southeastern corner of the field (fig. 3).

The contact between the Abo and the overlying Wichita varies from sharp to gradational. In many cores, the contact is marked by an interval (up to several feet thick) of intermixed clasts and fragments of Wichita tidal-flat deposits and Abo fusulinid-bearing subtidal deposits. The brecciated nature of this contact interval suggests strongly that it is the result of karst-related dissolution and collapse. These breccias and their distribution are discussed more fully in a later section of this report.

### *Wichita Formation*

The Wichita at Fullerton field consists of a diverse assemblage of peritidal to supratidal tidal-flat deposits. Integrated outcrop and subsurface studies indicate that the Wichita Formation represents an updip, proximal facies equivalent of both the Abo outer platform succession and the subtidal Lower Clear Fork. These data also suggest that the Wichita actually comprises parts of two depositional sequences: the highstand leg of sequence L1 and the transgressive leg of sequence L2 (fig. 19). The lower Wichita represents the updip, tidal-flat facies tract equivalent of the downdip, outer platform facies tract of the Abo in Leonardian sequence L1, whereas the upper Wichita represents the updip tidal-flat facies equivalent of the basal Lower Clear Fork subtidal facies in sequence L2 (fig. 11).

The Wichita is dominantly composed of dolostone; however, intervals of limestone are common in the upper Wichita in the northern part of the field (fig. 20). The limestone intervals

are relatively persistent laterally and are generally subparallel to stratigraphic markers in the field (fig. 8).

The thickness of the Wichita is fairly consistent over the northern two-thirds of the field, ranging from about 350 ft in the center of the field to about 280 ft along the western, northern, and eastern margins of the field area (fig. 21). Thickness decreases, however, to as little as 110 ft in the southeastern part of the field (fig. 21). This decrease in thickness, which occurs relatively abruptly along a generally northeast trending belt, marks the change from the updip Wichita tidal-flat facies to the downdip Abo outer ramp fusulinid facies. This relationship, is well displayed in figure 22, a NW-SE cross section through the field.

Correlations within the thick Wichita succession of relatively similar tidal-flat deposits are difficult owing to (1) the discontinuous nature of tidal-flat deposits, (2) the lack of any systematic vertical stacking relationships among facies to define cycles, (3) the nonuniform response of wireline logs to these facies, and (4) the overprinting effects of diagenesis. One exception to this is a thin (average 10 ft thick) bed of subtidal fusulinid to peloidal packstone that is apparent in the middle of the Wichita in many cores and logs (figs. 8, 22). Because of its subtidal character, this bed is actually well imaged by wireline gamma logs. Its low gamma-ray response provides a strong contrast to the generally high and variable gamma-ray aspect of the underlying and overlying tidal-flat deposits (figs. 6, 22). This subtidal deposit, which appears to be present over the entire field area, documents a widespread sea-level rise and transgression and is essentially the only definable time line in the Wichita succession. This marine flooding event appears to represent a late L1 transgression of the platform and probably correlates to the uppermost part of the Abo in downdip areas of the field.

## *Lower Clear Fork Formation*

Rocks assigned to the Lower Clear Formation represent the subtidal systems tract of the Leonardian 2 (L2) sequence. Core studies show that the Lower Clear Fork can be subdivided into three high-frequency sequences HFS (L 2.1, L2.2, L2.3) throughout most of the Fullerton field area (figs. 4 and 8). A fourth HFS (L 2.0) can be defined at the margins of the field. Each of these can be identified as having a transgressive, dominantly subtidal lower leg and an overlying, highstand upper leg.

### High-Frequency Sequence L 2.0

HFS L 2.0 documents the initial flooding of the platform following sea-level fall and exposure at the end of L1 deposition. In most of the field area, HFS 2.0 consists of amalgamated tidal-flat deposits of the upper Wichita. Subtidal Lower Clear Fork deposits of L 2.0 are only present at the margins the field (figs. 8 and 22). At the downdip edge of the field, HFS L 2.0 consists of a basal transgressive leg of peritidal tidal-flat deposits, a middle maximum flooding leg of subtidal, outer platform, fusulinid-rich packstones, and an upper leg of peritidal tidal-flat deposits (fig. 22).

### High-Frequency Sequence L 2.1

In most of the Fullerton field area, HFS L 2.1 forms the base of the Lower Clear Fork. As defined for this study, L 2.1 consists of a basal section of transgressive to early highstand subtidal platform facies and an upper section of highstand tidal-flat facies (figs. 8, 11, and 22). The basal transgressive subtidal facies of the Lower Clear Fork represent the first marine flooding of the platform and a sharp change in depositional style from the tidal-flat deposition of the Wichita to subtidal deposition of the Lower Clear Fork.

The basal transgressive leg of L2.1 consists dominantly of fusulinid wackestone-packstone and oncoid wackestone-packstone facies that document landward backstepping of outer platform facies across the platform. These rocks are generally overlain by a succession of peloid packstones and grain-dominated packstones that represent late transgression and early highstand. Locally, within this succession there are exposed tidal-flat facies indicating periodic exposure. L 2.1 is capped throughout most of the field by a succession of one to three tidal-flat-capped cycles that represent exposure during late highstand (figs. 8, 11, and 22). These tidal-flat facies typically exhibit an elevated gamma-ray log response that aids in their recognition (figs. 8 and 22).

Like most of the Lower Clear Fork in the Permian Basin, HFS 2.1 is dominantly dolostone. However limestone is locally common at Fullerton field, especially in the transgressive leg of 2.1. Areal, limestone is most abundant along the periphery of the northern half of the field and at the southern end of the field (fig. 23).

The thickness of L 2.1 is relatively constant across the Fullerton field area, ranging from about 140 to 150 ft across most of the area (fig. 24). In some cases, thickness changes appear to be a function of differential subsidence along deep-seated faults (see Jones and Ruppel, this report). This is especially apparent along the north-trending fault in the northeastern part of the field, where the thickness changes from less than 140 ft on the western, upthrown side of the fault to more than 160 ft on the eastern, downthrown side of the fault (fig. 23). Examination of modern structure (fig. 5) shows that considerable movement on this fault occurred even after Lower Clear Fork deposition.

Porosity can be developed in any part of L 2.1 but is most abundant in the subtidal (transgressive and early highstand) parts of the sequence. Pore space is dominated by



intercrystalline and moldic pores, the latter being especially abundant in limestone sections. Overall, these rocks are most porous in areas where limestone is present. Tidal-flat rocks are also locally porous but generally contain low permeabilities. The subtidal rocks of L 2.1 probably constitute the most productive reservoir interval in the field.

### High-Frequency Sequence L 2.2

HFS L 2.2 is similar to HFS L 2.1 in consisting of a basal transgressive leg composed of backstepping tidal-flat facies, a middle (late transgressive to early highstand) leg composed dominantly of subtidal facies, and an uppermost (late highstand) leg composed of tidal-flat facies (figs. 8, 11, and 22).

As is the case with L 2.1, there is good evidence that the marine flooding of the platform following the post L2.1 lowstand was progressive. Basal L2.2 tidal-flat deposits are thickest in the center of the field area but generally absent along the margins, reflecting greater accommodation and early flooding of downdip areas. The lower abundance of outer ramp fusulinid-rich facies in the TST of L 2.2 relative to L 2.1 suggests that the overall accommodation during the L2.2 sea-level rise was somewhat less than during L2.1. Lower accommodation and attendant lower wave energies are also suggested by the near absence of the oncoid wackestone-packstone facies in L 2.2. These rocks are found only in the most downdip core in the field. The fusulinid wackestone-packstone facies is also largely restricted to the eastern and southeastern parts of the area (fig. 22).

Throughout most of the field area, L 2.2 is dominated by peloid wackestones and packstones (figs. 8 and 22) typical of middle platform deposition. The sequence is capped by a thin succession of tidal-flat cycles (figs. 8 and 22).

HFS L 2.2 is composed dominantly of dolostone with two important exceptions. Like L 2.1, limestone is dominant in the southern part of the field (fig. 25). Dolomite in this area is largely restricted to mud-rich fusulinid wackestones; virtually all grain-rich facies in this area are limestone. Limestone is also abundant in a small area in the north-central part of the field.

The thickness of L 2.2 is generally significantly less than that of L 2.1 (fig. 26). L 2.2 ranges from about 85 to 90 ft across most of the central part of the area to about 100 ft along the northern and southern field margins.

Porosity development in L 2.2 is similar to that in L 2.1. Porosity is best developed in the subtidal (transgressive and early highstand) parts of the sequence and dominated by intercrystalline and moldic pores. Also like L 2.1, porosity is greatest in sections containing significant limestone.

### High-Frequency Sequence L 2.3

The uppermost Lower Clear Fork high-frequency sequence (L 2.3) is composed of tidal-flat-capped restricted subtidal cycles throughout most of the field area (figs. 8, 11, and 22). These tidal-flat caps typically contain fenestral and fine intercrystalline pore space that is definable on porosity logs. Log correlations suggest that these cycle-capping tidal-flat facies are relatively continuous across significant areas of the field. The underlying cycle-base subtidal rocks are dominantly mud-rich packstones and wackestones.

Porosity, as indicated, is mostly restricted to tidal-flat caps. Because these rocks are dominated by fine intercrystalline and moldic pores, they contain little if any reservoir permeability. Accordingly, they locally contain oil stain but rarely contribute to oil production. A possible exception to this occurs along the outer margins of the field where grain-rich peloidal

packstones of the middle ramp become more common (fig. 22). If reservoir permeability is anywhere present in L2.3, it is in these field marginal areas.

### *Tubb Formation*

The Tubb is characterized by fine-grained siliciclastics (coarse siltstone and fine sandstone), which are relatively easily defined by high-gamma-ray log response (fig. 8). These clastics have been interpreted to represent eolian deposits that were deposited during the post-L2 lowstand then reworked during the ensuing L3 sea-level rise. Because of this, most intervals are varying mixtures of siltstone/sandstone and carbonate (typically mud-rich, shallow-water facies). Although locally some Tubb beds appear correlative, they are highly variable in their distribution across the field area. The base of sequence L3 is picked at the first occurrence of siltstone/sandstone about 100 ft below the thickest clastic beds (fig. 8). A prominent marine flooding event of dolostone (peloidal wackestone and dolostone) immediately above these clastics is readily definable on wireline logs throughout the field because of its characteristic low-gamma-ray signature (especially on the spectral gamma-ray log) and provides the most correlative datum in the field. The Tubb is not part of the reservoir at Fullerton field.

### **Cycle-Scale Stratigraphy**

The fundamental goal of cycle stratigraphy is to develop a correlation framework based on time-equivalent surfaces. The basic underlying premise for this approach is the assumption that widely correlative depositional cycles are formed by punctuated, allocyclic processes (e.g., sea-level rise and fall) that affected sedimentation over broad areas. The methodology used to develop a cycle-scale stratigraphic framework in the Leonardian section at Fullerton field consists of the following: (1) characterization of facies stacking patterns and cycle development in analogous outcrops, (2) description, interpretation, and logging of facies, stacking patterns,

and possible cycle tops in cores, (3) integrated log- and core-based correlation of tentative cycle tops, and (4) definition of cycle architecture. At Fullerton field, nearly 15,000 ft of core (from 29 cored wells) was described in detail to provide the basic data for cycle definition.

### *Wichita Cyclicity*

As discussed previously, tidal-flat facies, such as those that characterize the Wichita, are typically highly discontinuous laterally; thus, depositional cycles are generally not definable in these rocks. This assertion is supported both by outcrop studies and by examination of such sediments in modern settings. Only one correlative cycle top has been defined in the Wichita on the basis of facies stacking relationships. This surface, which occurs in about the middle of the Wichita succession in most of the field, is marked by the sharp superposition of clearly subtidal rocks over the more typical tidal-flat facies of the Wichita. These subtidal rocks are in turn overlain by tidal-flat facies (peritidal mudstone-wackestone facies or exposed tidal-flat facies) that mark the cycle top. This cycle averages about 10 ft in thickness and is generally marked by a low-gamma-ray log response (fig. 8). It is probable that this lone subtidal cycle represents maximum transgression (i.e., maximum flooding) and accommodation developed on the inner Lower Clear Fork platform during the L 2.0 HFS sea-level rise. No other true depositional cycle tops (e.g., time surfaces) can be defined in the Wichita.

### *Lower Clear Fork Cyclicity: HFS L 2.1*

Facies stacking patterns define numerous apparent cycle tops, at thicknesses ranging from 2 to 15 ft (fig. 27). Cycles are typically characterized by having mud-rich facies at their bases and grain-rich facies at their tops. Basal transgressive systems tract (TST) cycles in HFS L2.1 contain abundant oncoids at cycle bases along with accompanying fusulinids (fig. 27). These cycles are capped by better sorted, peloid-rich facies. High frequency cycles (typically 5 to 10 ft

in thickness) stack into cycle sets that average 25 to 40 ft in thickness (fig. 27). Cycle sets display similar facies stacking patterns to cycles consisting of fusulinid-rich bases and peloid-rich caps. Locally, tidal-flat facies cap these cycle sets. Porosity is generally highest at both cycle tops and cycle set tops relative to bases. However, because cycles in the lower parts of cycle sets are generally more mud- and fusulinid-rich, overall porosity in these basal TST cycles is usually relatively low.

Cores and outcrop studies suggest that cycles and cycle sets are correlative over significant distances. However, where cores are not available, these correlations can be difficult to establish. Gamma-ray logs display virtually no systematic response to subtidal facies and cycles (figs. 27, 28) and thus cannot be reliably used for cycle-scale correlation throughout most of the Lower Clear Fork. [They are only useful for general definition of tidal-flat cycles at HFS contacts.] In the absence of gamma-ray logs, the most effective way of establishing cycle-scale correlations is through the use of porosity logs. This approach is based on the observation from outcrops and cores that cycle tops consistently contain the most grain-rich facies and that these rocks are most likely to contain high porosity. Accordingly, porosity logs can be used to correlate both the high-porosity facies in the upper part of the cycle and the overlying cycle top.

L2.1 highstand cycles are dominated by mud-rich peloidal facies at their bases and grain-rich peloid- or ooid-bearing facies at their tops (fig. 28). Fusulinids are usually uncommon in these highstand cycles reflecting the basinward shift in facies tracts. In general, these cycles are dominated by peloid packstones and grain-rich packstones. Porosity is commonly highest at both cycle tops and cycle set tops because of the abundance of these grain-rich facies. Cycles typically average 5 to 10 ft in thickness; cycle sets are commonly 20 to 30 ft thick (fig. 28).

### *Lower Clear Fork Cyclicity: HFS L 2.2*

Facies stacking and cycle development in HFS L 2.2 are very similar to those in L 2.1. Cycles average 5 to 10 ft in thickness, and porosity is best developed in cycle tops (fig. 29). L 2.1 cycles differ, however, in the lack of oncoid facies and the relative scarcity of fusulinid facies. This presumably reflects decreasing overall accommodation in L2.2 owing to platform aggradation and slowing rates of long-term sea-level rise. Additionally, cycle sets are not generally definable in L 2.2. This is largely due to the general absence of fusulinid facies that in L 2.1 define these intermediate-scale sea-level rise events.

### *Lower Clear Fork Cyclicity: HFS L 2.3*

High-frequency cyclicity in the Leonardian at Fullerton field is most readily definable in L2.3. These rocks, which are characterized by tidal-flat-capped shallow subtidal cycles (fig. 30), appear to be much more widely correlative than cycles in L 2.1 or L 2.2. Although neither facies nor cyclicity is defined by gamma-ray logs, both are distinguishable on porosity logs because of the typically well developed porosity associated with cycle-capping tidal-flat deposits. The porosity in these rocks is generally caused by the presence of fenestral pores and can be relatively high, especially relative to the generally low porosity exhibited by cycle-base mud-rich wackestones and packstones. However, because of the separate-vug fenestral pores, permeability is generally low and L 2.3 rarely contributes to hydrocarbon production in the field. Porosity-based wireline correlations suggest that cycle and facies continuity is high. This is somewhat unexpected considering outcrop observations that suggest that tidal-flat facies are highly discontinuous. The laterally continuous porosity development at these cycle tops probably reflects the effects of early diagenesis associated with sea-level fall and subsequent rise at these surfaces.

## MINERALOGY AND DIAGENESIS

The lower Leonardian section at Fullerton field is similar to most other platform Leonardian successions in the Permian Basin in showing evidence of significant post-depositional diagenesis. Principal products of this diagenesis are matrix-replacive and pore-filling dolomite and anhydrite. However, limestone is locally present in the Leonardian section at Fullerton, including the Abo, the Wichita, and the Lower Clear Fork.

### Dolomite and Limestone Distribution

Dolomite is by far the dominant mineral in the reservoir section. The Abo consists entirely of dolomite except in the most downdip wells. In core from the FM-1 well, perhaps the most downdip well in the field, the Abo contains alternating zones of limestone and dolostone. Dolostone is more commonly associated with mud-rich facies (peloid wackestone and fusulinid wackestone) in the Abo clinoformal succession, whereas limestone intervals are more commonly grain-rich, skeletal facies (fig. 22).

Limestone is locally very abundant in the Wichita, especially in the upper half of the formation (fig. 8). In all cases, calcite-rich rocks in the Wichita are peritidal mudstones or wackestones (the peritidal mudstone-wackestone facies). These calcite-dominated facies characteristically exhibit very low porosity (>2 %) and essentially no permeability. Log correlations suggest that limestone intervals are locally correlative (fig. 8). Although facies stacking patterns do not clearly reveal a systematic relationship between mineralogy and cyclicity, it is probable that these limestones are the result of cycle-punctuated diagenesis. Limestone is virtually absent from the lower Wichita (L1) but very common in the upper part (L2) of the formation (fig. 8). This distribution correlates closely with the position of the interpreted L1 – L2 sequence boundary that subdivides the Wichita (fig. 22); limestone is absent

from the L1 (highstand) Wichita but is locally very abundant in the L2 (transgressive) Wichita. Limestone abundance in the upper (L2) Wichita displays a systematic trend across the field. The highest abundance of limestone is in the northwestern part of the field; essentially no limestone is present in the southern part of the field (fig. 20). Because of the low porosity associated with limestones in the Wichita, porosity logs can be reliably used to define and correlate limestone even where cores, or dual porosity, or PE logs are unavailable.

Lower Clear Fork rocks at Fullerton field also contain locally abundant limestone. Limestone is common in HFS L 2.1 across most of the field (fig. 23). Highest abundance is in the southern part of the field where only mud-rich (typically fusulinid-bearing) facies contain significant dolomite. Essentially all grain-rich facies in this area are dominantly calcitic. In the northern part of the field, limestone is also common in L 2.1 but is complexly distributed among all subtidal facies.

Like HFS 2.1, limestone dominates L 2.2 in the southern part of the field. However, outside of this area, limestone is rare except in one small area in the northwestern part of the field (fig. 25).

Porosity is generally high in limestone-rich intervals in the Lower Clear Fork. However, porosity is also well developed in dolostones, so except where cores, dual-porosity log suites, or PE logs are available, it is not possible to differentiate limestone from dolostone in the Lower Clear Fork.

### Stable Isotope Chemistry

Samples of dolostone and limestone were collected from the Lower Clear Fork Formation in the FM-1 core and analyzed for stable isotopes. For both rock types  $\delta^{13}\text{C}$  data are similar; data average 4.89 ‰ PDB for limestones ( $n = 13$ ) and 5.44 ‰ PDB for dolostone ( $n = 2$ ). Such



heavy carbon isotope values are typical of most Permian Leonardian and Guadalupian carbonates (Ruppel and Cander, 1988a, b; Leary and Vogt, 1990; Saller and Henderson, 1998; Ruppel, 2002).

The  $\delta^{18}\text{O}$  data from limestones average  $-2.67\text{‰}$  PDB ( $n = 13$ , range:  $-1.55$  to  $-3.55\text{‰}$ ). These data are very different from previously reported values for other calcite-bearing samples in the Leonardian and Guadalupian. For example, most  $\delta^{18}\text{O}$  values for Guadalupian calcites have ranged from about  $-7.6$  to  $-10.4$  (Leary, 1985; Vogt, 1986, S. Ruppel, unpublished data from the Grayburg Formation at South Cowden field). These values, however, were recorded from “replacement calcite” interpreted to have precipitated from meteoric water possibly sourced from deep basin fluids. The  $\delta^{13}\text{C}$  values from these “replacement calcites” are also very depleted ( $-19$  to  $-30\text{‰}$  PDB), suggesting precipitation from bacterially mediated sulfate reduction (Leary, 1985; Vogt, 1986; S. Ruppel, unpublished data). The more “normal”  $\delta^{13}\text{C}$  values for the Lower Clear Fork limestones at Fullerton indicate a very different origin for these calcites. It should be noted that these Lower Clear Fork  $\delta^{18}\text{O}$  values are very similar to the current best estimate for marine calcite precipitates from seawater during the middle Permian ( $-2.8\text{‰}$  PDB; Lohman and Walker, 1989). One interpretation of these data is that these Lower Clear Fork limestones contain a preserved record of original seawater chemistry and by extension that these rocks have undergone relatively little chemical alteration.

The  $\delta^{18}\text{O}$  data obtained from Lower Clear Fork dolostones average  $2.30\text{‰}$  ( $n = 2$ ). These data are similar to previous Leonardian data reported by Ye and Mazzullo (1993), Saller and Henderson (1998), and Ruppel (2002) but very different from most data reported for younger Guadalupian rocks. Typical  $\delta^{18}\text{O}$  values for these younger Guadalupian (San Andres and Grayburg Formations) platform dolomites are  $3$  to  $6\text{‰}$  (Vogt, 1986; Ruppel and Cander,

1988a,b; Saller and Henderson, 1998; Ruppel and Bebout, 2001; Ruppel, 2002). The relatively enriched isotopic signatures of these Guadalupian dolomites have invariably been interpreted to have been produced during dolomitization by evaporatively concentrated seawater brines. The significantly depleted values for the Leonardian dolostones at Fullerton and in other Leonardian fields suggest that either (1) dolomitization was caused by brines that were less evaporatively concentrated than those that caused Guadalupian dolomitization, (2) dolomitization was caused by fluids of a mixed water origin, or (3) a combination of cases 1 and 2 above.

## Karst Development

### *Karst Fabrics*

Evidence of karst-related diagenesis and dissolution is common in the lower part of the reservoir section at Fullerton field; karst features occur within the Wichita and at the Wichita/Abo contact. These rocks are variable in fabric but include four basic types: (1) polymict conglomerates, (2) monomict breccias, (3) fractured and tilted beds, and (4) void-filling cement.

The predominant style of polymict conglomerate typically consists of rounded clasts of multiple peritidal lithologies (fig. 31). Clasts range in size from a few millimeters to several centimeters in maximum dimension and are usually subequant and rounded. Clasts are usually enclosed in mudstone or abut one another at stylolitic contacts. Polymict fabrics are most common in the middle of the Wichita (fig. 31). Intervals of polymict conglomerate of at least 25 ft to as much as 60 ft thick are present in the FCU 6122 core. The multiple facies character of these clasts and their rounded character indicate that they were formed by sediment transport. Their discontinuous nature and their association with other features indicative of karst processes suggest they originated as cave-fill deposits.

Although probably not true polymict conglomerates, superficially similar deposits that also indicate karst processes are present at the contact of the Wichita and the Abo in the FM-1 core at the downdip edge of the field area. These rocks are usually characterized by a mixture of two or more facies types including Wichita tidal-flat facies, green silty carbonate, dark-gray silty carbonate, and Abo subtidal facies (figs. 32, 33). Rather than being interbedded with one another the first three appear to surround the Abo facies in many cores (fig. 33). This suggests that these “polymict conglomerates” actually represent dissolution and/or erosion of the top of the Abo and subsequent infilling of the irregular surface or differential compaction of the Abo (L1) and overlying transgressive Wichita sediments (L2) at the Abo/Wichita contact. In rare instances, there are also features suggestive of collapse brecciation. All of these features have been observed in analogous outcrops of the Abo/Wichita contact in Apache Canyon in the Sierra Diablo (Kerans and others, 2000). The outcrop succession reveals that karst features (sinkholes and caves) were formed during the post L1 sea-level fall, then filled with transgressive L2 tidal-flat deposits (i.e., Wichita facies). These tidal-flat facies in some instances were brecciated and intermixed with the underlying Abo as sinkholes and caves collapsed.

Monomict conglomerates or breccias consist of broken and rotated clasts of constant lithology and facies (fig. 34). These rocks are restricted to the Wichita, usually the middle of the section. Commonly associated with these deposits are fractures, sediment infill (cracks and fissures), void-filling cement (chiefly anhydrite), and other evidences of dissolution. Most of these features can also be formed by nonkarst processes in tidal-flat intervals not exposed to true karst (e.g., tepee formation is usually accompanied by broken and rotated blocks, cracks and fissures, and cement and sediment infill). Thus it is possible that some of these deposits may not

be the result of true karst processes. However, their thickness, abundance, and association with other features of karst formation suggest that many are also karst related.

Fractured and tilted beds are also observed in some cores especially in the middle of the Wichita section. Tilted beds have clearly been formed by postdepositional collapse. In the FCU 5927 core, they form part of a succession that very much resembles the classic cave fill–cave roof succession described by Loucks (1999). The succession in the 5927 well consists of 20 ft of polymict cave-fill conglomerate composed of mixed tidal-flat facies overlain by 20 ft of fractured and locally tilted but apparently generally in situ beds of tidal-flat and subtidal facies probably representative of a cave roof.

Large zones of void-filling anhydrite cement are also strong indicators of karst-related dissolution. Zones of massive anhydrite up to 1½ ft thick are present in cores in the Wichita at Fullerton field (e.g., FCU 6122, 5927). Smaller anhydrite-filled voids and fractures are ubiquitous within the Wichita and at the Wichita/Abo contact (e.g., fig. 32) and also point to late cementation of dissolution voids by diagenetic fluids associated with reflux dolomitization of the succession.

### *Causes and Timing of Karst*

Outcrop studies demonstrate that major karsting of the Leonardian sequence occurred at the sea-level fall/rise event that is defined by the L1/L2 sequence boundary (Kerans and others, 2000). In downdip areas of Fullerton field, cores demonstrate this same relationship. Here, the top surface of the Abo outer platform facies succession (L1) is karsted and is infilled and overlain by brecciated Wichita tidal-flat facies (L2). In updip areas, however, establishing a spatial and temporal relationship between karst formation and the L1/L2 sequence boundary is more problematic. Most karst features in the Fullerton field area are found in an interval of about

150 ft in the middle of the Wichita section (fig. 8). In general, this interval correlates approximately to the marine flooding event identified within the Wichita in cores and logs that is thought to represent the L2 transgression (fig. 22). However, karst features are developed both below and above this horizon, indicating that karst-related diagenesis was not limited to the L1 sequence. Instead, it appears that two types of karst-related processes occurred as outlined below.

Primary karsting and dissolution probably occurred during the post-L1 lowstand. At this time, the exposed top L1 surface (consisting of Abo subtidal sediments downdip and lower Wichita tidal-flat sediments updip) developed local caves, sinkholes, and an irregular topography. During the subsequent L2 sea-level rise, transgressive peritidal deposits of the Wichita filled the irregular karsted surface including sinkholes and caves. With continued sedimentation and compaction, parts of the overlying L2 (upper Wichita tidal flat) succession underwent local brecciation and collapse probably due to stress differences set up over underlying karst features. This scenario is consistent with outcrops (Kerans and others, 2000) and fits the distribution of karst features seen at Fullerton field.

### *Impact of Karsting on Reservoir Quality*

Some karst-related deposits most certainly exhibit at least local differences in petrophysical properties (i.e., porosity, permeability, and saturation) from surrounding undisturbed and unaltered deposits. Polymict conglomerates and anhydrite voids are two obvious examples of this. However, two factors make quantification of the importance of these differences difficult. First, most karst deposits do not record significantly different porosity or permeability than surrounding nonkarsted deposits based on both wireline and core data. This is probably due to the fact that most karst fills are composed of the same facies as nonkarsted

intervals. Anhydrite void fills are an obvious exception to this, as they contain no porosity or permeability, but they are generally very small and probably of little impact on reservoir flow.

Second, with the exception of areas in which there are cores, the distribution of karst features in the reservoir section is not definable. Efforts to identify karst fill using logs and 3-D seismic appear to be negated by the similar lithological and petrophysical properties these features share with surrounding rocks. It is tempting to conclude from these observations that karst features have no impact of reservoir heterogeneity or fluid flow. However, there are anomalies in water production and flow rates in the Wichita that cannot be readily explained by matrix petrophysical properties (T. Anthony, personal communication, 2003). These phenomena may be the result of karst development.

## RESERVOIR IMAGING

Accurate definition of reservoir architecture and the distribution of rock fabrics within this architecture is the key to defining improved methods for recovery of hydrocarbons remaining in these systems. We utilized several methods to better image the reservoir at Fullerton field. Especially important in defining the geologic architecture of the reservoir are (1) the calibration and use of borehole image logs to aid in the identification and mapping of facies, cyclicity, and rock fabrics, and (2) the use of 3-D seismic data to constrain the geologic framework.

### Identifying Facies and Cyclicity from Borehole Image Logs

Image logs are highly underutilized in the characterization of carbonate reservoirs. To most, the principal use of such logs is in the identification of fractures. However, image logs also have the potential to accurately image many matrix properties that are key to the proper characterization, modeling, and exploitation of carbonate reservoirs.

Traditionally, cores have been obtained to provide the key data needed for constraining the distribution of reservoir facies, cyclicity, and rock fabrics. However, because of cost, the number of cores typically obtained is generally far smaller than needed to accurately constrain these aspects. If properly calibrated with core observations, borehole image logs can provide most of the required data to construct an accurate reservoir model at a fraction of the cost.

To test this premise and to add to the core database, a borehole image log was obtained in a new well drilled in the field at the beginning of the study. This well (FCU 2564, fig. 3) was drilled in an area where no cores exist. Accordingly, the development of a robust methodology for deriving key geological information from this well such as facies, rock fabric, and cyclicity from this image log has tremendous potential value for efforts to construct a more accurate image of the reservoir architecture.

A critical first step in utilizing image logs for geological analysis is the calibration of the images to known geological features. This is best done with a core taken from the well in which the image log is recovered. However, when a companion core is not available, as was the case with this image log, a satisfactory calibration can often be established by examination and correlation of nearby cores.

It is important to keep in mind that resistivity image logs, like the FMI log, display differences in resistivity. Thus, only those sedimentary features that are associated with resistivity contrasts can effectively be imaged. High-resistivity features are usually those that have very low porosity. In most color scales used on such image logs, the highest resistivity (lowest porosity) features are shown in white). In these rocks, white usually indicates anhydrite. At the other end of the color scale, black indicates lowest resistivity and usually higher porosity.

However, dark colors can also indicate low resistivity associated with clay-rich sediments (e.g., shales).

Examination, correlation, and comparison of the FCU 2664 image log with nearby cores show that seven facies can reliably be identified from the image log. This is fewer than the 12 defined from core studies but is sufficient to provide necessary information to define major facies successions and cyclicity and to provide a strong basis for accurate correlation and interpretation of facies and cyclicity to nearby wells. Facies recognizable on the image log include (1) tidal-flat facies, (2) peloid wackestone-packstone, (3) nodular wackestone-packstone, (4) cross-bedded grainstone, (5) fusulinid wackestone-packstone, (6) karst breccia, and (7) clay-rich mudstone. Additionally, siltstone-sandstone facies can be identified from many wireline logs.

Tidal-flat facies are characterized on image logs principally by their closely spaced parallel and horizontal laminations (fig. 35). The common presence of fenestral pores and small burrows in tidal-flat facies is typically shown on image logs by abundant small black (low resistivity indicating fluid-containing open pores) spots. Tepee structures and sheet cracks are also well imaged where present. The identification of tidal-flat facies is crucial for defining both reservoir architecture and reservoir quality. Because they generally occupy cycle tops their definition makes it possible to define cycle boundaries and thereby facilitates cycle-scale correlation. Equally important is the identification of tidal-flat facies and their petrophysical significance. As discussed previously, tidal-flat facies commonly display relatively high porosities but low permeability. Because of this, it is critical for accurate reservoir-quality mapping to distinguish tidal-flat rocks from subtidal rocks that are typically higher in permeability.



Fusulinid wackestones (fig. 36) are identified on image logs by the presence of small black patches that are in some cases similar to those representing fenestral pores in tidal-flat facies. However, fusulinid pores are typically larger and more irregular in shape. Fusulinid facies can also be distinguished from tidal-flat facies by the general lack of closely spaced laminations. Fusulinid-bearing rocks generally represent the deepest water facies in the Leonardian succession and typically are found at cycle bases. They are thus important indicators of sea-level rise and guides to cycle definition and correlation.

Although generally rare in the Leonardian, cross-bedded grainstones are well imaged on image logs because of their dipping laminations (fig. 37). These rocks also indicate cycle tops and thus are guidelines to cycle definition and correlation. Additionally, where porous, these grainstones can contain very high permeability.

Other subtidal rocks are typically difficult to subdivide using image logs. Peloid-skeletal wackestones and packstones commonly all display a grainy texture, probably caused by their small pore size, and intercrystalline porosity (fig. 38). Burrowing of these rocks is ubiquitous, however, and image logs can readily reveal where this burrowing has caused changes in porosity or promoted differential diagenesis. Nodular wackestones, for example, contain abundant anhydrite nodules that were precipitated in the enhanced permeability pathways created by burrowing organisms (fig. 39). The anhydrite that fills these burrows is easily imaged on the image log as whitish subspherical patches (fig. 39b). Commonly, burrow margins still preserve some of the porosity enhancement caused by the burrowing. These high-porosity margins are expressed on the image logs as black rims around the nodules (fig. 39b). Where anhydrite has not filled the burrows, the result is patches of high porosity (fig. 40a). These are displayed on the

## RESERVOIR ARCHITECTURE

A critical component of a robust reservoir model is a geologically constrained reservoir framework. Geologically accurate models must be based on correlations of time stratigraphic units, the most readily correlative of which are cycle and sequence boundaries. At Fullerton field, we utilized correlations of cycle tops to construct the reservoir model for the Clear Fork. Although these correlations are ultimately based on correlations of wireline logs (porosity and gamma ray), the underlying basis for the interpretation and correlation of these logs is a knowledge of 1D and 2D facies and cycle-stacking relationships developed from integrated studies of cores and outcrops.

### Cyclicity and Flow-Unit Definition

Reservoir flow units are most appropriately based on the definition and mapping of depositional cycle boundaries. This is because, when properly defined and correlated, depositional cycles represent the best available indicator of original depositional surfaces or time lines. The procedure for identifying utilizing cycle boundaries for flow unit definition has been well described by Ruppel and Ariza (2002) and Lucia and Jennings (2002) for the South Wason Clear Fork reservoir.

Ideally, the correlation of depositional cycle tops should be based on a log that can be directly tied to facies and one that is independent of diagenesis or porosity development. The gamma-ray log in certain ideal settings serves this function. However, throughout most of the Leonardian carbonate succession (in fact, throughout most of the Permian carbonate section in the Permian Basin) the gamma-ray log is not accurate for detailed correlation because of variable volumes of uranium, potassium, and thorium. The spectral gamma-ray log can help to distinguish variations in these elements and thus is useful in separating clastic-rich sections (that contain

through this interval is potentially better than that attainable from cores (because of uncertainties of core/well depth ties). Cycles defined from these facies successions range in thickness from 3 to 20 ft. Highest facies and cycle resolution was obtained in intervals characterized by alternating subtidal and tidal-flat facies in the Lower Clear Fork because of the marked contrast in image log character of these two facies types.

Particularly noteworthy observations from the image log in FCU 2564 is the clear indication that this well occupies a significantly different depositional setting than the nearest cored wells to the east. The greater thickness of relatively deep water fusulinid wackestone-packstone facies in L 2.1 here strongly suggests that accommodation increases to the west. This is counter to the regional trend in depositional dip and paleogeography and would not be recognized without this image (or a continuous core). This finding has potential petrophysical significance for the western part of the field by suggesting that deeper water facies of more favorable petrophysical character may be more prevalent in this area than would otherwise be expected. Thus, because of the ability to image key facies and thus facilitate the definition of cycles, sequences, and rock fabrics, the image log adds critical data that are extremely pertinent to the accurate modeling of reservoir architecture and permeability across the field.

### Imaging Stratigraphic Architecture and Reservoir Development from 3-D Seismic

Like image logs, 3-D seismic data are remarkably underutilized in the characterization of carbonate reservoirs. A critical need in developing approaches that lead to improving recovery from reservoirs containing significant volumes of remaining hydrocarbons is a better understanding of the 3-D distribution of reservoir attributes. The approaches outlined in this report for assembling and interpreting well data are the most critical part of this effort. However, because they are limited to well control, they leave important gaps in our understanding. Three-

dimensional seismic data offer valuable data on interwell and extrawell areas (meaning areas of the field where usable well data are absent) and when properly interpreted and applied can greatly improve and thus constrain reservoir attribute models. Here we provide some brief insights into how 3-D data can be used to better image both reservoir framework and porosity distribution. A far more detailed and rigorous application of these 3-D data to the construction of the geological model at Fullerton is described by Zeng (this report).

### *Constraining Reservoir Architecture*

Two- and three-dimensional data at Fullerton field provide important guides to the stratal architecture of the reservoir succession. Seismic amplitude sections through the entire reservoir interval reveal that much of the section is characterized by generally parallel seismic reflectors (fig. 42). This is not unexpected considering the shallow-water-platform depositional setting indicated by the cores and the apparently subhorizontal correlations suggested by wireline logs. However, 3-D and some 2D data suggest a very different architecture for the basal Leonardian, Abo Formation. Seismic data reveal sets of clinoformal reflectors in the Abo that dip generally basinward (toward the east). This apparent clinoformal architecture of the Abo is consistent with observations of clinoformal fusulinid wackestones and packstones in outcropping Abo-equivalent sections in the Sierra Diablo. These clinoforms demonstrate that conventional horizontal correlations of wireline log data are inappropriate for the Abo. In most cases, it is not possible to resolve cycle-scale correlations of either facies or time surfaces in such settings.

### *Defining Reservoir Quality*

Seismic data can also be robust indicators of porosity distribution in carbonate reservoirs. Zeng (this report) demonstrates the strong agreement between 3-D seismic impedance data and reservoir porosity at Fullerton field. Because of this robust relationship, even simple amplitude

because these Leonardian rocks rarely contain cycle-base flow barriers and flow probably does locally cross cycle boundaries. In any case, the porosity log correlation method, if properly constrained by core and outcrop calibration of facies, porosity, and cyclicity, is the most geologically sound basis for constructing cycle correlations and establishing the basis for true flow-unit correlations.

It is also important, however, to correlate geologically defined cycle tops at the highest resolution possible. For example, outcrop studies demonstrate that cycles less than 10 ft thick can be correlatable over large areas of the platform. Where wireline data permit, an effort should be made to correlate these thin cycles through the reservoir as well, even if later upscaling is planned for reservoir modeling. This is important for two reasons. First, coarser scale correlations are much more likely to be in error. At Fullerton, we found that early correlations made at the sequence or cycle set scale were later proven to be off by a cycle or two after we recorrelated the succession at the cycle scale. From a reservoir modeling point of view, this means that flow units defined by coarse scale correlations are more likely to cross-connect flow layers than those defined by finer scale correlations. Second, upscaling (grouping of cycles into thicker flow-unit packages for modeling) is more likely to retain the original geological architecture if based on fine-scale (i.e., cycle scale) correlations. Accordingly, we attempted to correlate the reservoir succession at the highest possible level of detail supported by outcrop and core observations and wireline resolution.

### *Lower Clear Fork Reservoir Architecture*

The robustness of the use of porosity logs for defining facies and cyclicity is apparent from core and log relationships in HFS L 2.3. A comparison of core data and porosity logs in the FCU 6122 well (fig. 45) shows that porosity is nearly entirely associated with cycle-top tidal-flat

facies. Thus, porosity logs can be used to define both facies and cyclicity. Other cored wells in the field exhibit the same core/log relationship. Although not an oil-producing part of the reservoir, the L 2.3 section demonstrates the log/porosity calibration that underlies all cycle-based correlation in the field. The cycles apparent from the porosity log response, which average about 10 ft in thickness, are relatively easily correlated across of the field.

The same approach is applicable to the subtidal sections in the Lower Clear Fork. However, in these cases, cycle tops are typically composed of grain-rich subtidal facies. Here too, however, there is a strong relationship in cored wells between cycle-top facies and porosity (fig. 46).

Using this approach at Fullerton, we defined and correlated 15 cycles in the Lower Clear Fork (fig. 4). The average thickness of these cycles is about 17 ft for the entire interval of L 2.1 and L 2.2. However, cycle thickness varies systematically by sequence within this interval. HFS L 2.2 cycles average about 11 ft in thickness, whereas L 2.1 cycles, with the exception of low-accommodation tidal-flat cycles at the base and top of the sequence, are nearly twice as thick (fig. 8). This is probably due to two factors. First, L 2.1 deposits record the maximum flooding of the platform and probably the development of maximum accommodation. The overall upward thinning of cycles from L2.1 to L 2.2 is consistent with an overall upward decrease in accommodation. Second, lateral changes in facies stacking in L 2.1 cycles suggest local variations in sediment accumulation patterns that may have been caused by topographic relief on the platform during L 2.1 flooding. The resultant complex vertical and lateral facies distribution patterns make accurate definition of cycles difficult. As a result, cycles defined for L 2.1 may actually reflect combinations of cycles or cycle sets.

## *Wichita Reservoir Architecture*

Rigorous cycle definition is not possible for the Wichita because of the preponderance of very low accommodation, tidal-flat facies. Both core and outcrop studies show that rocks deposited in such settings rarely display systematic trends in vertical facies stacking and generally exhibit very low lateral facies continuity. Accordingly, patterns of depositional facies do not define extrinsic controls (e.g., sea-level rise and fall) but rather local controls on sediment accumulation (e.g., paleotopography and climate). Thus for the Wichita, it is necessary to use diagenetic features to develop a reservoir framework.

Key diagenetic features used to define Wichita "cycles" are mineralogy and porosity. In the northern part of the field, the upper Wichita contains multiple intervals of low-porosity limestone (figs. 8, 20). Because these intervals are generally parallel to overlying and underlying cycle and sequence boundaries and because they are relatively continuous (fig. 8), we suspect that their formation was related to cycle deposition, exposure, and diagenesis. For example, early dolomitization of peritidal cycle tops has been widely documented in low-accommodation carbonate platform successions of all ages. By analogy, these limestone beds probably represent undolomitized cycle bases, whereas the intervening dolostone beds define cycle tops. As such, the architecture of these diagenetic "cycles" is closely tied to depositional surfaces and thus represents a good approximation of time surfaces. These surfaces are also especially useful from a reservoir point of view because they define layers of low and high porosity and permeability. The top four "cycles" in the Wichita are defined on the basis of these cyclic dolostone (high porosity) - limestone (low porosity) couplets (fig. 4).

However, no limestone is present in the upper Wichita in the southern part of the field area (fig. 20) nor in the lower part of the Wichita in any part of the field (fig. 8). In these areas, it is necessary to use porosity alone to construct the reservoir framework. Although it still likely

that porosity variations in these areas are closely tied to diagenesis associated with depositional surfaces (i.e., cycle tops), we have little independent evidence (i.e., mineralogical variations) with which to demonstrate this. Accordingly, the framework established for these parts of the Wichita is far less geologically robust than that defined for other parts of the reservoir. For this part of the reservoir we defined and correlated 12 surfaces on the basis of porosity. We have confidence that these surfaces are subparallel to time surfaces on the basis of their parallelism to overlying Lower Clear Fork cycle-top surfaces and to the middle Wichita marine floodback that marks the L1–L2 boundary. However, we cannot tie them rigorously to cyclicity.

### *Abo Reservoir Architecture*

The Abo is dominated by clinoformal bedding typical of outer ramp carbonate deposits; this is demonstrated both by outcrop studies (Kerans and others, 2000) and by 3-D seismic data at Fullerton (fig. 42). It is therefore certain that the Abo architecture differs significantly from the generally subparallel character of the depositional surfaces of the platform-top Wichita and Lower Clear Fork successions. Outcrop studies and seismic studies at Fullerton and elsewhere (Kerans others, 2000; Ruppel and others, 2000) also demonstrate that clinoformal outer platform successions like the Abo do not contain readily correlatable cyclic successions. This is due to changes in sources and distributional patterns and to extreme variations in lateral textures and fabrics of these transported sediments. Accordingly, it is not possible to establish an accurate internal architecture for these deposits. For purposes of reservoir modeling, we have created a series of conceptual clinoform surfaces to constrain the reservoir architecture. Although these surfaces do not accurately describe the architecture of the Abo, they do illustrate the nonparallel and nonhorizontal nature of these deposits.



## *Reservoir Model*

The architecture of the reservoir framework developed for the Clear Fork reservoir at Fullerton is depicted by Figure 47. Key aspects of this model are (1) the subhorizontal and subparallel nature of Clear Fork and upper Wichita (L 2) surfaces, (2) the effective pinch-out of lower Wichita (proximal L 1) surfaces at the facies change from Wichita tidal flats to Abo subtidal, and (3) the clinoformal nature of Abo (distal L 1).

## **Porosity Distribution**

Core and log data from wells that penetrate the Abo indicate that the Abo locally contains high porosity. However, well control is too sparse and incomplete to accurately map porosity distribution. Wang (this report) presents an estimation of the 3-D distribution of Abo porosity using a full field based on available porosity data and a conceptual geological framework. However, the accuracy of this distribution must be considered relatively low.

The Wichita Formation contains higher  $\phi_{\text{ih}}$  than either the Abo or the Lower Clear Fork (fig. 48). This total  $\phi_{\text{ih}}$  map reveals that highest  $\phi_{\text{ih}}$  lies along the field structural crest (compare figs. 48 and 5), suggesting that porosity development may have been a function of structure. However, when  $\phi_{\text{ih}}$  is examined by stratigraphic horizon this interpretation seems less obvious. The key element of porosity distribution in the lower parts of the Wichita is the marked decrease in  $\phi_{\text{ih}}$  to the southeast due to the southeastward facies transition from Wichita tidal flat to Abo subtidal facies (and accompanying decrease of Wichita thickness) along the margin of the inner platform (fig. 49). Lower Wichita porosity distribution in the interior platform of these L 1 Wichita tidal-flat deposits shows no obvious trend, although localized areas of high porosity are apparent in both intervals.

The lower part of the upper Wichita (Fig. 50), which represents the base of the L 2 composite sequence and the beginning of L2 transgression (HFS L 2.0), displays a very well defined, arcuate trend of porosity that generally parallels the underlying L 1 Wichita/Abo facies transition (fig. 49). Note that both the wireline log data (fig. 50b) and the 3-D seismic amplitude extraction data (fig. 50c) image this trend well. The transition from L 2.0 upper Wichita rocks to L2.0 Lower Clear Fork rocks is located just eastward of this belt of porosity. The decrease in porosity southeastward from this belt is thus associated with a change from tidal-flat rocks to subtidal-flat rocks, presumably the result of topographic dip and changes in bathymetry and accommodation downdip on the lower Wichita-Abo platform. The decrease in porosity to the northwest, however, is not associated with any apparent change in depositional facies. Wichita rocks in the northern part of the field are depositionally similar facies. Accordingly, the cause of porosity development must be more a function of diagenesis than deposition. A model for this diagenesis is presented in the following section.

The uppermost Wichita also displays strong differential development of porosity across the field area that does not appear to be related to depositional facies. Areas of highest porosity are located in the northern and southern parts of the field. Low porosity is encountered in the center and northwest parts of the area (fig. 50a). Like the lower Wichita, there are no apparent systematic differences between the tidal-flat deposits across the field. Thus, these variations must be the result of differential diagenesis. Porosity patterns suggest that upper Wichita porosity may exhibit a similar, albeit westwardly displaced, arcuate trend much like that in the lower Wichita. The high-porosity area in the north extends southwestward and may continue west of the field to link up with the porosity in the southern end of the field. If so, this would imply a link between reservoir development and platform geometry similar to that suggested for the lower Wichita.

The more westward development of this porosity trend is consistent with progressive transgression of the L2 platform and backstepping of the Wichita tidal-flat systems tract.

Limestone is common in the upper Wichita tidal-flat succession throughout the northern part of the field but is not related to areal trends in porosity. It does, however, affect fluid flow through this part of the reservoir.

The Lower Clear Fork HFS L 2.1 displays an arcuate trend in porosity development that is very similar to that seen in the upper Wichita (fig. 51b, c). Like the uppermost Wichita (fig. 50a), there is a strong suggestion that the northern trend may extend west of the field and curve south to link up with the southern areas of porosity as does the lower upper Wichita (fig. 50b). As is the case with the Wichita porosity development, depositional facies do not appear to be the dominant controlling factor in the development of this trend. The eastward decrease in porosity (in the southern part of the field) is associated with a gradual change from middle ramp grain-rich packstones to outer ramp fusulinid-rich wackestones. The area of high porosity may represent a low-energy ramp crest because the abundance of ooid-skeletal grain-dominated packstones and grainstones is somewhat greater. But the change in depositional facies associated with the major decrease in porosity into the northwestern part of the field appears subtle (fig. 51b). Instead, it is apparent that, like the Wichita, high porosity in L 2.1 is dominantly the result of diagenetic patterns. There is almost a 1:1 relationship between the presence of limestone and high-porosity areas (compare figs. 23 and 51b). Areas of high porosity in the northern part of the field contain mixtures of porous dolostones and porous limestone; the high-porosity area at the south end of the field is nearly all limestone.

No obvious trend in porosity is apparent in HFS L 2.2 (fig. 51a). However, like L2.1, the areas of highest porosity are associated with limestone. For L2.2 this is dominantly in the

southern end of the field; however, a small area of limestone also exists in the northwest corner of the field (compare figs. 25 and 51a).

### *Models for Porosity Development*

As we have discussed, porosity is developed in all parts of the Abo–Wichita– Lower Clear Fork reservoir section. However, there are obvious areal variations in porosity that reflect a combination of depositional, diagenetic, and structural controls on reservoir development. Most of the major reservoir intervals exhibit spatial variations in porosity development that parallel platform paleotopography. This is particularly apparent in the lower and upper parts of the upper (L2) Wichita and in the Lower Clear Fork (HFS 2.1) (fig. 20E). In each of these cases, trends of high porosity are situated immediately up depositional dip from the position of the underlying Wichita-Abo facies boundary. However, the mechanism for porosity development must differ between the Wichita (fig. 20Ea,b) and the Lower Clear Fork (fig. 20Ec).

In the case of both Wichita intervals, depositional facies in the high-porosity trend are essentially identical to those in low-porosity areas both updip and downdip depositionally (fig. 20Ea, b). This indicates that porosity formation is the result of local diagenetic processes. Stable isotope data reported for the Fullerton field reservoir by Kaufman (1991) are consistent with those reported herein and suggest that high-porosity dolomites in the Wichita were formed by seawater-dominated fluids perhaps mediated by meteoric mixing. This is indicated by light  $\delta^{18}\text{O}$  values (average: 0.1 ‰ ;  $\delta^{13}\text{C} = 2.6$  ‰ PDB). The restriction of high-porosity rocks to the downdip margin of the Wichita tidal flat suggests the possibility that porosity development may be the result of early seawater-dominated dolomitization and stabilization along the seaward margin of the Wichita tidal flat. Available data suggest that less porous, updip Wichita tidal-flat deposits were dolomitized during a later event by very different fluids. These rocks contain

heavier isotopes ( $\delta^{18}\text{O} = 2.7 \text{ ‰}$ ;  $\delta^{13}\text{C} = 3.0 \text{ ‰}$  PDB) that are typical of younger, Lower and Upper Clear Fork rocks and are more indicative of brines that were evaporatively concentrated (Saller and Henderson, 1998; Ruppel, 2002). Possible sources for such brines based on stratigraphic data are updip tidal flats at the top of HFS 2.1, 2.2, and 2.3 or those developed during Tubb deposition. The presence of limestone interbeds in the Wichita in the northern, less porous part of the field suggests such a distal diagenetic setting (i.e., one that is distal to the source of diagenetic fluids). The lack of porosity in the updip Wichita tidal flats may reflect compaction as well as porosity reduction caused by dolomitization and sulfate emplacement during Clear Fork/Tubb reflux dolomitization.

The Lower Clear Fork HFS 2.1 also displays a trend in porosity development that closely parallels the Wichita-Abo facies transition as well as the Wichita–Clear Fork facies transition (fig. 20Ec). In this case, however, there is a relationship between both facies and mineralogy and porosity development. Facies data suggest that the trend of high porosity may represent a platform ramp crest: an area characterized by more common ooid-bearing, grain-rich packstones and grainstones and by locally more abundant tidal-flat caps. Ramp-crest development was probably controlled by inherited paleotopography over the L1 (Wichita-Abo) inner ramp margin and/or differential subsidence over deep-seated faults in the same way that the position of the Wichita-Abo facies transition is most likely controlled by such deep structures. Mineralogical data show that this trend is also an area of abundant calcite; lower porosity areas to the east and west are nearly entirely dolomite (see fig. 23). Strontium and oxygen isotope data from these calcites indicate that they are essentially unaltered original marine precipitates. Updip dolomites display values that indicate that they were formed from evaporatively concentrated brines after deposition. These data together suggest the HFS L2.1 porosity trend may have been formed by

early marine calcite cementation in well-agitated and -oxygenated conditions along the ramp crest. Lower porosity in updip dolomites is probably the result of predolomitization compaction and possibly by porosity occlusion by dolomite and anhydrite cementation. Both compaction and dolomitization, and thus porosity loss, were probably limited in the ramp crest because of the early calcite cementation and stabilization that took place there.

## SUMMARY

Both the procedure used to develop the reservoir framework at Fullerton field and many of the attributes of this framework offer important guidelines for the characterization of Clear Fork reservoirs and for the development of predictive models of the distribution of reservoir properties. Key findings from this study include the following.

The Leonardian reservoir succession in the Permian Basin consists of three formations or facies successions: Abo, Wichita, and Lower Clear Fork. Each of these is characterized by distinctive facies, cyclicity, depositional architecture, and porosity development.

The Abo consists largely of porous outer ramp, open-marine, fusulinid/crinoid facies whose clinoformal architecture is clearly expressed on seismic. Lateral facies continuity is poor. As a result, porosity distribution is complex and probably highly discontinuous.

The Wichita, which includes both highstand systems tract updip equivalents of the Abo (Leonardian sequence L1) and transgressive systems tract updip equivalents of the basal Lower Clear Fork (Leonardian sequence L2), consists of a thick succession of aggradational, restricted tidal-flat facies. These rocks contain high porosity but usually relatively low permeability and display poor small-scale continuity. Cyclicity is poorly developed; reservoir architecture is more controlled by diagenesis than by depositional facies. Limestone intervals in the dominantly

dolomitic Wichita display extremely low porosity and permeability and act as local fluid-flow baffles between the higher porosity intervals of dolostone.

The Lower Clear Fork consists of a succession of three high-frequency sequences (HFS), each of which records sea-level rise (transgression) and fall (regression). Reservoir development is largely restricted to subtidal facies (late transgression and early highstand). Highest porosity and permeability in the Lower Clear Fork is associated with incompletely dolomitized grain-rich packstones and grainstones. Cyclicity is well developed. However, facies are discontinuous at the cycle scale.

Karst features (including inclined beds and monomict and polymict cave-fill breccias) are common in the Wichita. Neither wireline log data nor core analysis data reveal any definitive differences between karsted and unkarsted sections of Wichita. Nevertheless, these karst zones, which are only definable on image logs and cores, may locally affect fluid flow.

Gamma-ray logs are useful for general correlations only. As in other Leonardian reservoirs, high gamma-ray response is usually an indication of the presence of clays and silt in tidal-flat facies; low gamma-ray response indicates subtidal facies. Porosity logs or image logs must be used for high-resolution, cycle-scale correlation. Three-dimensional seismic provides excellent resolution of both the reservoir architecture and the distribution of reservoir porosity at the HFS scale.

Porosity development is largely a function of early diagenesis controlled by platform-margin geometry. Zones of highest porosity in the Wichita are the result of early dolomitization and stabilization along the outer margin of the Wichita inner platform. A similar subparallel zone in the Lower Clear Fork was created by early calcite cementation and mineralogical stabilization in the platform ramp crest.

## ACKNOWLEDGMENTS

The results presented in this paper are part of continuing research into the styles and causes of heterogeneity in shallow-water platform carbonate reservoirs in the Permian Basin by the Bureau of Economic Geology. Frequent, sometimes vigorous, discussions with colleagues at the Bureau, including Charlie Kerans, Robert Loucks, Jerry Lucia, and Jim Jennings, have been especially helpful in formulating the interpretations presented herein. Funding for the study was provided by contract no. DE-FC26-01BC15351 from the U. S. Department of Energy. Additional funding was provided by member sponsors of the Bureau's Carbonate Reservoir Characterization Research Laboratory, including Anadarko, Aramco, BP, ChevronTexaco, ExxonMobil, Great Western Drilling, Kinder Morgan, Marathon, Occidental Petroleum, Petroleum Development Oman, Shell International, Statoil, and TotalFinaElf. Additional funding for the study was provided by ExxonMobil and The University of Texas System. Special thanks are extended to David Smith, Terry Anthony, Steve Krohn, and Amy Powell of ExxonMobil and Jeff Simmons, Craig Kemp, and John Stout of Oxy for their contributions to organizing the project and providing data. David Smith and Terry Anthony have been especially helpful in providing insights into the field geology and engineering issues. We also express our appreciation to Stephen Hartman and Tim Hunt of The University of Texas System West Texas Operations Office for providing both collaborative funding and data.



## REFERENCES

- Atchley, S. C., Kozar, M. G., and Yose, L. A., 1999, A predictive model for reservoir characterization in the Permian (Leonardian) Clear Fork and Glorieta Formations, Robertson field area, West Texas: American Association of Petroleum Geologists Bulletin, v. 83, p. 1031–1056.
- Bebout, D. G., and others, 1987, Characterization of the Grayburg reservoir, University Lands Dune field, Crane County, Texas: The University of Texas at Austin, Bureau of Economic Geology Report of Investigations No. 168, 98 p.
- Dutton, S. P., Kim, E. M., Broadhead, R. F., Breton, C. L., Raatz, W. D., Ruppel, S. C., and Kerans, C., 2004, Play analysis and digital portfolio of major oil reservoirs in the Permian Basin: application and transfer of advanced geological and engineering technologies for incremental production opportunities: The University of Texas at Austin, Bureau of Economic Geology, Final report to the Department of Energy, contract DE-FC26-02NT15131, 408 p.
- Fitchen, W. M., Starcher, M. A., Buffler, R. T., and Wilde, G. L., 1995, Sequence stratigraphic framework and facies models of the early Permian platform margins, Sierra Diablo, West Texas, *in* Garber, R. A., and Lindsay, R. F., eds., Wolfcampian-Leonardian shelf margin facies of the Sierra Diablo - seismic scale models for subsurface exploration: West Texas Geological Society Publication 95-97, p. 23–66.
- Garber, R. A., and Harris, P. M., 1990, Depositional facies of the Grayburg/San Andres dolomite reservoirs; Central Basin Platform, Permian Basin, *in* Bebout, D. G., and Harris, P. M. (eds.), Geologic and engineering approaches in evaluation of San Andres/Grayburg hydrocarbon reservoirs - Permian Basin: The University of Texas at Austin, Bureau of Economic Geology, p. 1–20.
- Hardie, L. A., and Garrett, P., 1977, General environmental setting, *in* Hardie, L. A., ed., Sedimentation on the modern carbonate tidal flats of the northwest Andros Island, Bahamas: The Johns Hopkins University Press, Baltimore and London, p. 12–50.
- Holtz, M. H., and Garrett, C. M., 1990, Geologic and engineering characterization of Leonardian carbonate oil reservoirs: a framework for strategic recovery practices in four oil plays (abs.), *in* Flis, J. E., and Price, R. C., eds., Permian Basin oil and gas fields: innovative ideas in exploration and development: West Texas Geological Society Publication No. 90-87, p. 76.
- Holtz, M. H., Ruppel, S. C., and Hocott, C. R., 1992, Integrated geologic and engineering determination of oil-reserve-growth potential in carbonate reservoirs: Journal of Petroleum Technology, November, p. 1250–1258.
- Jones, R., and Ruppel, S., 2004, Evidence of post-Wolfcampian fault movement and its impact on Clear Fork reservoir quality: Fullerton field, West Texas, *in* Trentham, R. C., Banking

- on the Permian Basin: plays, field studies, and techniques: West Texas Geological Society Fall Symposium: West Texas Geological Society Publication #04-112, p.207.
- Kaufman, J., 1991, A predictive model for early dolomitization in the Permian Basin: Exxon Production Research Unpublished report EPR.6X.91, 31 p.
- Kerans, Charles, Kempter, K., Rush, J., and Fisher, W. L., 2000, Facies and stratigraphic controls on a coastal paleokarst: Lower Permian, Apache Canyon, West Texas, *in* Lindsay, R., Trentham, R., Ward, R. F., and Smith, A. H. (eds.), Classic Permian geology of West Texas and Southeastern New Mexico, 75 Years of Permian Basin oil & gas exploration & development: West Texas Geological Society Publication 00-108, p. 55–82.
- Kerans, Charles, Lucia, F. J., and Senger, R. K., 1994, Integrated characterization of carbonate ramp reservoirs using Permian San Andres Formation outcrop analogs: American Association of Petroleum Geologists Bulletin, v. 78, no. 2, p. 181–216.
- Kerans, Charles, and Fitchen, W. M., 1995, Sequence hierarchy and facies architecture of a carbonate ramp system: San Andres Formation of Algerita Escarpment and Western Guadalupe Mountains, West Texas and New Mexico: The University of Texas at Austin, Bureau of Economic Geology Report of Investigations No. 235, 86 p.
- Kerans, Charles, and Ruppel, S. C., 1994, San Andres sequence framework, Guadalupe Mountains: implications for San Andres type section and subsurface reservoirs, *in* Garber, R. A., and Keller, D. R., eds., Field guide to the Paleozoic section of the San Andres Mountains: Permian Basin Section - SEPM, Publication No. 94-35, p. 105–115.
- Kerans, Charles, and Kempter, Kirt, 2002, Hierarchical stratigraphic analysis of a carbonate platform, Permian of the Guadalupe Mountains: The University of Texas at Austin, Bureau of Economic Geology (American Association of Petroleum Geologists/Datapages Discovery Series No. 5), CD-ROM.
- King, P. B., 1942, Permian of West Texas and southeastern New Mexico: American Association of Petroleum Geologists Bulletin v. 26, no. 4, p. 535–763.
- King, P. B., 1965, Geology of the Sierra Diablo region, Texas: U.S. Geological Survey Professional Paper 480, 185 p.
- Leary, D. A., 1985, Diagenesis of the Permian (Guadalupian) San Andres and Grayburg Formations, Central Basin Platform, Permian Basin, West Texas: unpublished Master's thesis, The University of Texas at Austin, 125 p.
- Leary, D. A., and Vogt, J. N., 1990, Diagenesis of the San Andres Formation (Guadalupian) reservoirs, University Lands, Central Basin Platform, *in* Bebout, D. G., and Harris, P. M., eds., Geologic and engineering approaches in evaluation of San Andres/Grayburg hydrocarbon reservoirs - Permian Basin: The University of Texas at Austin, Bureau of Economic Geology, p. 21–28.

- Loucks, R. G., 1999, Paleocave carbonate reservoirs: origins, burial-depth modifications, spatial complexity, and reservoir implications: American Association of Petroleum Geologists Bulletin, v. 83, p. 1795–1834.
- Lohman, K. C., and Walker, J. C. G., 1989, The  $\delta^{18}\text{O}$  record of Phanerozoic abiotic cements: Geophysical Research Letters v. 16, p. 319–322.
- Longacre, S. A. , 1990, The Grayburg reservoir, North McElroy Unit, Crane County, Texas, *in* Bebout, D. G., and Harris, P. M. (eds.), Geologic and engineering approaches in evaluation of San Andres/Grayburg hydrocarbon Reservoirs - Permian Basin: The University of Texas at Austin, Bureau of Economic Geology, p. 239–273.
- Lucia, F. J. and Jennings, J. W., Jr., 2002, Calculation and distribution of petrophysical properties in the south Wasson Clear Fork field, in Lucia, F. J. (editor), Integrated outcrop and subsurface studies of the interwell environment of carbonate reservoirs: Clear Fork (Leonardian-age) reservoirs, West Texas and New Mexico: Final technical report to the Department of Energy, Contract No. DE-AC26-98BC15105, p. 95-142.
- Major, R. P., Vander Stoep, G. W., and Holtz, M. H., 1990, Delineation of unrecovered mobile oil in a mature dolomite reservoir: East Penwell San Andres Unit, University Lands, West Texas: The University of Texas at Austin, Bureau of Economic Geology Report of Investigations No. 194, 52 p.
- Mazzullo, S. J., 1982, Stratigraphy and depositional mosaics of lower Clear Fork and Wichita groups (Permian), northern Midland Basin, Texas: American Association of Petroleum Geologists Bulletin, v. 66, p. 210–227.
- Mazzullo, S. J., and Reid, A., 1989, Lower Permian platform and basin depositional systems, northern Midland Basin, Texas, *in* Crevello, P. D., Wilson, J. J., Sarg, J. F., and Read, J. F., eds., Controls on carbonate platform and basin development: Society of Economic Paleontologists and Mineralogists Special Publication, v. 44, p. 305–320.
- Presley, M. W., 1987, Evolution of Permian evaporite basin in Texas Panhandle: American Association of Petroleum Geologists Bulletin, v. 71, p. 167–190.
- Presley, M. W., and McGillis, K. A., 1982, Coastal evaporite and tidal-flat sediments of the upper Clear Fork and Glorieta Formations, Texas Panhandle: The University of Texas at Austin, Bureau of Economic Geology Report of Investigations No. 115, 50 p.
- Ruppel, S. C., Kerans, Charles, Major, R. P., and Holtz, M. H., 1994, Controls on reservoir heterogeneity in Permian shallow-water platform carbonate reservoirs, U.S.A.: implications for secondary recovery: The Arabian Journal for Science and Engineering, v. 19, no. 2B, p. 215–236.
- Ruppel, S. C., and Cander, H. S., 1988a, Effects of facies and diagenesis on reservoir heterogeneity: Emma San Andres field, West Texas: The University of Texas at Austin, Bureau of Economic Geology Report of Investigations No. 178, 67 p.

- Ruppel, S. C., and Cander, H. S., 1988b, Dolomitization of shallow-water platform carbonates by sea water and seawater-derived brines: San Andres Formation (Guadalupian), West Texas, *in* Sedimentology and geochemistry of dolostones: Society of Economic Paleontologists and Mineralogists, Special Publication No. 43, p. 245–262.
- Ruppel, S. C., and Bebout, D. G., 2001, Competing effects of depositional architecture and diagenesis on carbonate reservoir development: Grayburg Formation, South Cowden field, West Texas: The University of Texas at Austin, Bureau of Economic Geology Report of Investigations No. 263, 62 p.
- Ruppel, S. C., Park, Y. J., and Lucia, F. J., 2002, Applications of 3-D seismic to exploration and development of carbonate reservoirs: South Cowden Grayburg field, West Texas, *in* Hunt, T. J., and Lufholm, P. H., eds., The Permian Basin: preserving our past—securing our future: West Texas Geological Society, Publication No. 02-111, p. 71–87.
- Ruppel, S. C., 1992, Styles of deposition and diagenesis in Leonardian carbonate reservoirs in West Texas: implications for improved reservoir characterization: Society of Petroleum Engineers Annual Exhibition and Technical Conference, 24691, p. 313–320.
- Ruppel, S. C., 2002, Geological controls on reservoir development in a Leonardian (Lower Permian) carbonate platform reservoir, Monahans field, West Texas: The University of Texas at Austin, Bureau of Economic Geology Report of Investigations No. 266, 58 p.
- Ruppel, S. C., and Ariza, E. E., 2002, Cycle and sequence stratigraphy of the clear fork reservoir at South Wasson field: Gaines County, Texas, *in* Lucia, F. J. (editor), Integrated outcrop and subsurface studies of the interwell environment of carbonate reservoirs: Clear Fork (Leonardian-age) reservoirs, West Texas and New Mexico: Final technical report to the Department of Energy, Contract No. DE-AC26-98BC15105, p. 59-94.
- Ruppel, S. C., Ward, W. B., Ariza, E. E., and Jennings, J. W., Jr., 2000, Cycle and sequence stratigraphy of Clear Fork reservoir-equivalent outcrops: Victorio Peak Formation, Sierra Diablo, Texas, *in* Lindsay, R., Trentham, R., Ward, R. F., and Smith, A. H. (eds.), Classic Permian geology of West Texas and Southeastern New Mexico, 75 years of Permian Basin oil & gas exploration & development: West Texas Geological Society Publication 00-108, p. 109–130.
- Saller, A. H., and Henderson, N., 1998, Distribution of porosity and permeability in platform dolomites: insights from the Permian of West Texas: American Association of Petroleum Geologists Bulletin, v. 82, no. 8, p. 1528–1550.
- Shinn, E. A., 1983, Tidal flat, *in* Scholle, P. A., Bebout, D. G., and Moore, C. H., eds., Carbonate depositional environments: American Association of Petroleum Memoir 33, p. 171–210.
- Tyler, Noel, and Banta, N. J., 1989, Oil and gas resources remaining in the Permian Basin: targets for additional hydrocarbon recovery: The University of Texas at Austin, Bureau of Economic Geology Geological Circular 89-4, 20 p.

- Vogt, J. N., 1986, Dolomitization and anhydrite diagenesis of the San Andres (Permian) Formation, Gaines County, Texas: unpublished Master's thesis, The University of Texas at Austin, 202 p.
- Ye, Q., and Mazzullo, S. J. , 1993, Dolomitization of lower Permian platform facies, Wichita Formation, north platform, Midland Basin, Texas: Carbonates and Evaporites v. 8, no. 1, p. 55–70.
- Zeng, Hongliu, and Kerans, Charles, 2003, Seismic frequency control on carbonate seismic stratigraphy: a case study of the Kingdom Abo sequence, West Texas: American Association of Petroleum Geologists Bulletin, v. 87, no. 2, p. 273–293.

SERIES	STAGE	SUBSURFACE					OUTCROP				
		CENTRAL BASIN PLATFORM		NORTHERN SHELF			GUADALUPE MOUNTAINS/ SIERRA DIABLO				
Lower Permian	LEONARDIAN	NEW MEXICO		TEXAS					PLATFORM	MARGIN	SEQUENCE
		San Andres	San Andres	San Andres		San Andres	Cutoff	Guad 1			
		Glorieta	Glorieta	Glorieta		Glorieta	Victorio Peak	Leo 7-8			
		Paddock	upper Clear Fork	Clear Fork Group	upper Clear Fork	Clear Fork Group		Leo 6			
		Blinebry			middle Clear Fork			Leo 5			
		Tubb			Tubb			Leo 4			
		Drinkard			lower Clear Fork			Leo 3			
		Abo	Wichita	Wichita		Victorio Peak	Bone Spring	Leo 2			
			Abo	Abo				Leo 1			
		Wolfcamp	Wolfcamp	Wolfcamp				Hueco	Hueco	Wolf 3	

Figure 1. Chart showing the Leonardian stratigraphic section in the Permian Basin including the Clear Fork Group and analogous units in New Mexico and in outcrop.

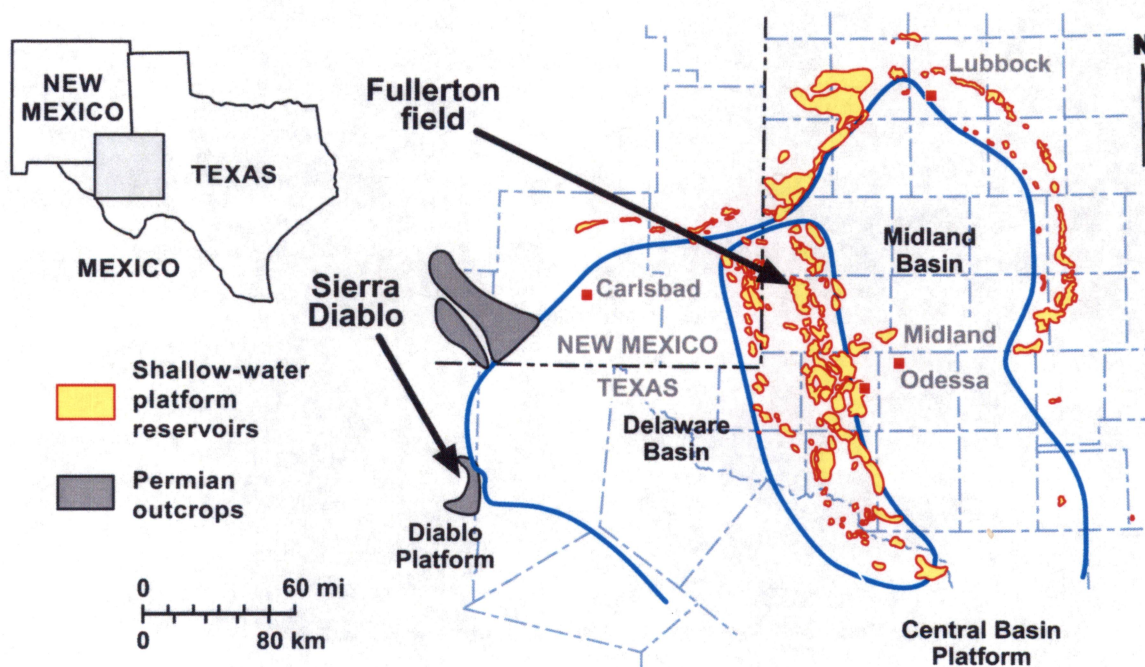


Figure 2. Regional map of the Permian Basin showing location of Fullerton field and analogous outcrops in the Sierra Diablo mountains.



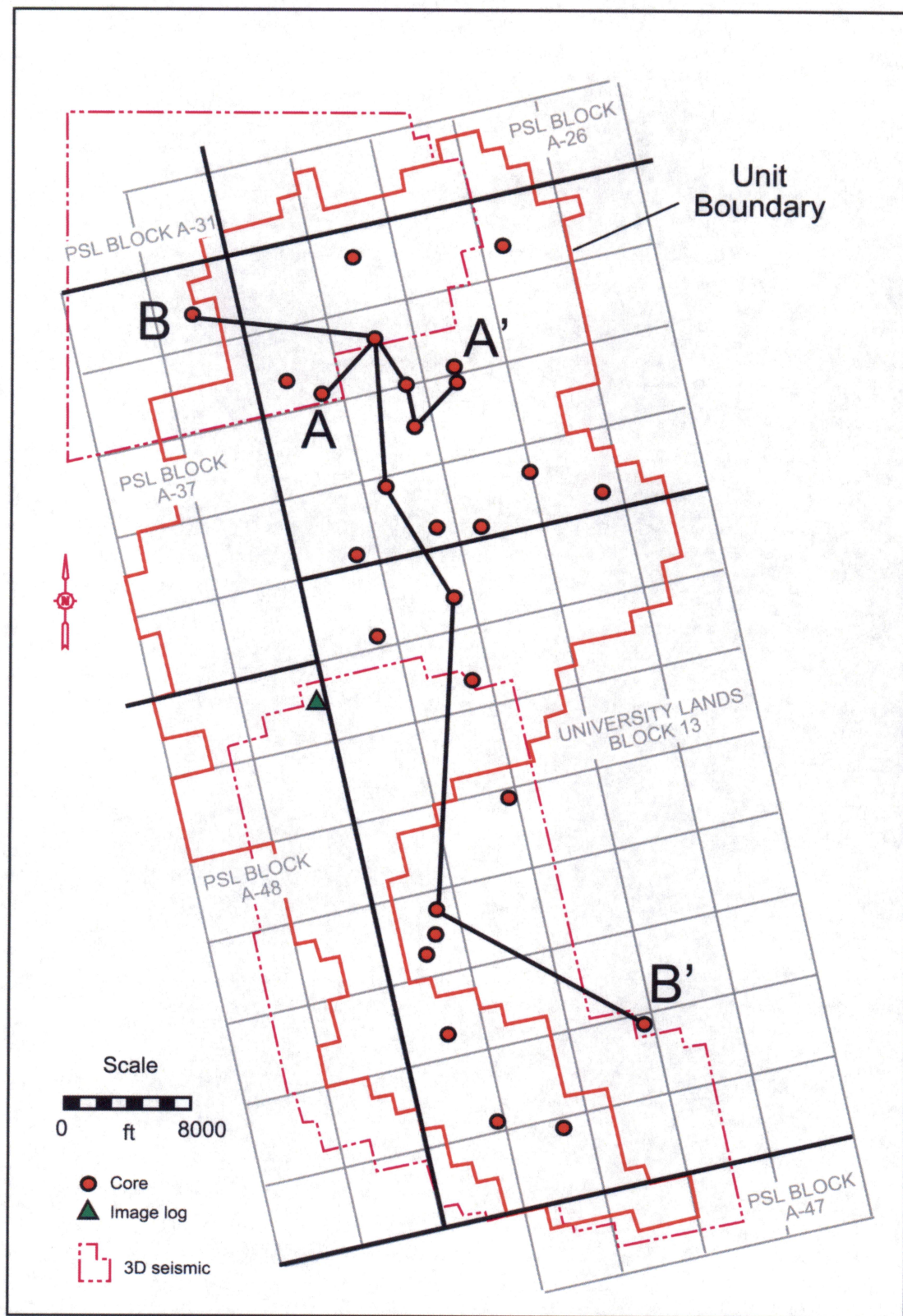


Figure 3. Map of Fullerton Clear Fork field showing location of focused study areas, cores, and 3-D seismic data.



The figure is a geological profile of the Tubb section. The vertical axis represents depth in feet, with major markers at 6500, 3500, 7000, and 4000. The horizontal axis at the top is labeled 'Sequence/Cycle Tops' and includes 'CGR', 'SGR', 'Depth', 'PE', 'Neu', and 'Den'. The profile shows several stratigraphic units: Tubb, HFS 2.3, Lower Clear Fork, HFS 2.2, HFS 2.1, Wichita, HFS 2.0, and Abo. The profile is divided into two main sections: 'Upper Staining' (above 3500 feet) and 'Lower Clear Fork' (below 3500 feet). The 'Wichita' unit is further divided into sub-units W1 through W12. The 'Reservoir Zones' are labeled on the right: Zone 1, Zone 2, Zone 3, Zone 3B, Zone 4, and Zone 5. A legend at the bottom indicates that the orange color represents 'Peritidal/Tidal Flat' and the blue color represents 'Subtidal'.

75



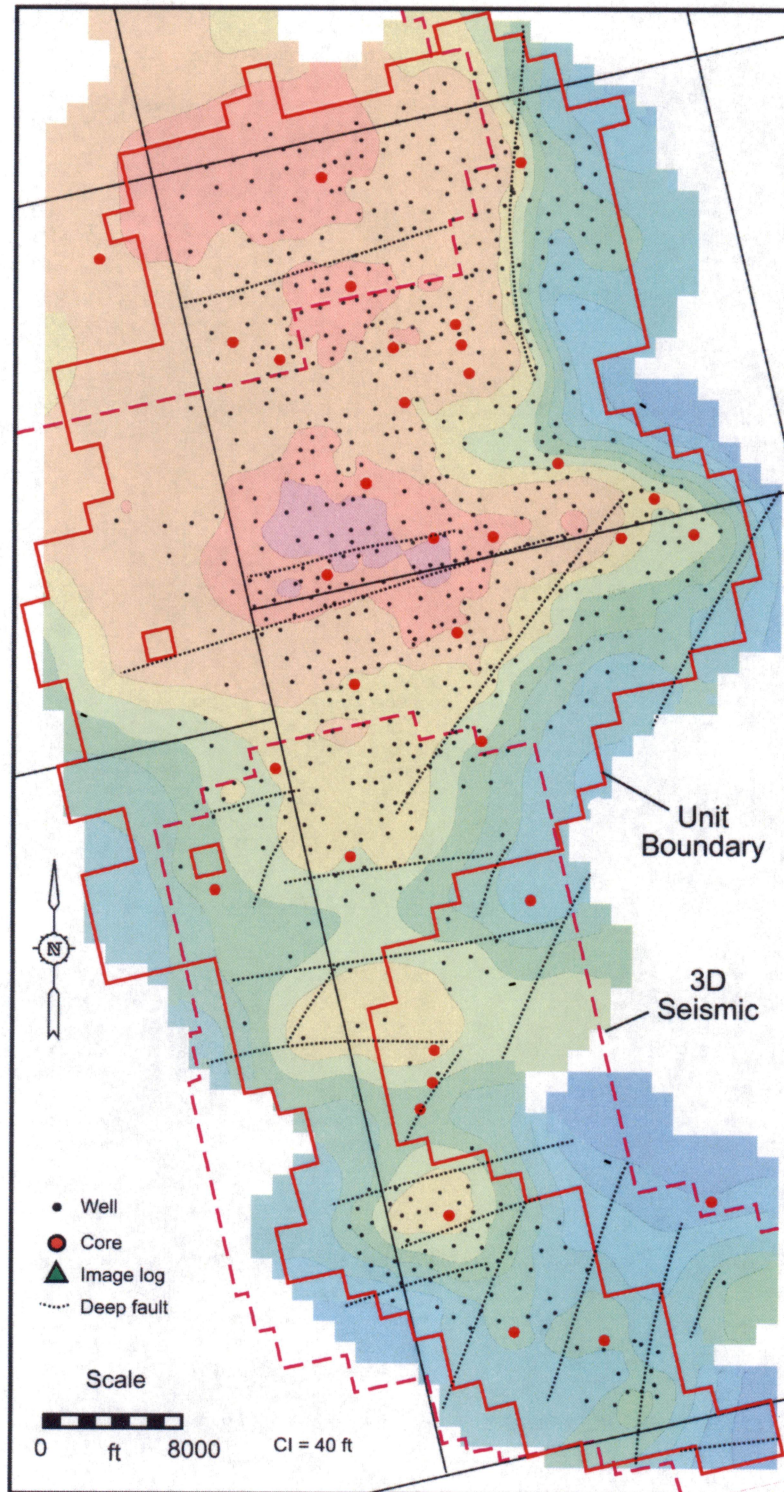


Figure 5. Structure of the Fullerton Clear Fork field. Datum is a prominent subtidal flooding event near the base of the Tubb Formation (see figures 4, 8).



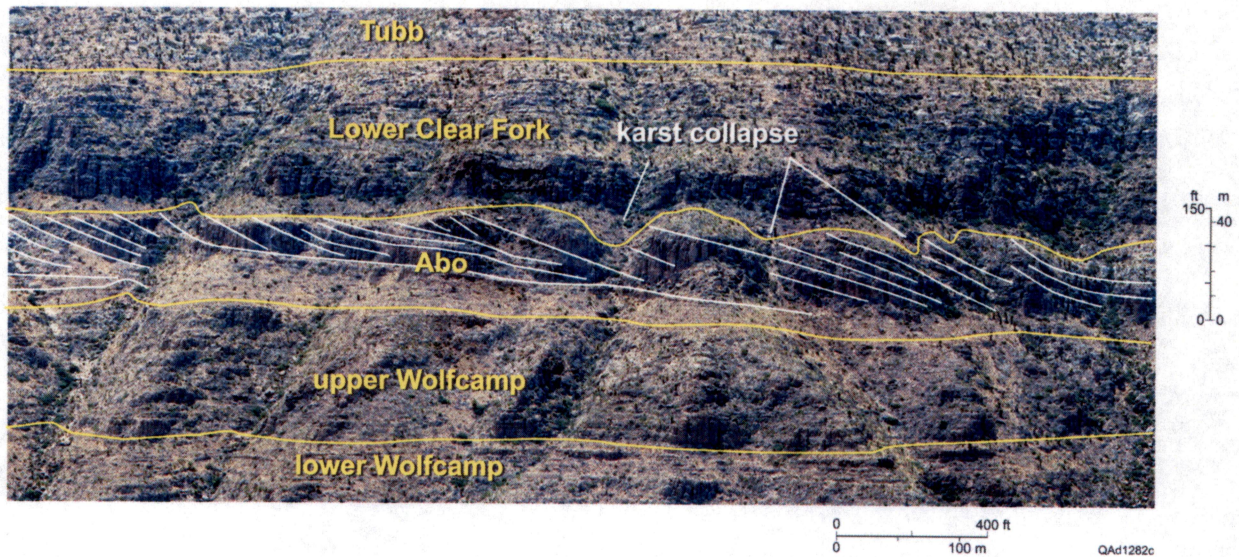


Figure 6. Outcrop photographs showing Abo–Lower Clear Fork section equivalent to producing reservoir interval at Fullerton field. Note top-lapping clinoformal geometry in the Abo and karst development at the Abo–Lower Clear Fork contact. Karst features are filled with locally collapsed peritidal tidal-flat deposits.

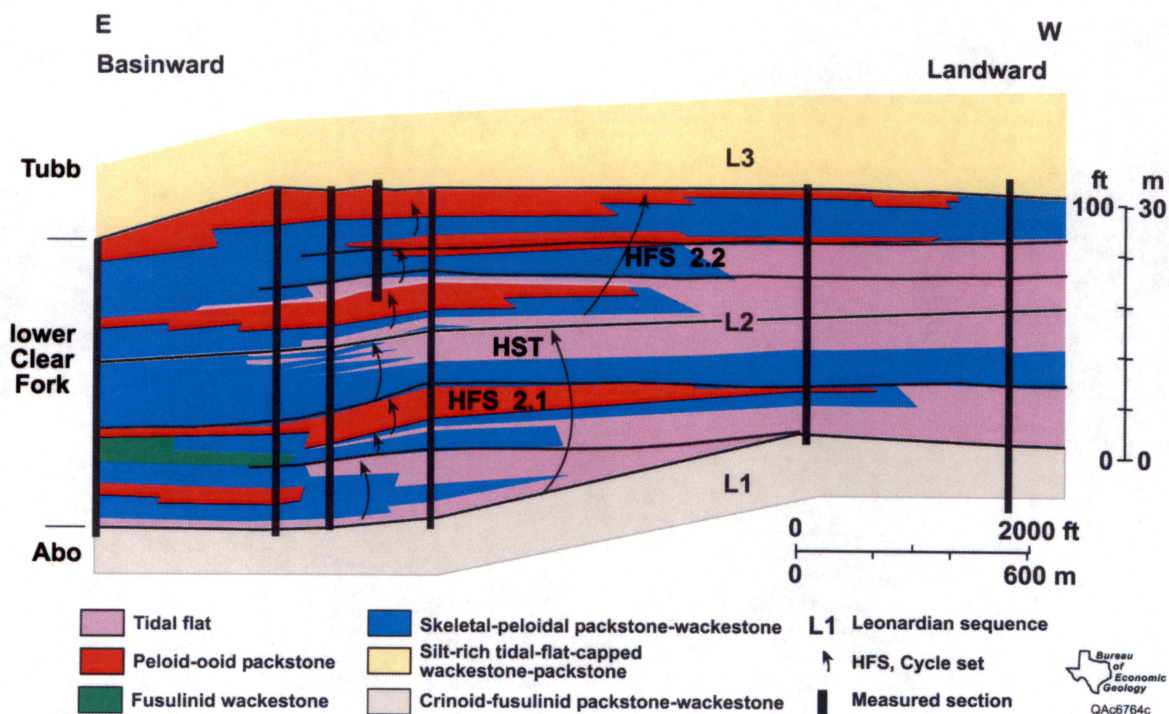


Figure 7. Cross section depicting lateral changes in facies and cyclicity in Sierra Diablo outcrops partly equivalent to Lower Clear Fork (sequence L2) reservoir rocks at Fullerton field. Note generally parallel, flat-lying contacts, and overall backstepping architecture.



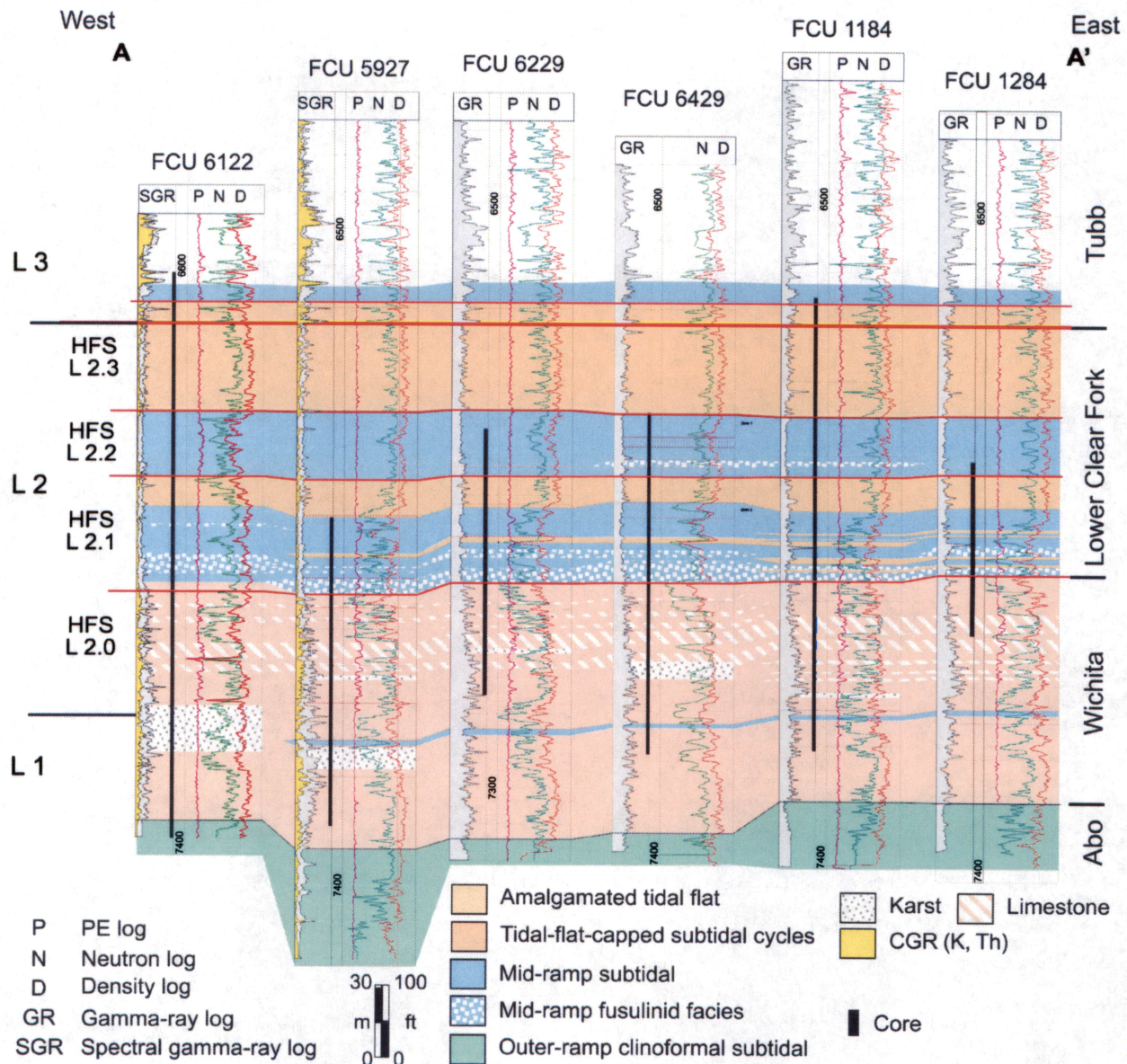


Figure 8. Cross section (A-A') illustrating sequence stratigraphy and facies in the central part of the Clear Fork reservoir at Fullerton field based on cores. The generally isopachous character of the reservoir section (Wichita–Lower Clear Fork) is consistent over most of the field area. Line of section shown in figure 3.



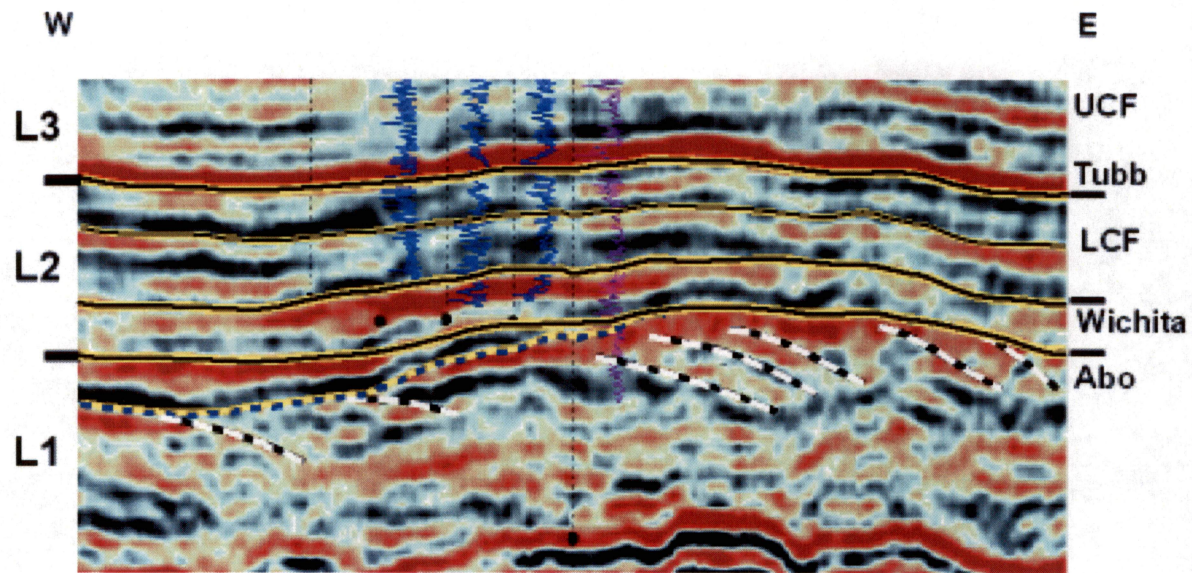


Figure 9. 3-D seismic section from southern part of Fullerton field showing seismic definition of the Clear Fork reservoir section. Yellow lines are time-line boundaries; dotted line defines the top of Abo Formation. Note that whereas the upper Wichita and Lower Clear Fork (LCF) intervals are essentially isopachous and continuous across the field, the lower Wichita and Abo display reciprocal thickness relationships. Blue lines define top-lapping Abo clinoforms. UCF = Upper Clear Fork.



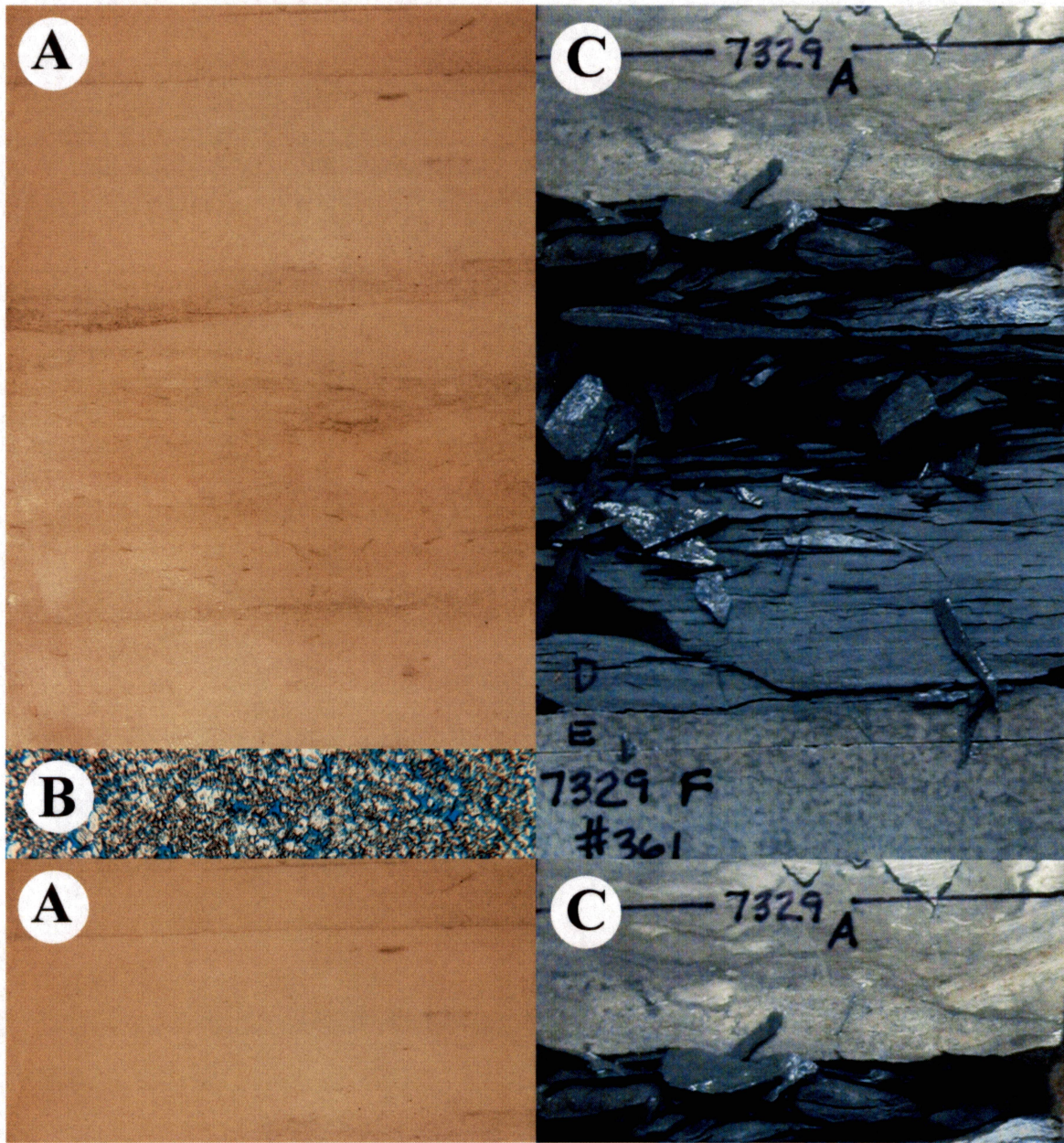


Figure 10. Core and thin-section photographs of typical Wichita tidal-flat facies. A. Slab photo of peritidal mudstone-wackestone showing weak laminations and local burrowing. Core is 4 inches wide. FCU 5927, depth: 7,021 ft. B. Photomicrograph of peritidal mudstone-wackestone facies showing abundant intercrystalline porosity. FCU 6122, depth: 7,092 ft; porosity: 13.8 percent; permeability: 1.6 md. Scale bar is 1 mm. C. Slab photo of clay-rich carbonate mudstone facies in the Wichita. Core is 4 inches wide. FM1 depth: 7,329 ft. Note underlying fenestral mudstone.



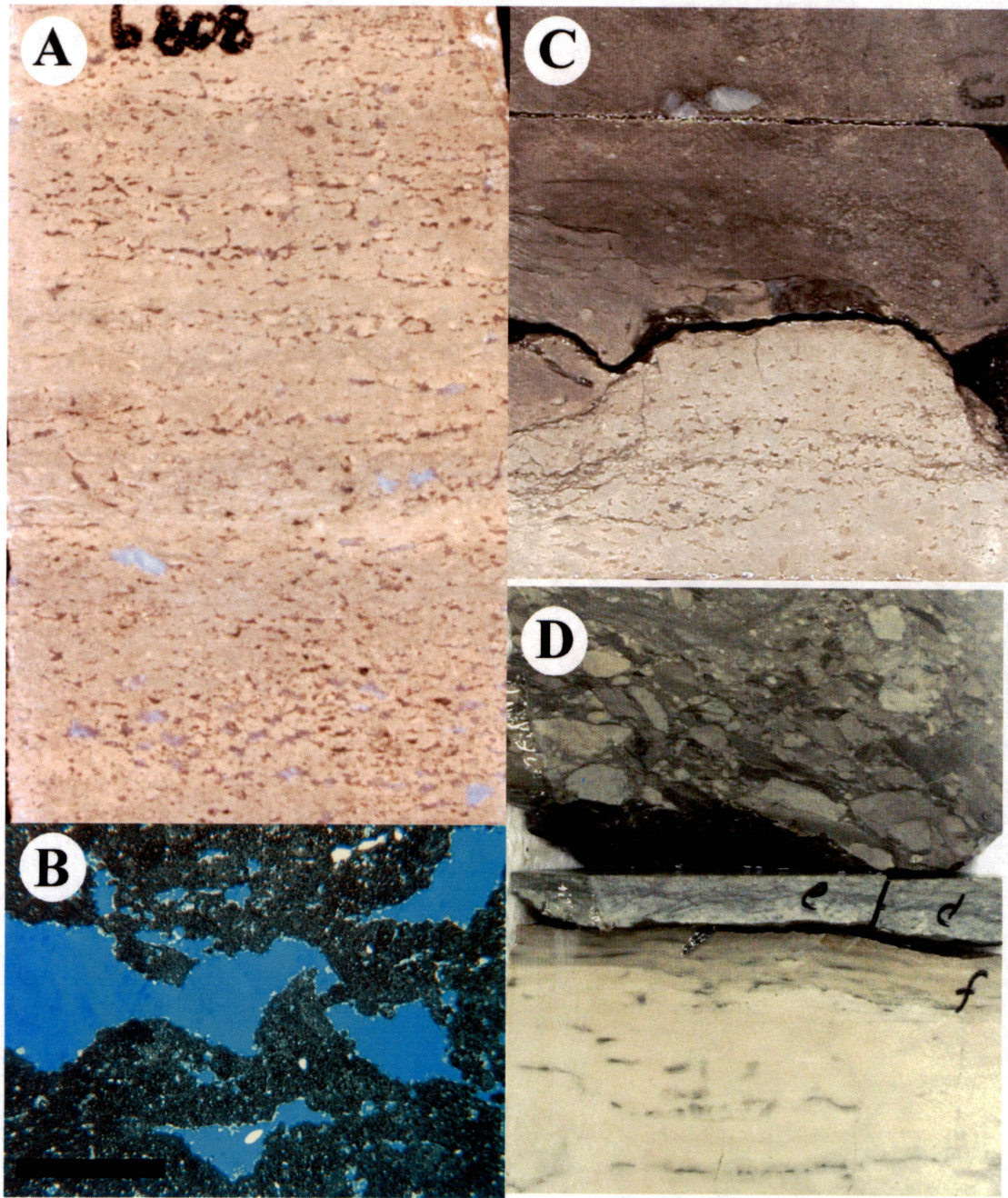


Figure 11. Core and thin-section photographs of typical tidal-flat facies and shallow subtidal facies in the Wichita and Lower Clear Fork. A. Slab photo of exposed tidal-flat facies showing typical parallel laminations and fenestral pores. Core is 4 inches wide. Lower Clear Fork FCU 7322, depth: 6,808 ft. Scale bar is 2 mm. B. Photomicrograph of exposed tidal-flat facies showing fenestral vuggy porosity. Lower Clear Fork FCU 6122, depth: 6,903 ft. Photo is 6 mm wide. C. Slab photo of cycle top showing fenestral exposed tidal-flat facies overlain by subtidal, burrowed peloid wackestone. Note small lithoclasts above cycle top. Lower Clear Fork, top HFS L 2.2. Core is 4 inches wide. FCU 7322, depth: 6,804 ft. D. Slab photo of large rip-up clasts overlying cycle top peritidal mudstone. Wichita FCU 7322, depth: 6,804 ft.



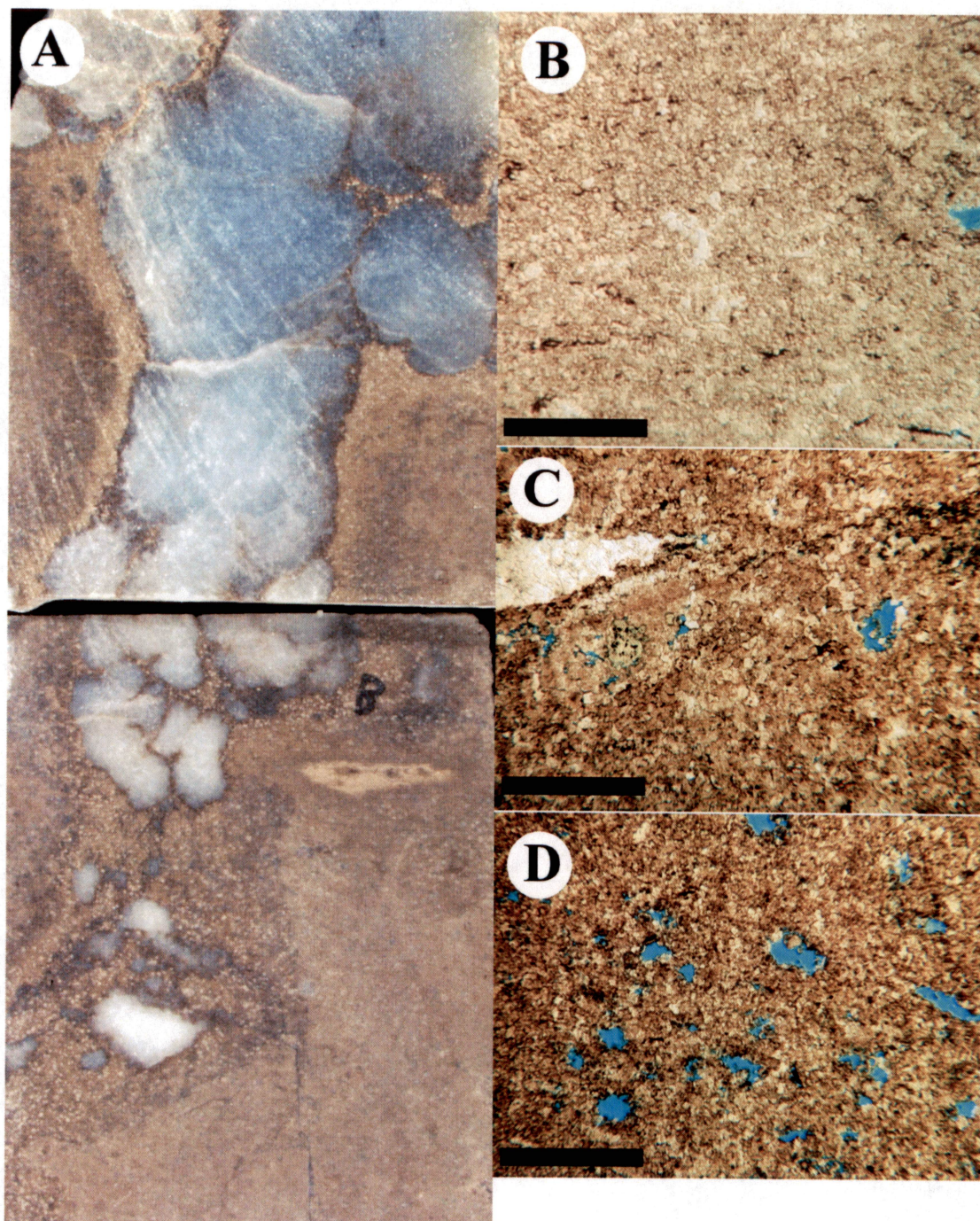


Figure 12. Core and thin-section photographs of typical peloid wackestone facies in the Lower Clear Fork. A. Slab photo of peloid wackestone with anhydrite-bearing, solution-widened vertical burrow. Lower Clear Fork, HFS L 2.2. Core is 4 inches wide. FCU 7322, depth: 6,874 ft. B. Thin-section photomicrograph of low-porosity burrowed, peloid wackestone. FCU 6429, depth: 6,817 ft. Scale bar is 1 mm. C. Thin-section photomicrograph of low-porosity burrowed, peloid wackestone. FCU 6229, depth: 6,820 ft. Scale bar is 1 mm. D. Thin-section photomicrograph of peloid wackestone with moldic pores. FCU 6229, depth: 6,841 ft. Scale bar is 1 mm.



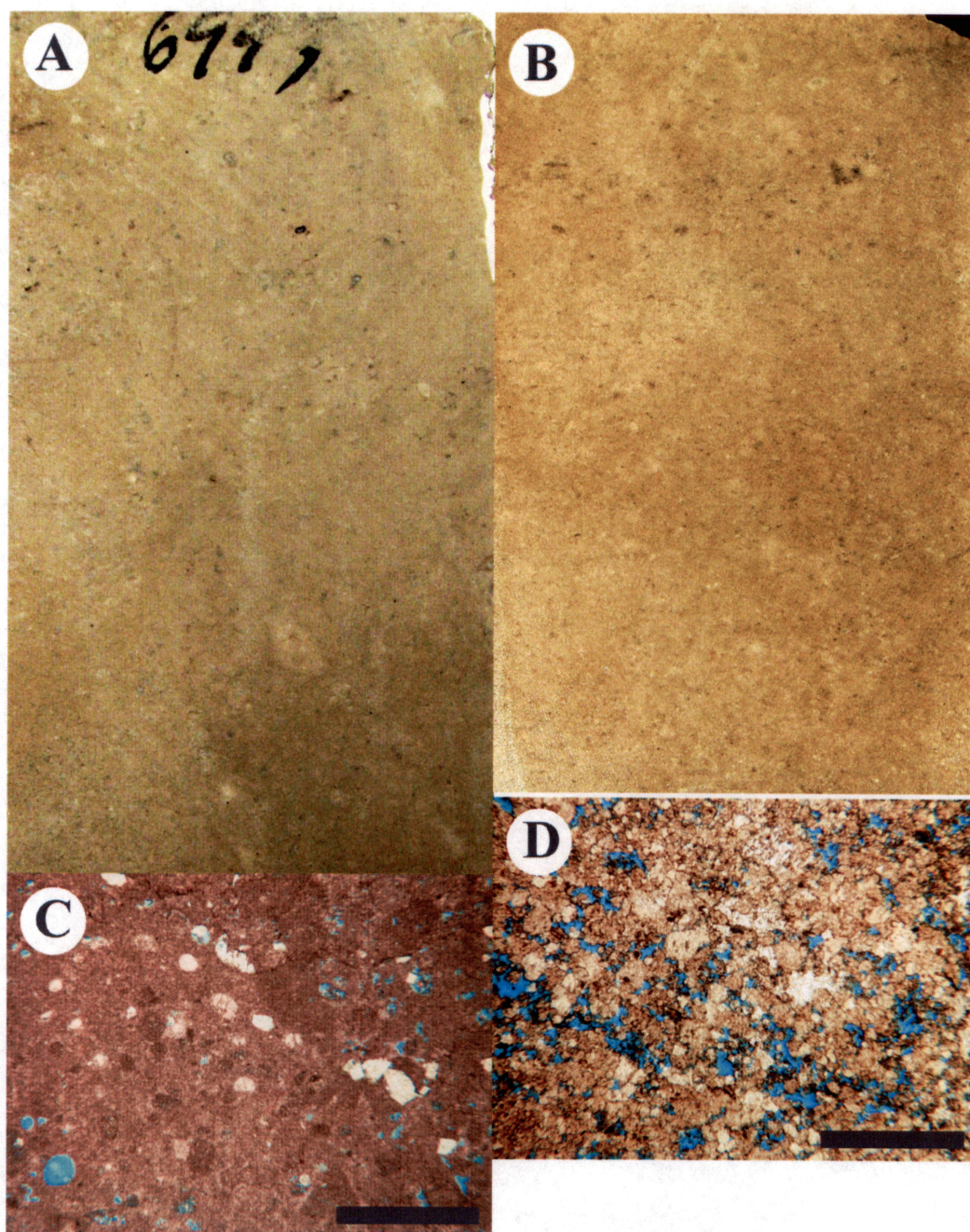


Figure 13. Core and thin-section photomicrographs of mud-rich peloid packstone-wackestone. A: Slab photo of burrowed Lower Clear Fork peloid packstone (dolostone). FCU 6229, depth: 6,997 ft. Core is 10 cm wide. B. Slab photo of Wichita peloid packstone (dolostone). FCU 5927, depth: 7,038 ft. Core is 10 cm wide. C. Photomicrograph of Lower Clear Fork peloid packstone (limestone) with moldic porosity. FCU 5927, depth: 6,903 ft. Scale bar is 1 mm. D. Photomicrograph of Lower Clear Fork peloid packstone (limestone) with moldic porosity. FCU 6229, depth: 6,817 ft. Scale bar is 1 mm.



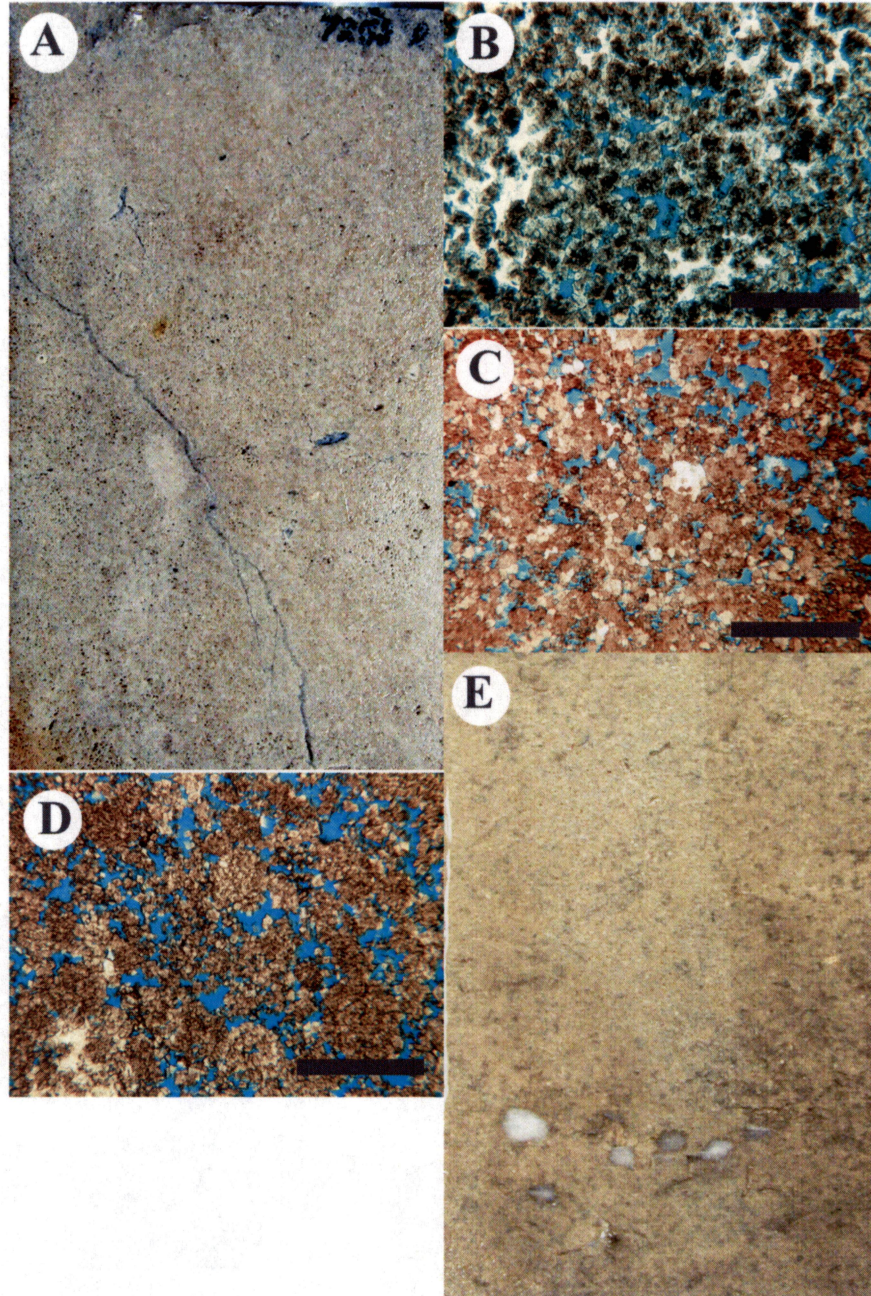


Figure 14. Core and thin-section photomicrographs of peloid, grain-rich packstones and grainstones. A. Slab photo of Abo peloid grain-dominated packstone. University Consolidated IV-25, depth: 7,252 ft. Core is 10 cm wide. B. Photomicrograph of Lower Clear Fork peloid dolostone grain-dominated packstone showing interparticle porosity. White areas are poikilotopic anhydrite. FCU 6122, depth: 6,976 ft. Scale bar is 1 mm. C. Photomicrograph of Lower Clear Fork peloid (ooid?) dolostone grain-dominated packstone-grainstone with interparticle porosity. FCU 6946, depth: 6,835 ft. Scale bar is 1 mm. D. Photomicrograph of Lower Clear Fork peloid grain-dominated packstone dolostone showing interparticle porosity. FCU 6229, depth: 6,816 ft. Scale bar is 1 mm. E. Slab photo of Lower Clear Fork (L 2.2) peloid grain-dominated packstone (dolostone). FCU 6229, depth: 6,822 ft. Core is 10 cm wide.



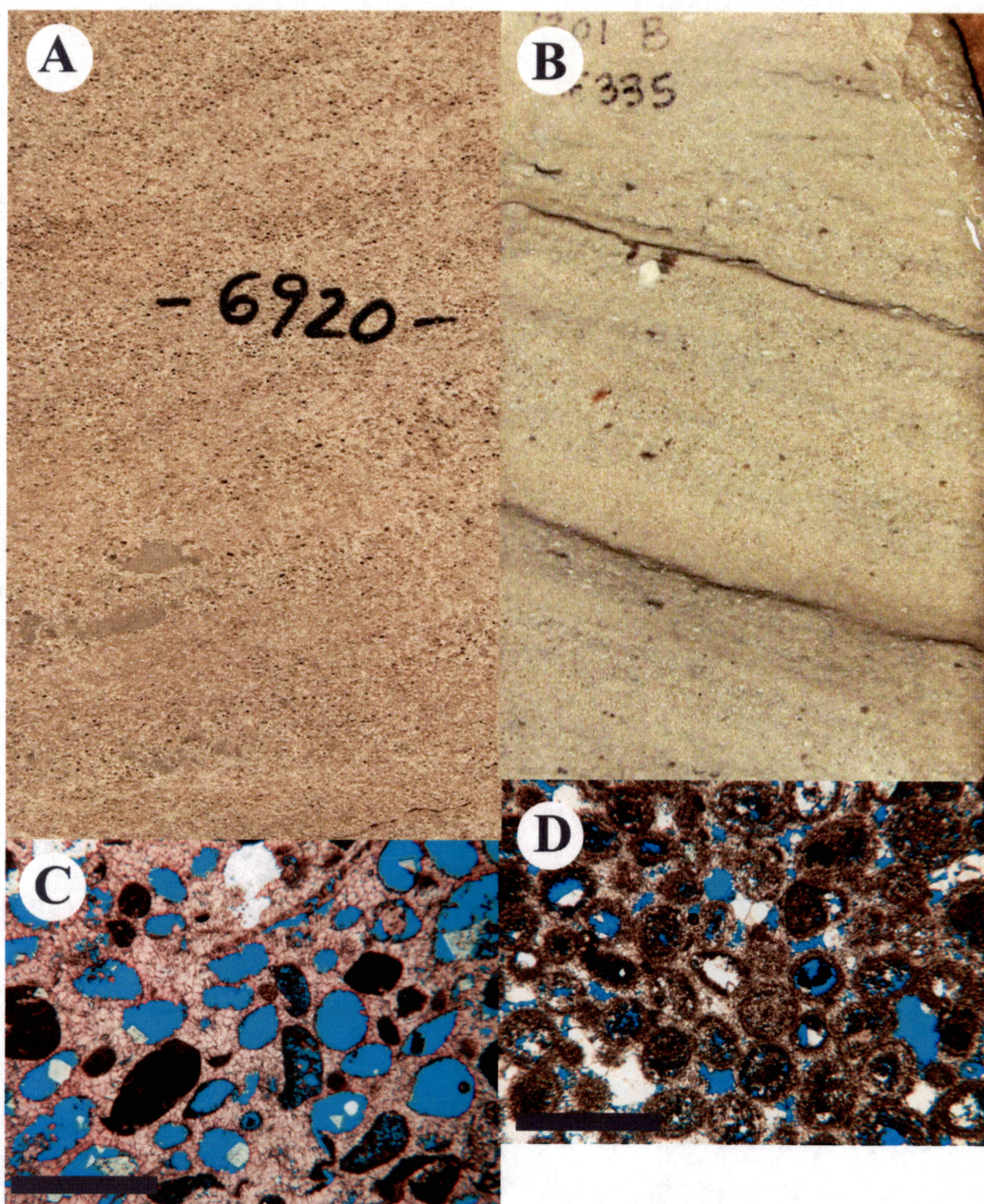


Figure 15. Core and thin-section photomicrographs of Lower Clear Fork and Abo grainstones. A. Slab photo of Lower Clear Fork ooid grainstone showing cross laminations. FCU 6122, depth: 6,920 ft. Core is 10 cm wide. B. Slab photo of Abo skeletal grainstone showing inclined laminations. FCU 7322, depth: 7,301 ft. Core is 10 cm wide. C. Photomicrograph of Lower Clear Fork ooid limestone grainstone showing oomoldic pores. FCU 5927, depth: 6,913 ft. Scale bar is 1 mm. D. Photomicrograph of Lower Clear Fork ooid dolostone grainstone wackestone showing interparticle and minor moldic pores. FCU 4828, depth: 7,137 ft. Scale bar is 1 mm.



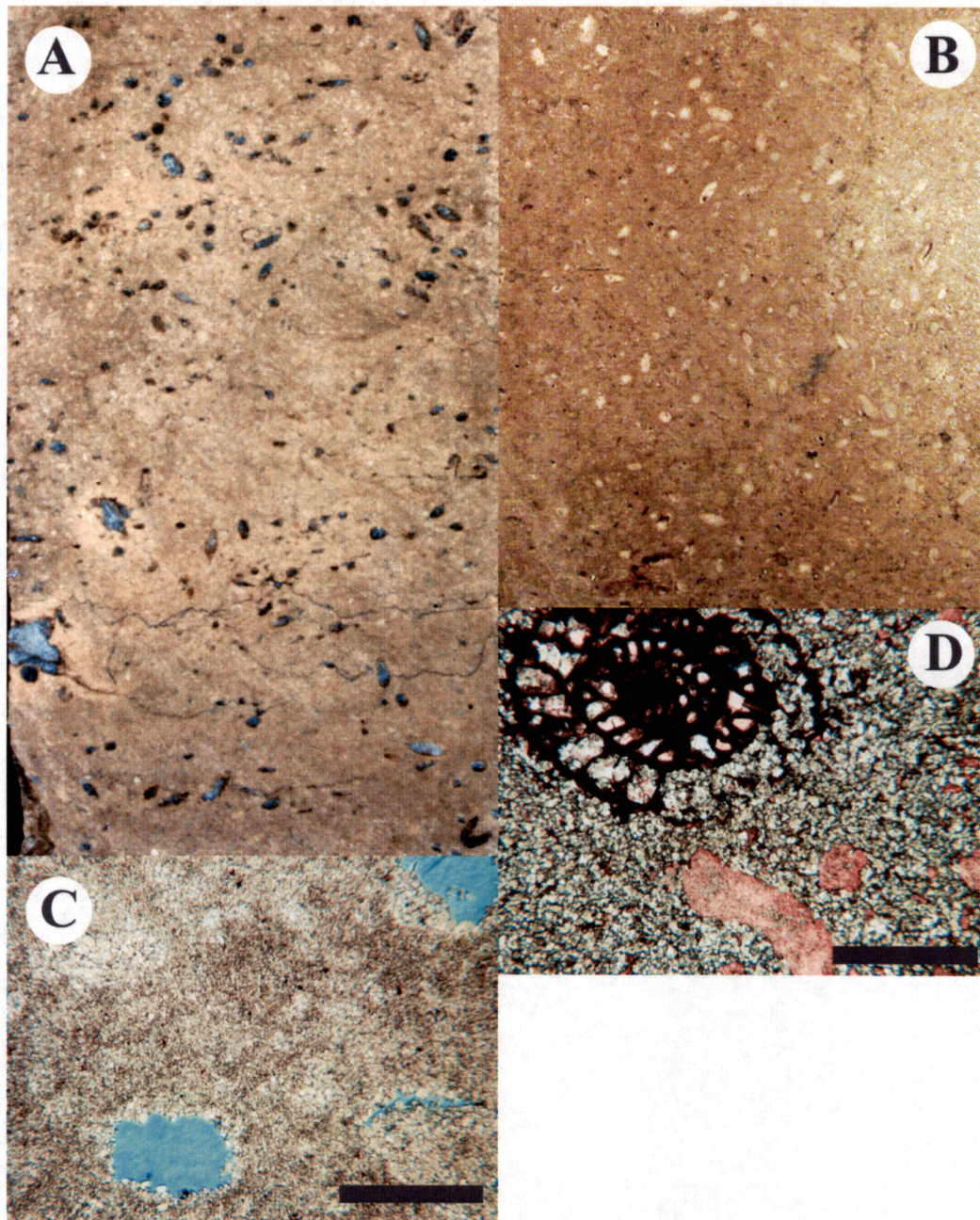


Figure 16. Core and thin-section photomicrographs of the fusulinid wackestone-packstone facies. A. Slab photo of fusulinid wackestone with open and anhydrite-filled fusu-moldic pores. FCU 7322, depth: 6,996 ft. Core is 10 cm wide. B. Slab photo of fusulinid wackestone with anhydrite-filled fusu-molds. FCU 7322, depth: 6,994 ft. Core is 10 cm wide. C. Photomicrograph of fusulinid wackestone showing open fusu-molds. FCU 7630, depth: 6,778 ft. Scale bar is 1 mm. D. Photomicrograph of fusulinid wackestone showing well-preserved fusulinids but little or no porosity. FCU 4828, depth: 7,018 ft. Scale bar is 1 mm.



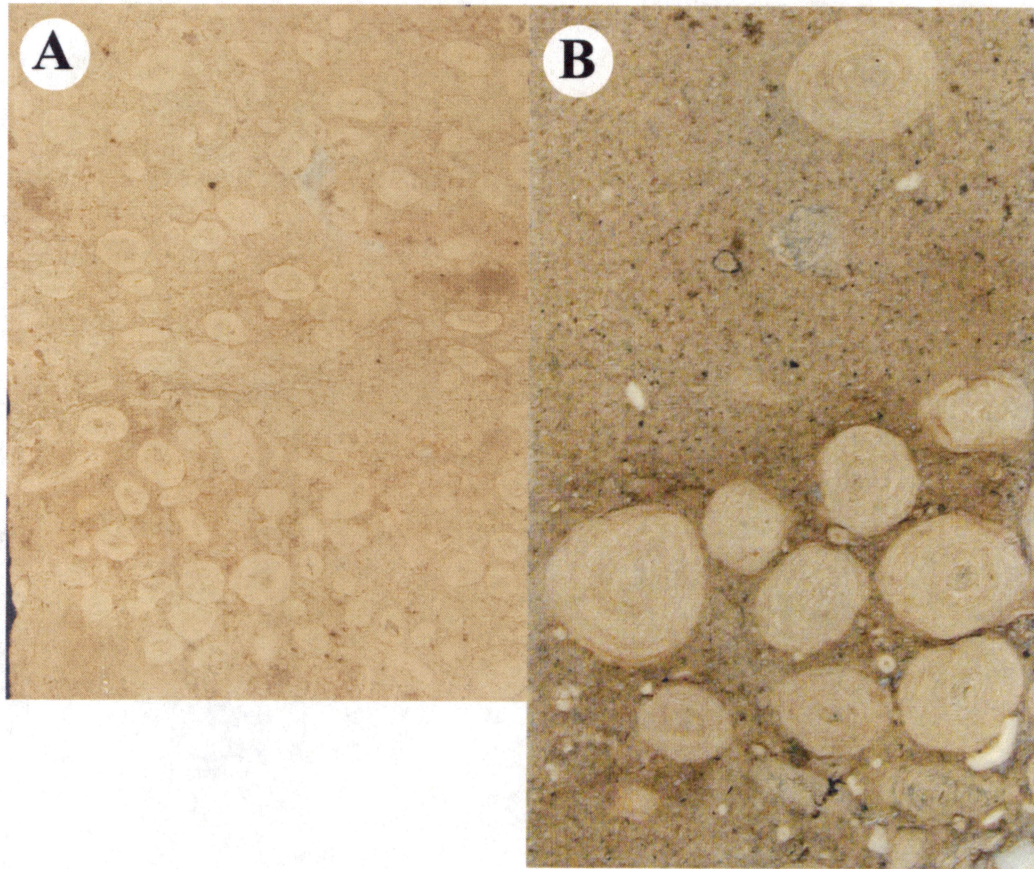


Figure 17. Core and thin-section photomicrographs of the oncoïd, wackestone-packstone facies. A. Small, algal-coated fusulinids. Lower Clear Fork, FCU 5927, depth: 6,980 ft. B. Large oncoïds. Lower Clear Fork, FM-1 well, depth: 7,160 ft. Cores are 4 inches wide.



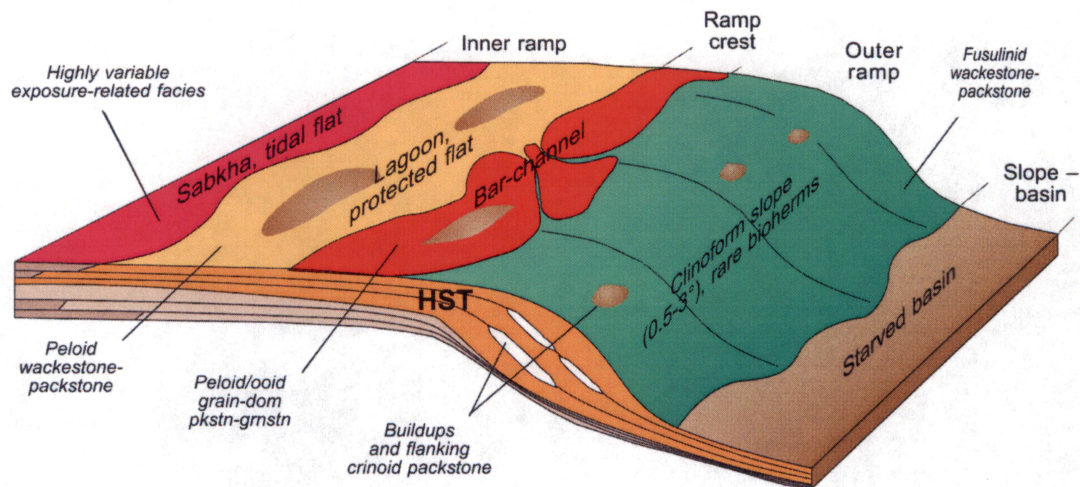


Figure 18. Depositional model for Permian shallow-water carbonate platforms in the Permian Basin. This model is applicable to most Leonardian and Guadalupian carbonate platform successions, including the reservoir succession at Fullerton field. After Kerans and Ruppel (1994).

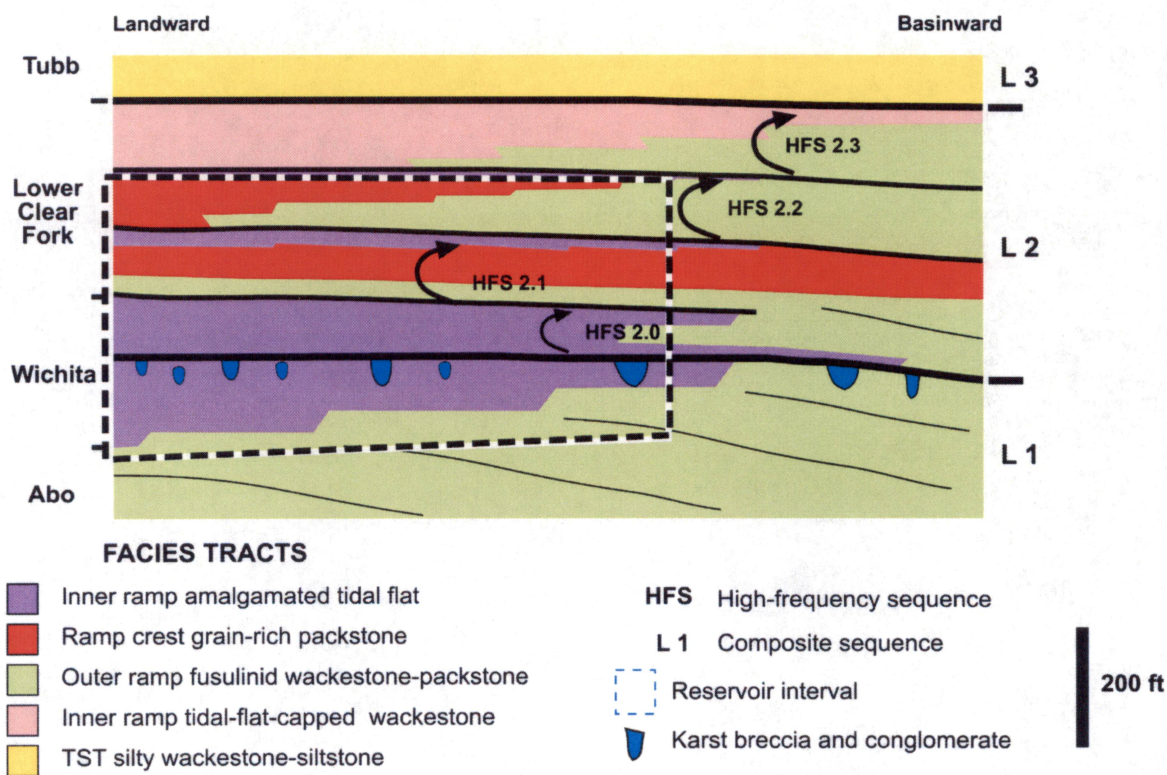


Figure 19. Generalized sequence-stratigraphic model of the lower Leonardian succession at Fullerton field showing primary facies tracts and stratigraphic nomenclature.

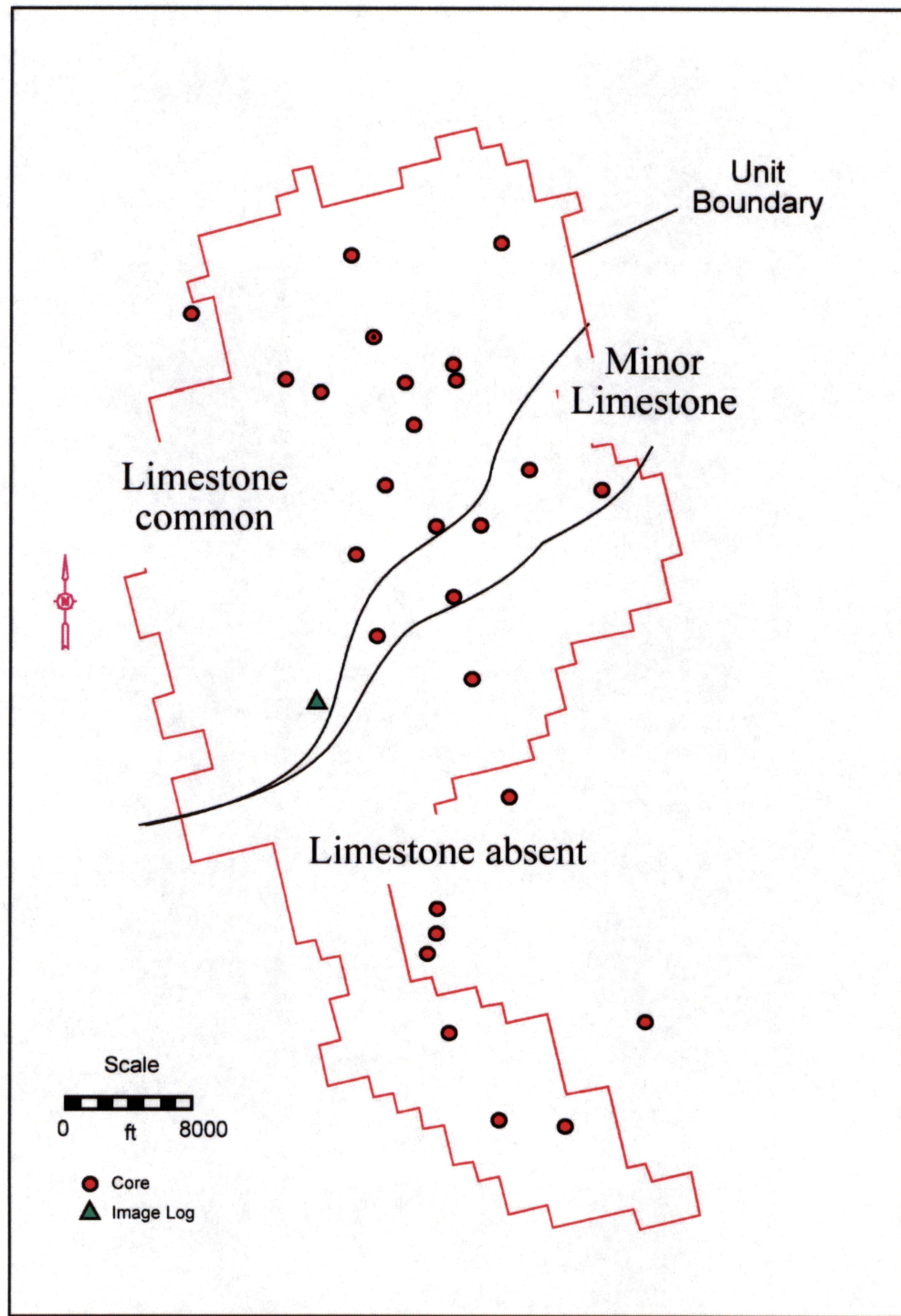


Figure 20. Map of limestone abundance in the Wichita Formation.



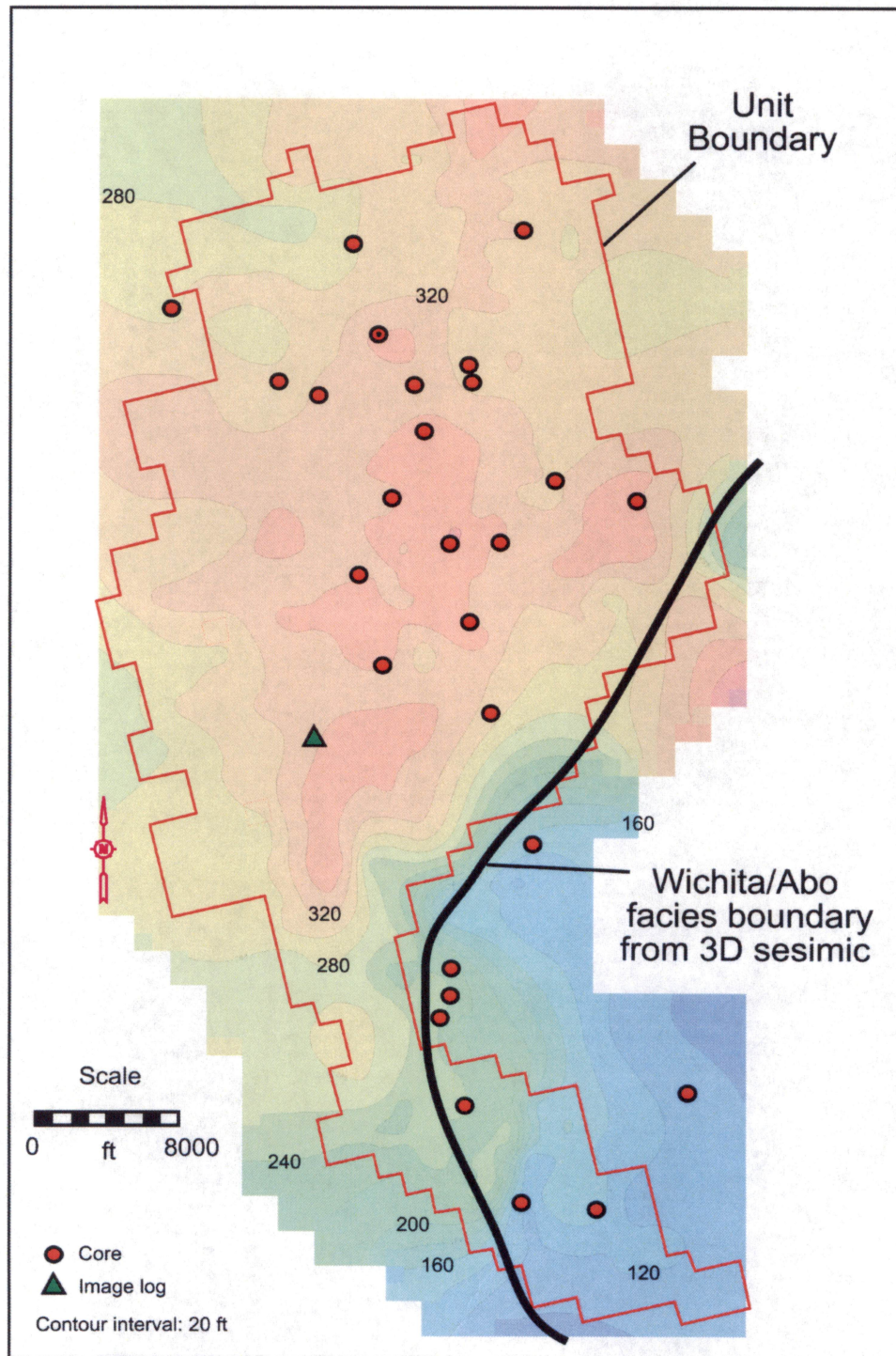


Figure 21. Thickness of the Wichita Formation in the Fullerton field area. The relatively sharp decrease in thickness in the southeastern part of the area is caused by the change in facies from Wichita tidal-flat facies to time-equivalent subtidal Abo facies.



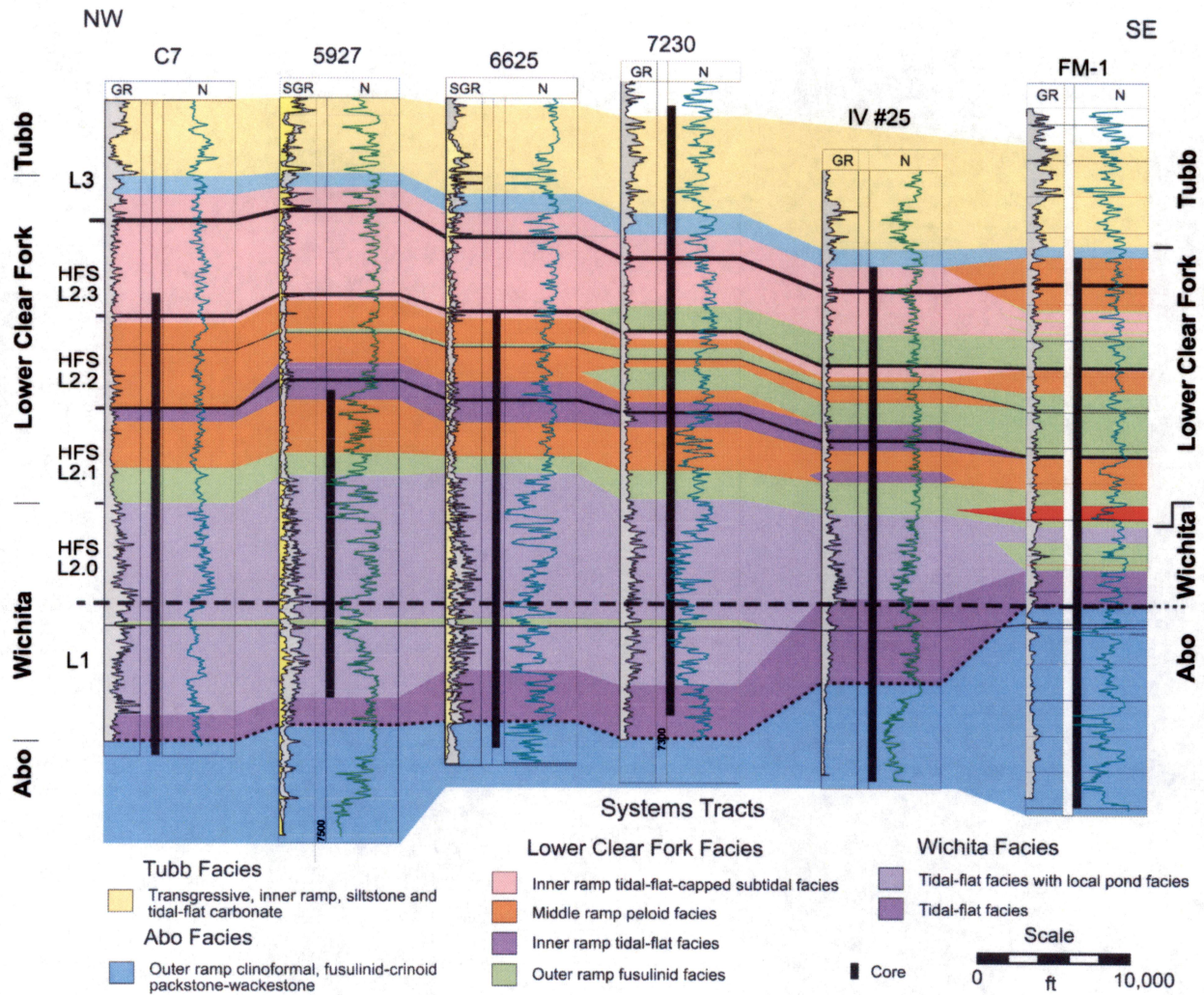


Figure 22. Northwest-southeast cross section (B-B') across the Fullerton field area showing the sequence architecture and general facies development based on cored well control. Line of section shown in figure 3.



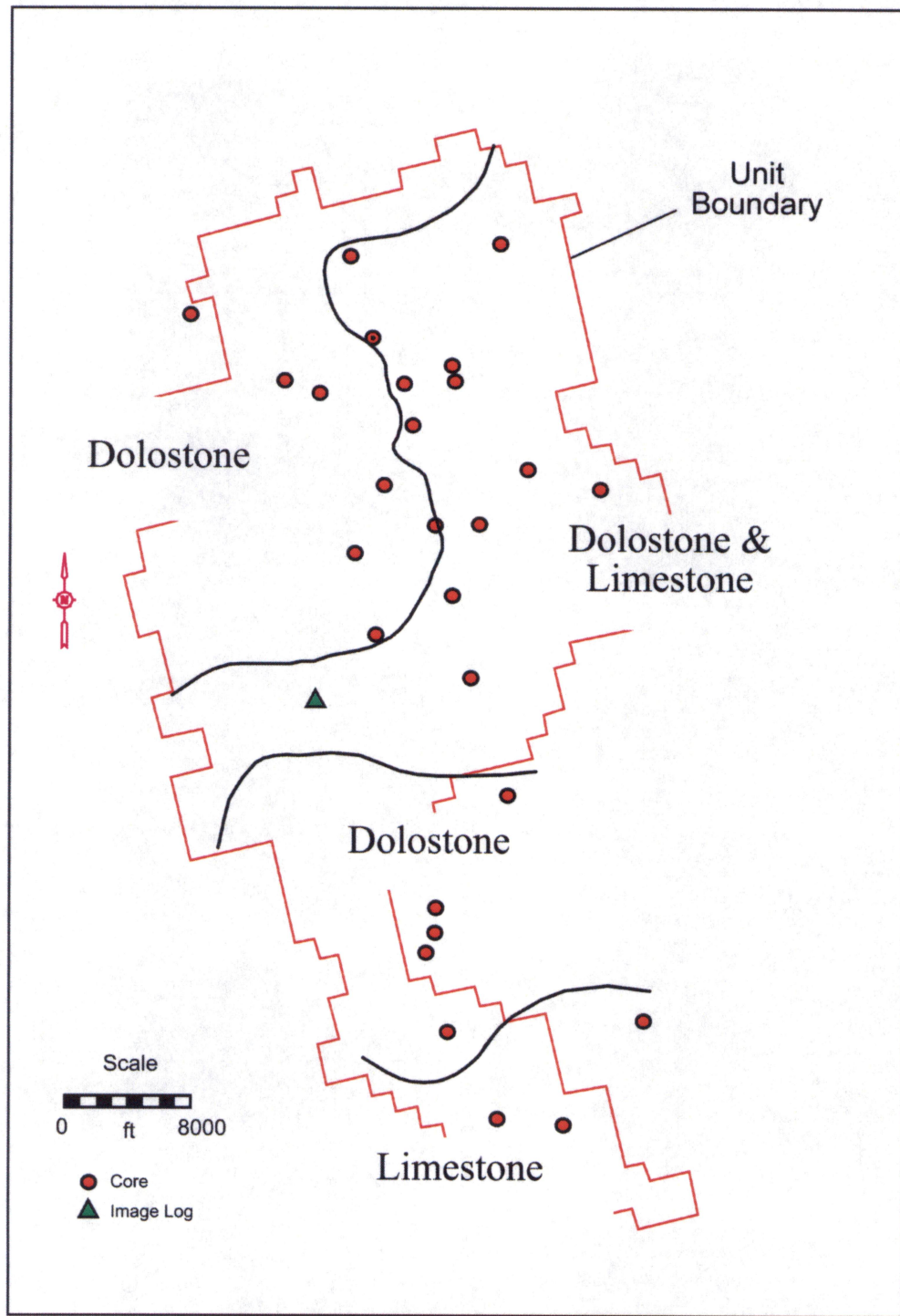


Figure 23. Map showing the distribution of limestone and dolostone in Lower Clear Fork HFS L 2.1 based on cores and wireline logs. Note: Most areas actually contain complexly interbedded limestone and dolostone. Limestone is generally more abundant in the south.

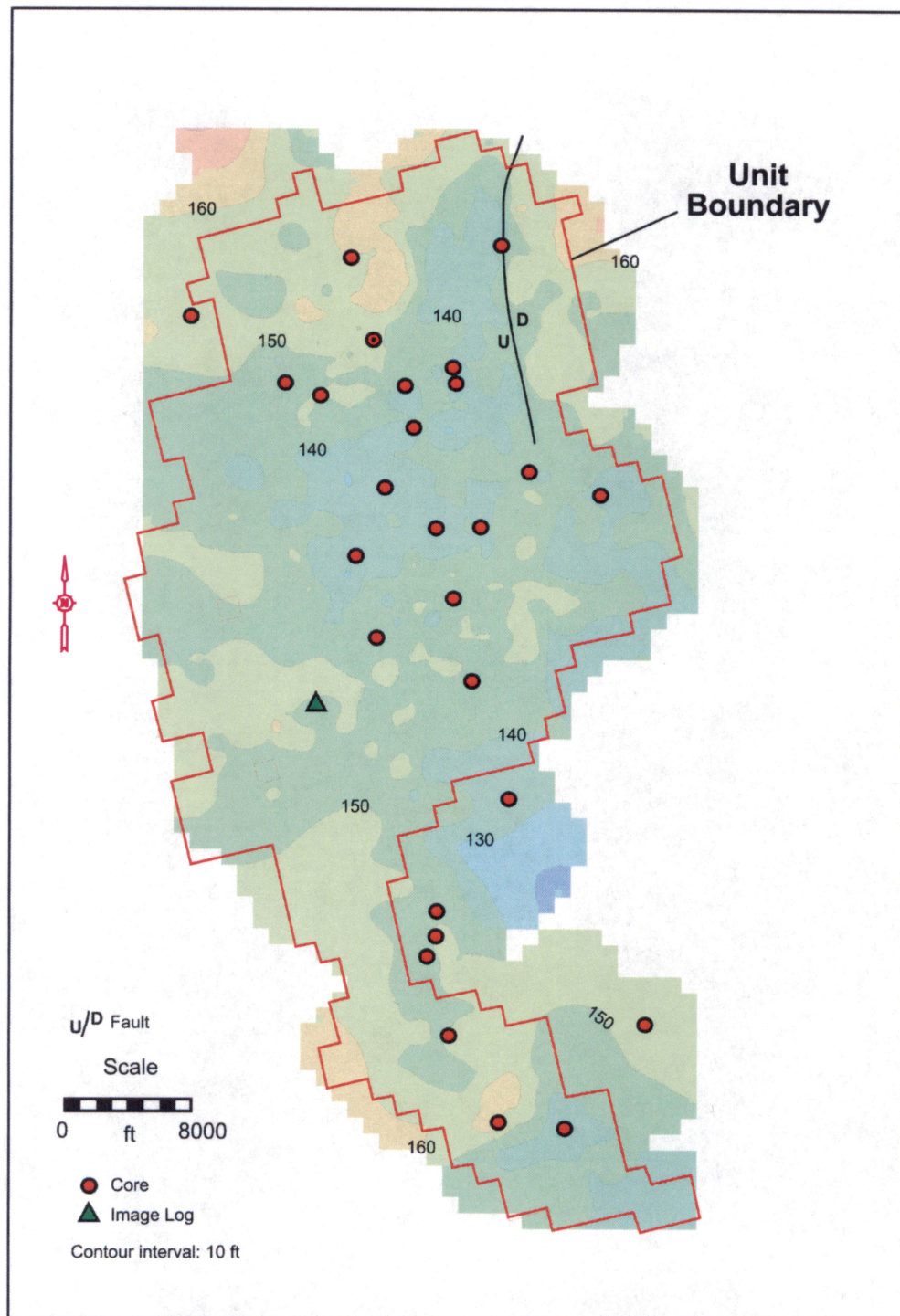


Figure 24. Map of the thickness of the Lower Clear Fork L 2.1 sequence at Fullerton field. Note the abrupt change in thickness along the north-trending fault in the northeastern part of the field.



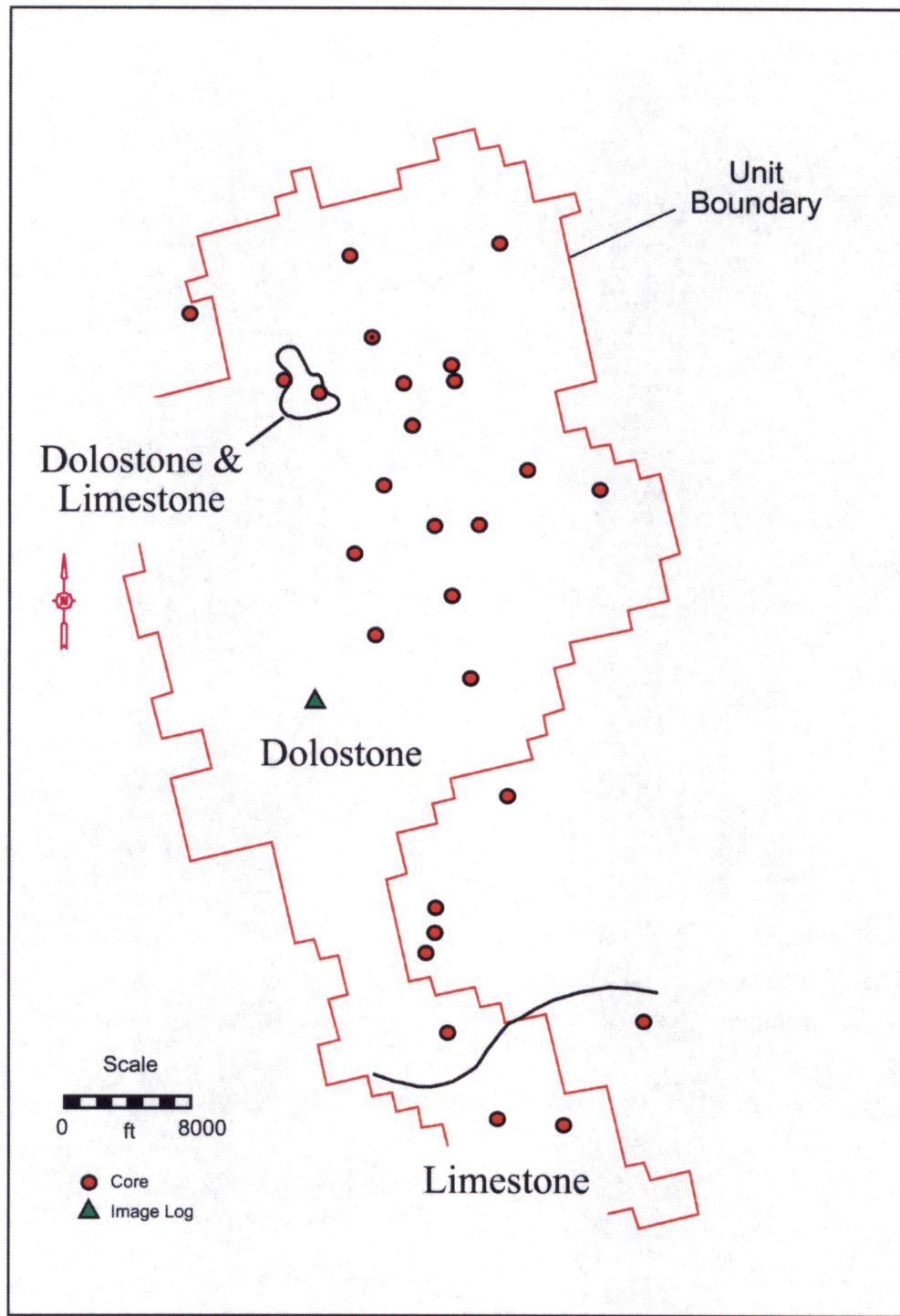


Figure 25. Map showing the distribution of limestone and dolostone in Lower Clear Fork HFS L 2.2 based on cores and wireline logs.

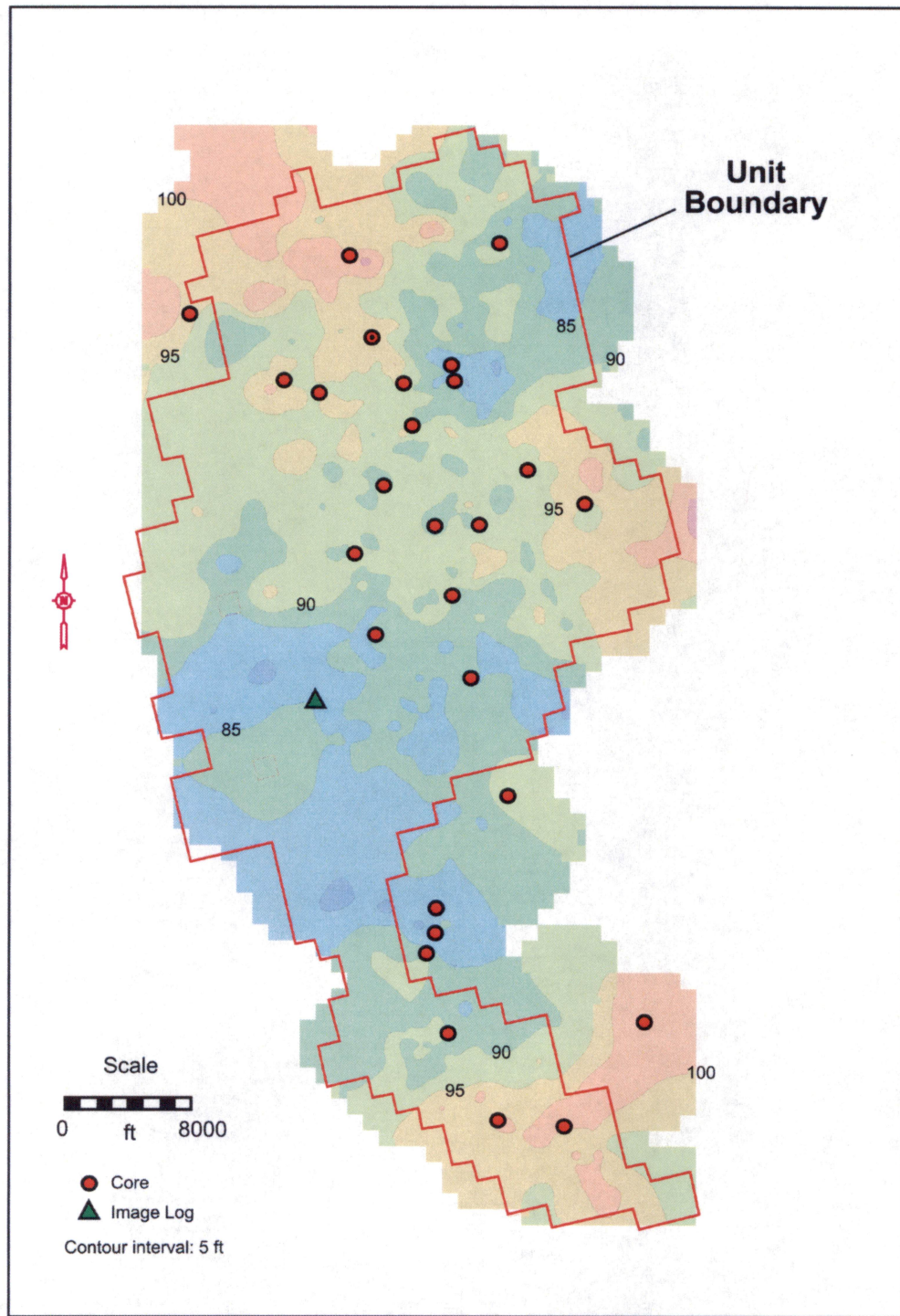


Figure 26. Map of the thickness of the Lower Clear Fork L 2.2 sequence at Fullerton field.



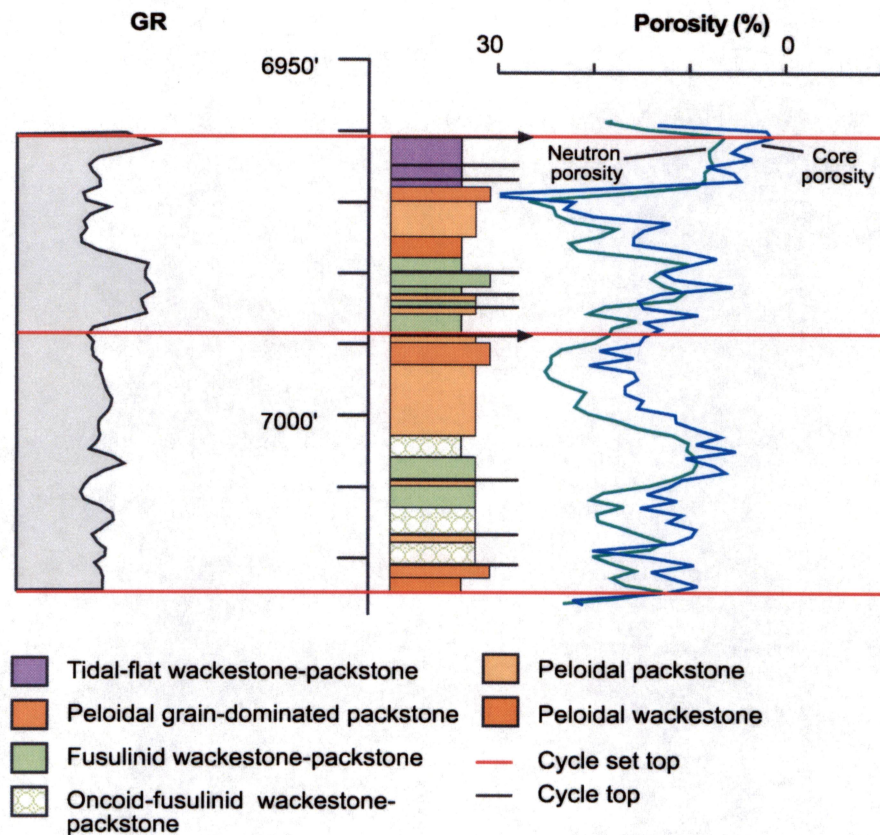


Figure 27. Facies stacking and cycle development in the fusulinid- and oncoïd-rich, transgressive systems tract (TST) of Lower Clear Fork HFS L 2.1. Note that porosity is typically developed at or near cycle tops. Note also the lack of any systematic relationship between gamma-ray log and facies or cyclicity.

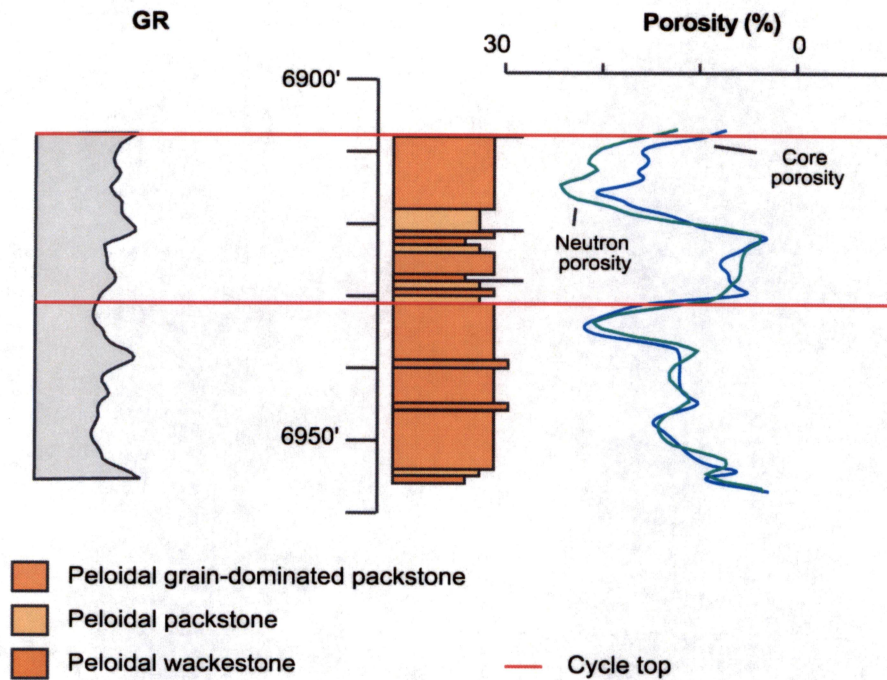


Figure 28. Facies stacking and cycle development in the grain-rich, highstand systems tract (HST) of Lower Clear Fork HFS L 2.1. Note that porosity is typically developed at or near cycle tops. As with other Lower Clear Fork successions, gamma-ray logs do not show a systematic response to facies or cyclicity.



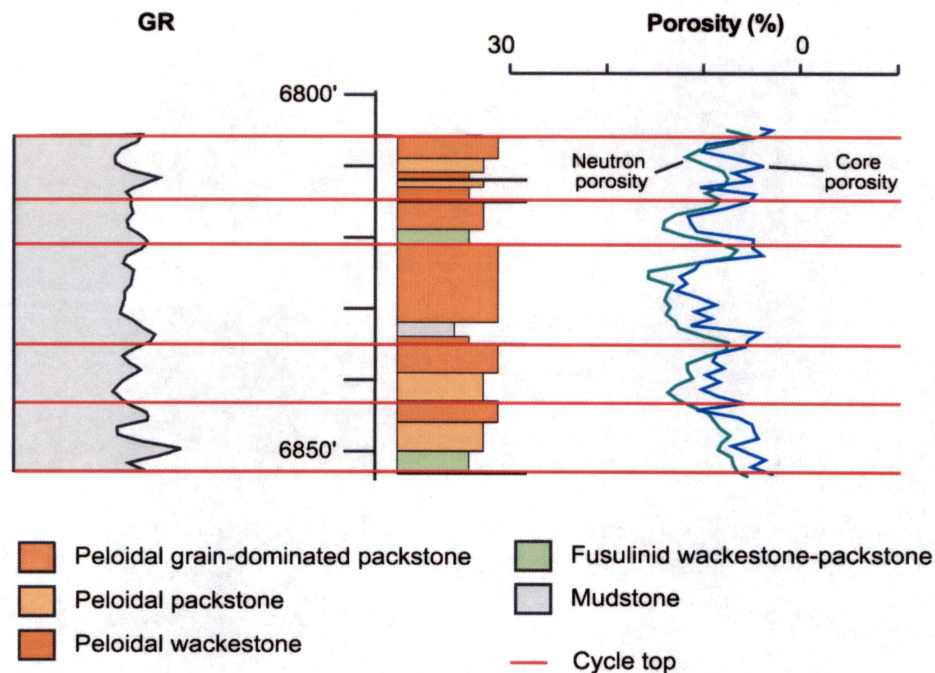


Figure 29. Facies stacking and cycle development in the grain-rich, late transgressive systems tract/early highstand systems tract of Lower Clear Fork HFS L 2.2. Note that porosity is typically developed at or near cycle tops. Note here again that gamma-ray logs do not display any relationship to facies or cycle development.

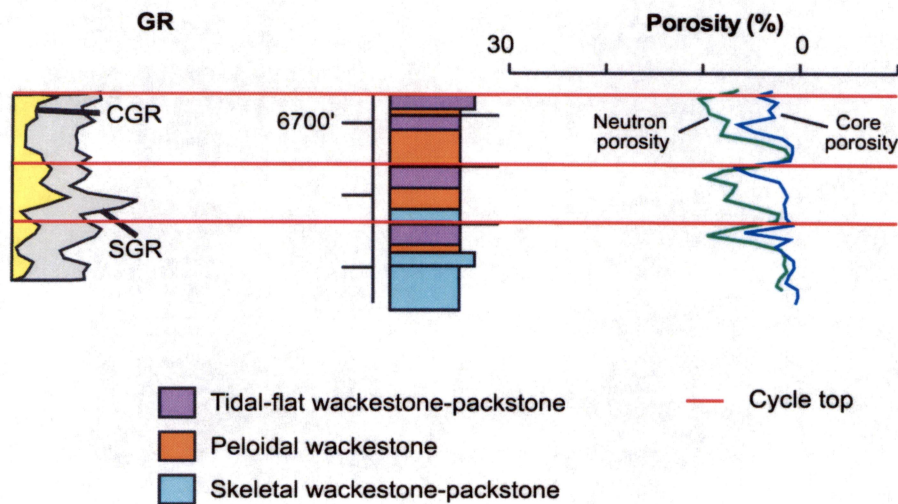


Figure 30. Facies stacking and cycle development in the nonreservoir Lower Clear Fork HFS L 2.3. Porosity is typically developed in cycle-capping tidal-flat facies at cycle tops, but little or no permeability is associated with the fenestral pores that dominate these caps.



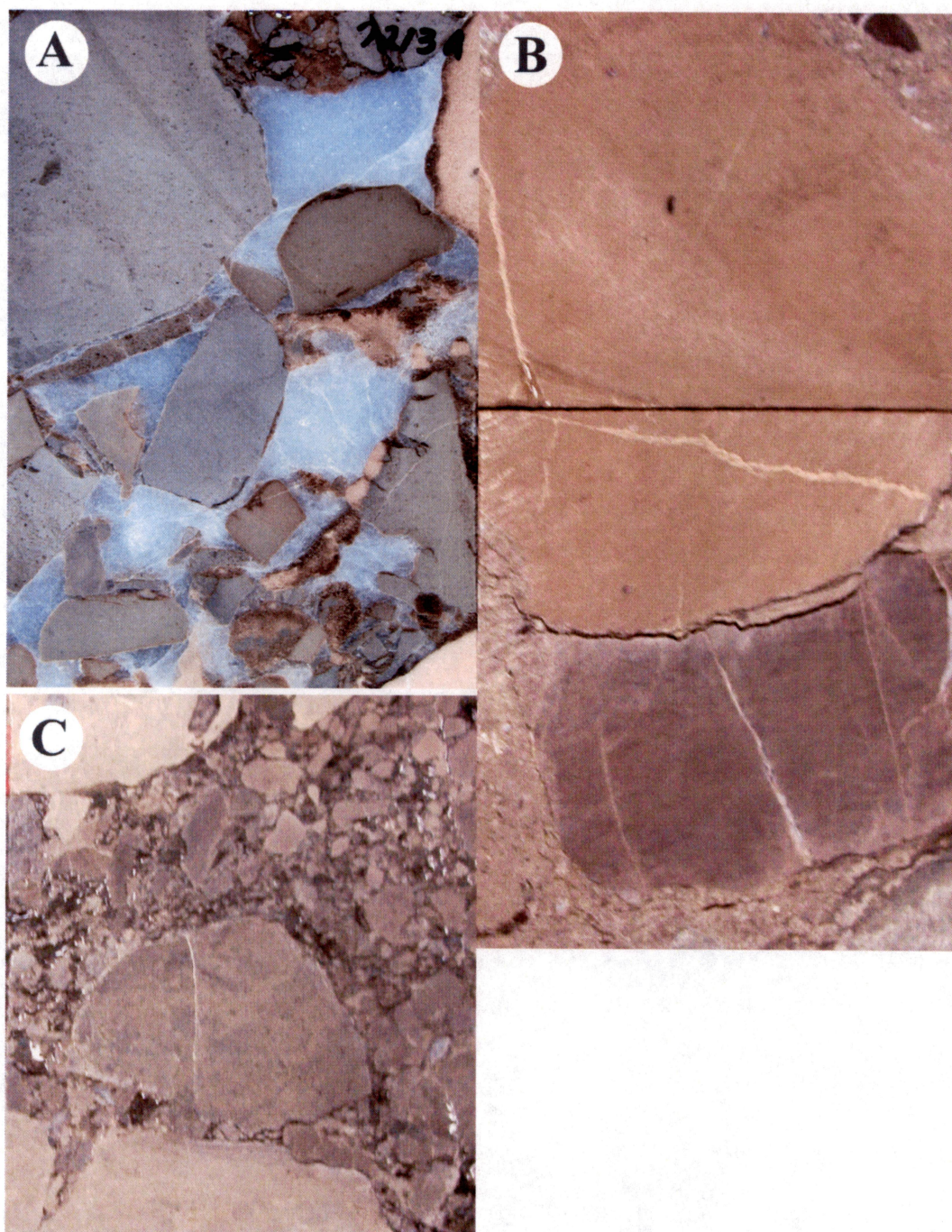


Figure 31. Core slab photos of polymict conglomerate in the Wichita Formation of probable karst origin. A. Amoco University Consolidated # IV-25, depth: 7,213 ft. B. FCU 6122, depth: 7,254 ft. C. FCU 6122, depth: 7,201 ft. All cores are 4 inches wide.





Figure 32. Core slab box photo of breccias developed at the Abo/Wichita contact in FM-1 core. Amoco University Consolidated # IV-25, depths: 7,211–7,228 ft. Core pieces are 4 inches wide.



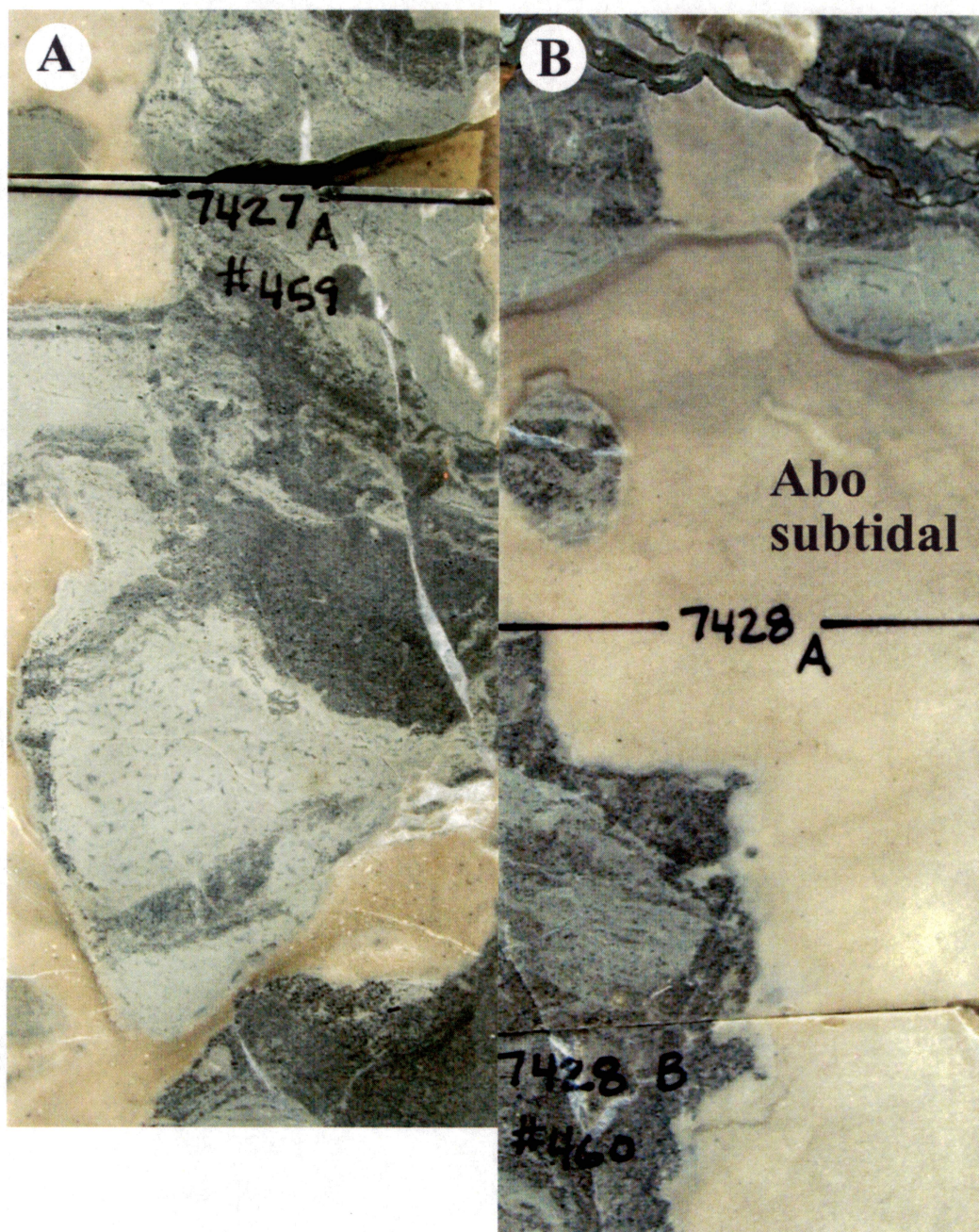


Figure 33. Core slab photos of contact zone of Abo/Wichita. Interrelationships between Abo subtidal facies (light-brown) and silty peritidal wackestones of the Wichita suggest that the contact represented a karsted locally collapsed interval.



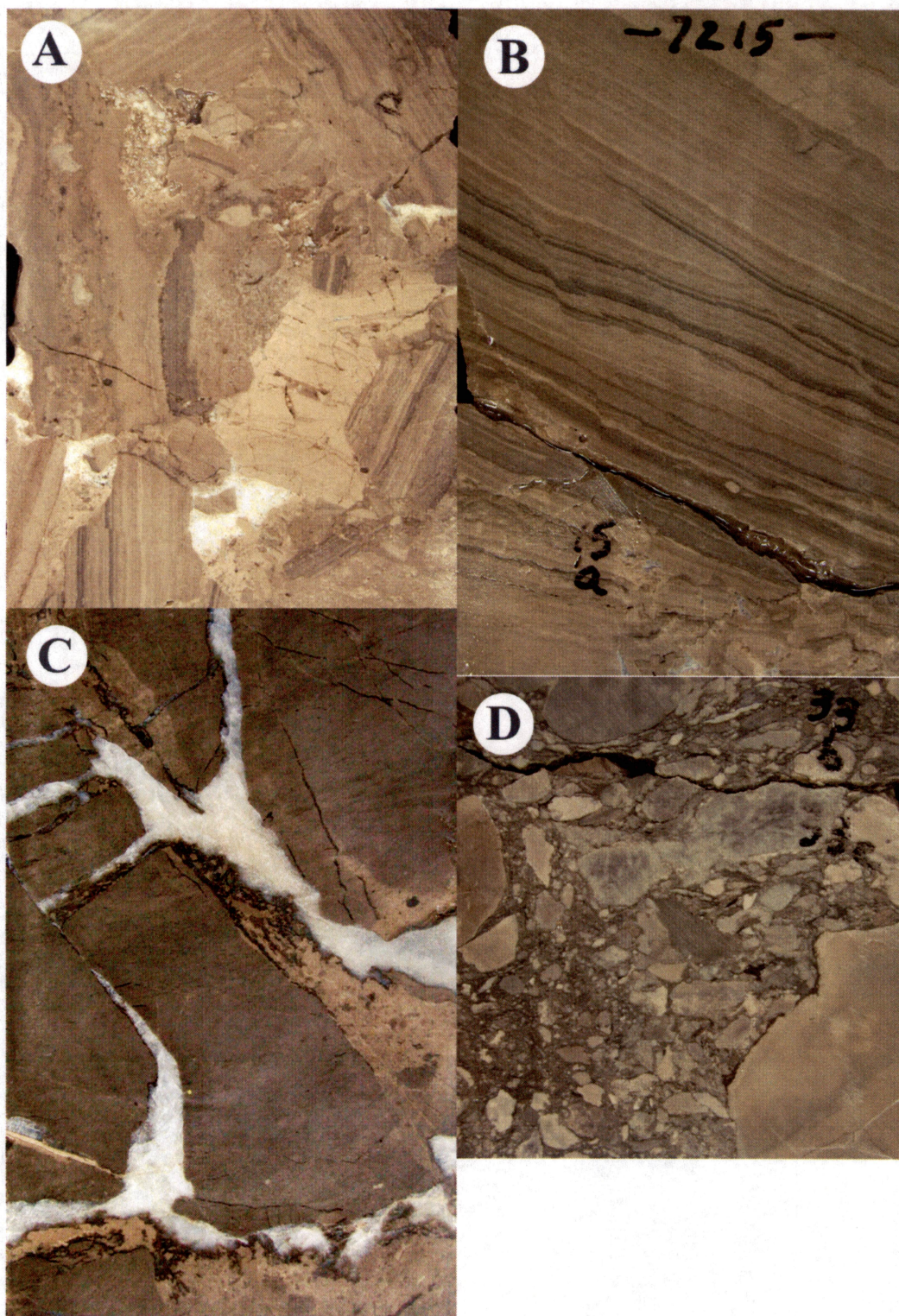


Figure 34. Core slab photos of monomict breccias from the Wichita. A. Rotated clasts of tidal-flat facies. B. Tilted blocks of laminated peritidal facies. Depth: 7,215 ft. C. Brecciated clasts of peloidal wackestone. University Consolidated V 15, depth: 6,899 ft. D. Clasts of peritidal mudstone-wackestone. All cores are 4 inches wide.



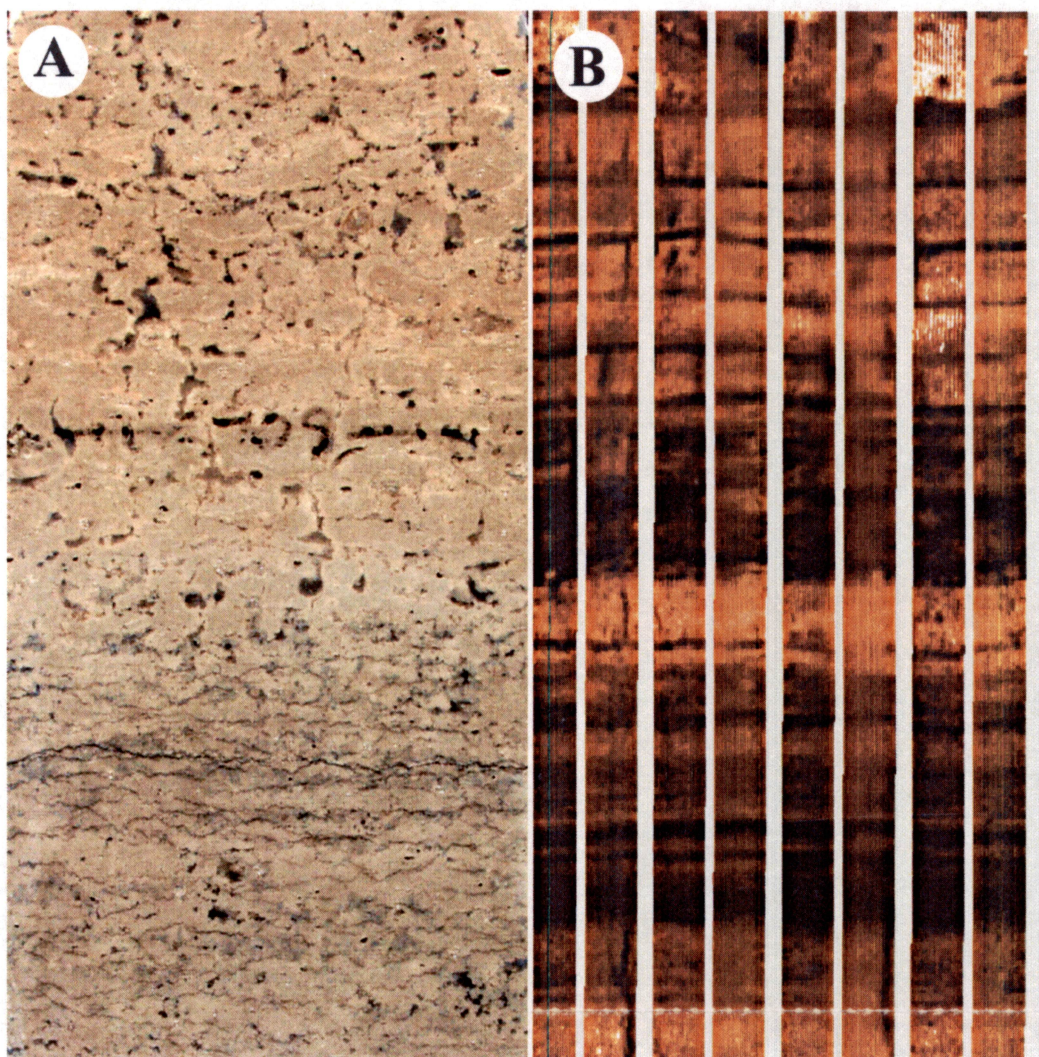


Figure 35. Image log and core photo images of laminated tidal-flat facies. Core: FCU 7322, depth: 6,909 ft. Image log: FCU 2564, depth: 6,900–6,904 ft. Core is 4 inches wide. Lower Clear Fork, HFS L 2.1.



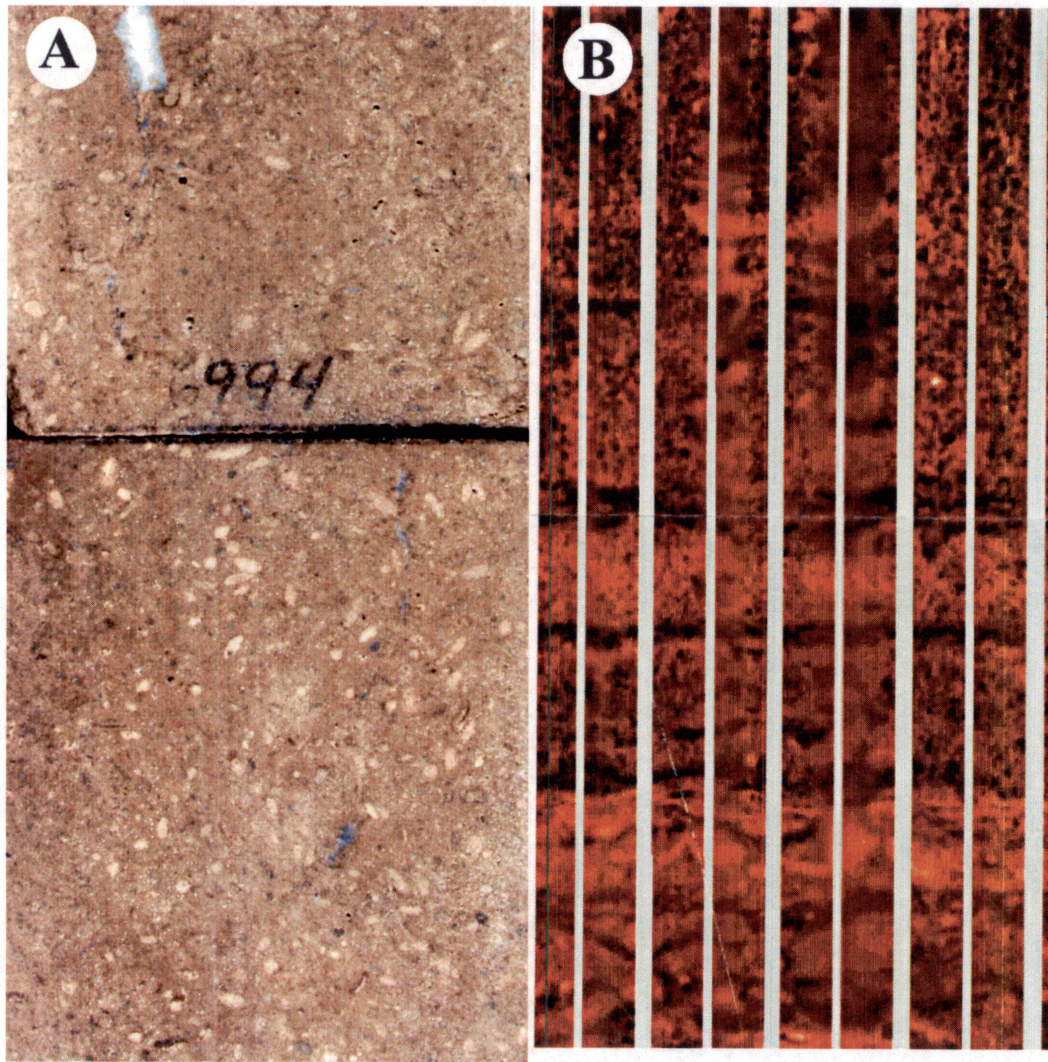


Figure 36. Image log and core photo images of fusulinid wackestone-packstone facies. Lower Clear Fork. Core: FCU 7322, depth: 6,994 ft. Image log: FCU 2564, depth: 6,990–6,994 ft. Core is 4 inches wide.



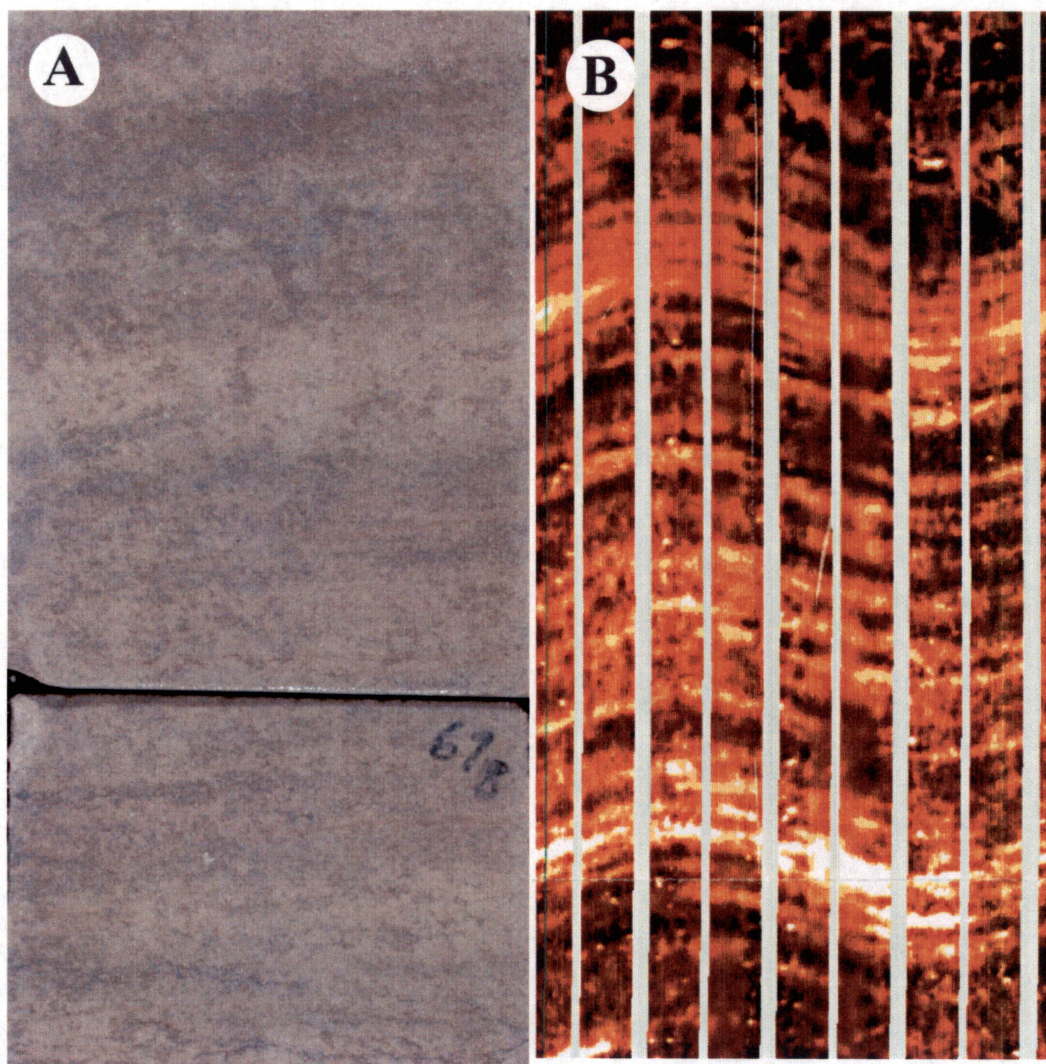


Figure 37. Image log and core photo images of crossbedded grainstone. Lower Clear Fork. Core: FCU 7322, depth: 6,967 ft. Image log: FCU 2564, depth: 7,002–7,005 ft. Core is 4 inches wide.



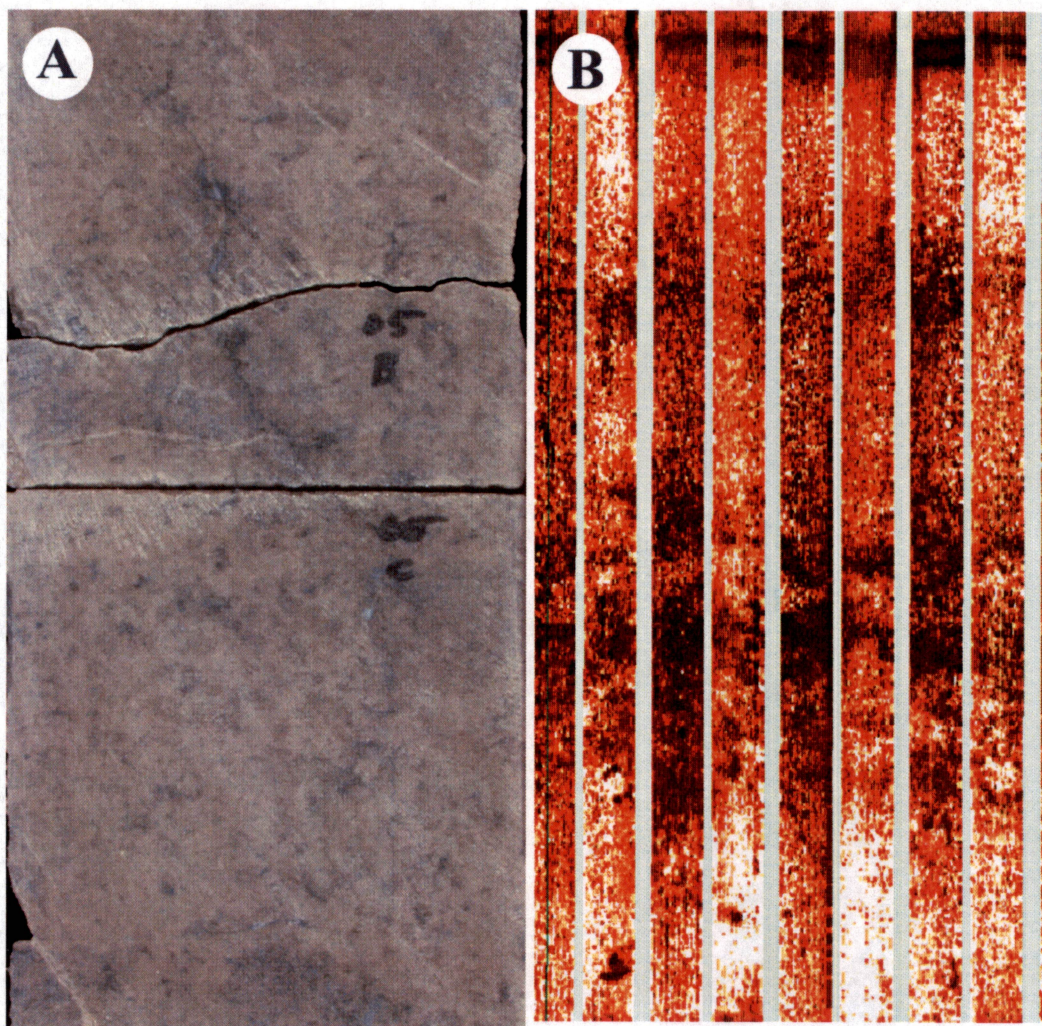


Figure 38. Image log and core photo images of peloid wackestone-packstone facies. Core: FCU 7322, depth: 6,905 ft. Image log: FCU 2564, depth: 6,905–6,909 ft. Core is 4 inches wide. Lower Clear Fork, HFS L 2.2.



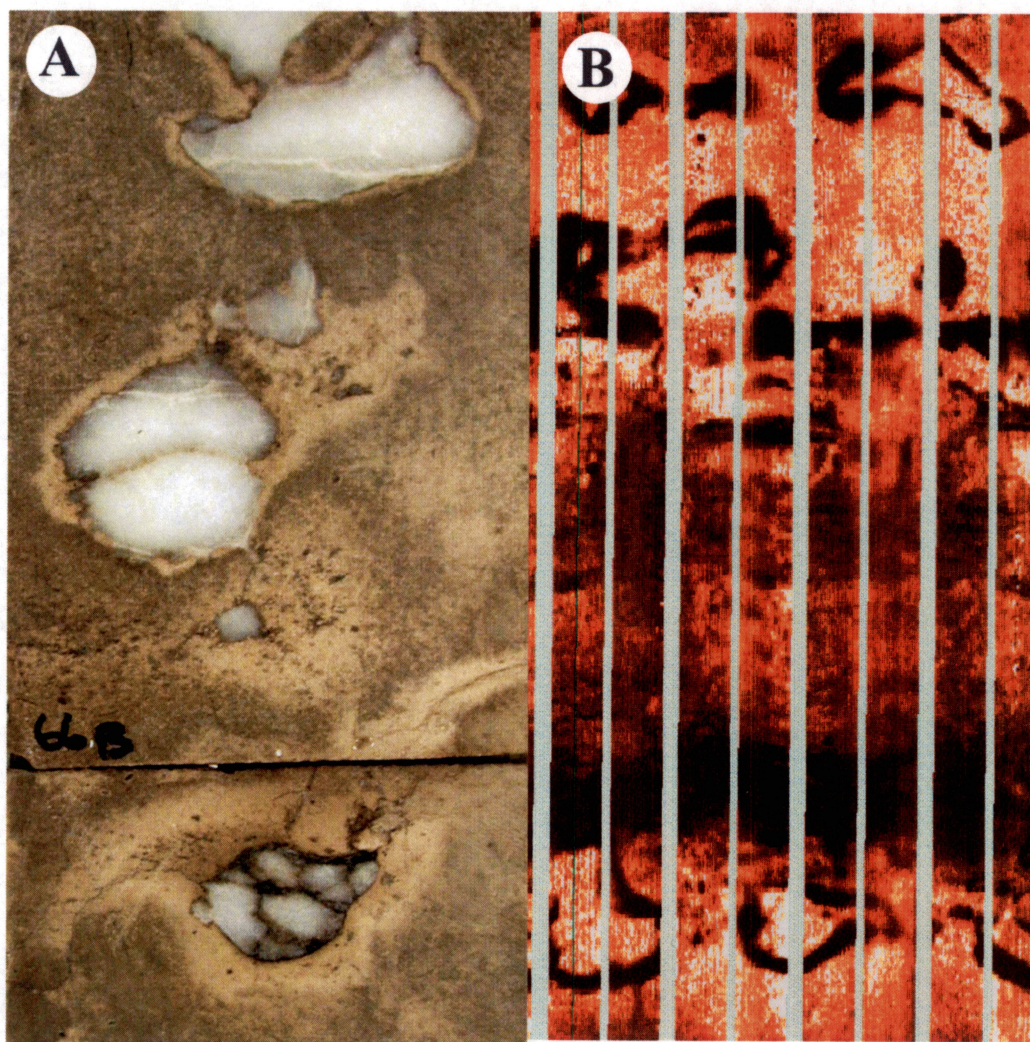


Figure 39. Image log and core photo images of nodular peloid wackestone typical of the Lower Clear Fork HFS L 2.2. Core photo shows anhydrite nodules surrounded by light-colored haloes of higher porosity. Image log displays the same features as white (high-resistivity) masses surrounded by black (low-resistivity owing to the fluid-filled pore space) rims. Core: FCU 6739, depth: 6,989 ft. Image log: FCU 2564, depth: 6,879–6,883 ft. Core is 4 inches wide.



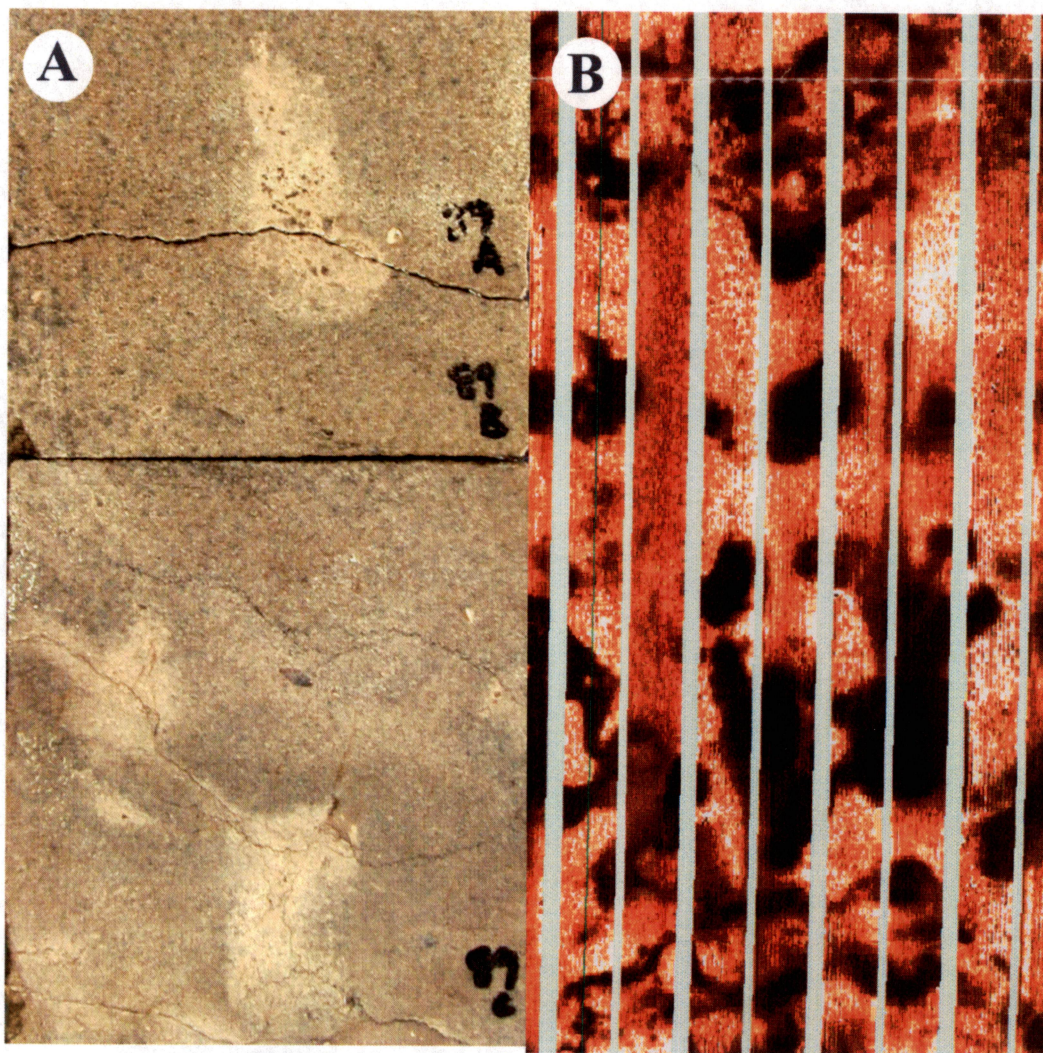


Figure 40. Image log and core photo images of “vuggy” fabric. Image log shows low-resistivity (black) features commonly interpreted to be open vugs. Core photo reveals that “vugs” are actually burrow fills (light-colored) of higher porosity. Lower Clear Fork. Core: FCU 6739, depth: 6,966 ft. Image log: FCU 2564, depth: 6,873–6,877 ft. Core is 4 inches wide.



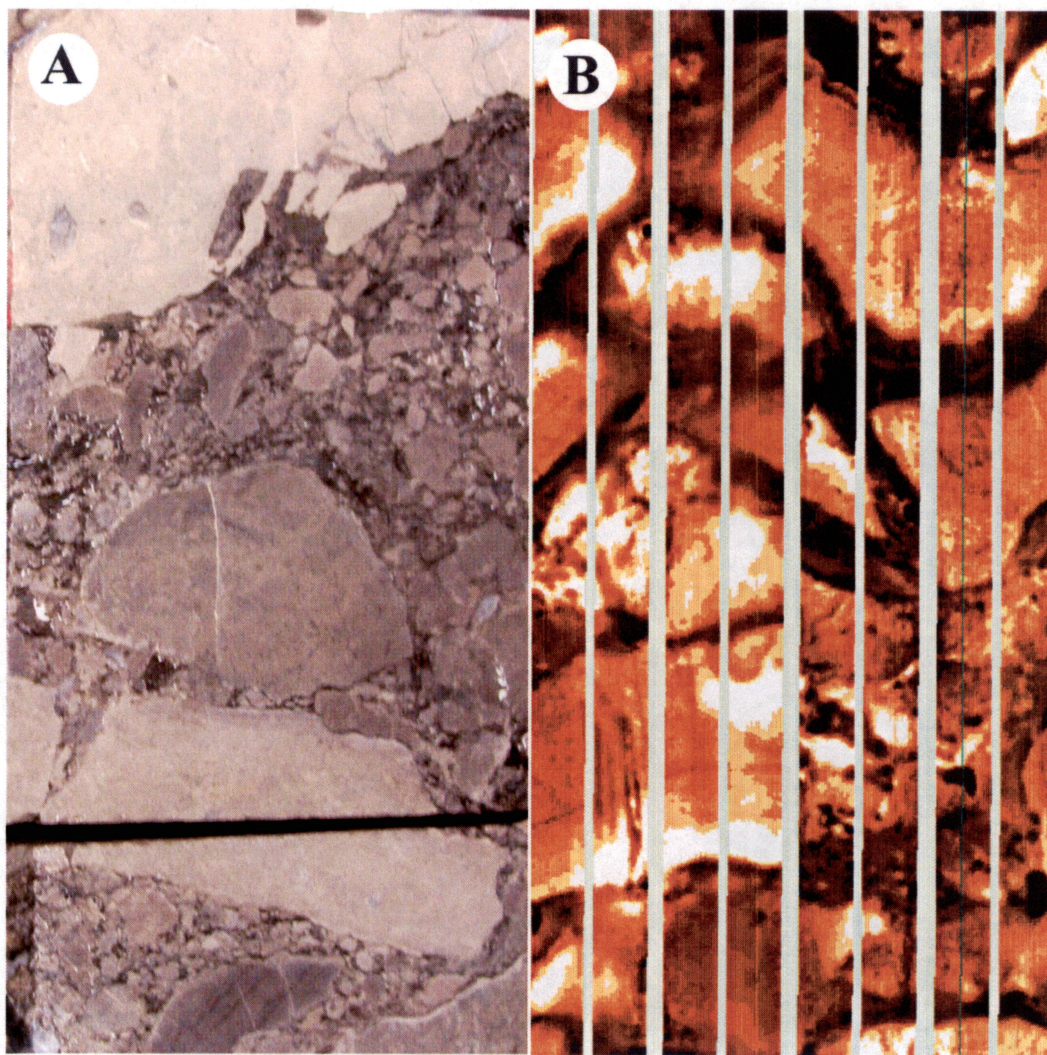


Figure 41. Image log and core photo images of polymict karst conglomerate. Wichita. Core: FCU 6122, depth: 7,201 ft. Image log: FCU 2564, depth: 7,171–7,182 ft. Core is 4 inches wide.



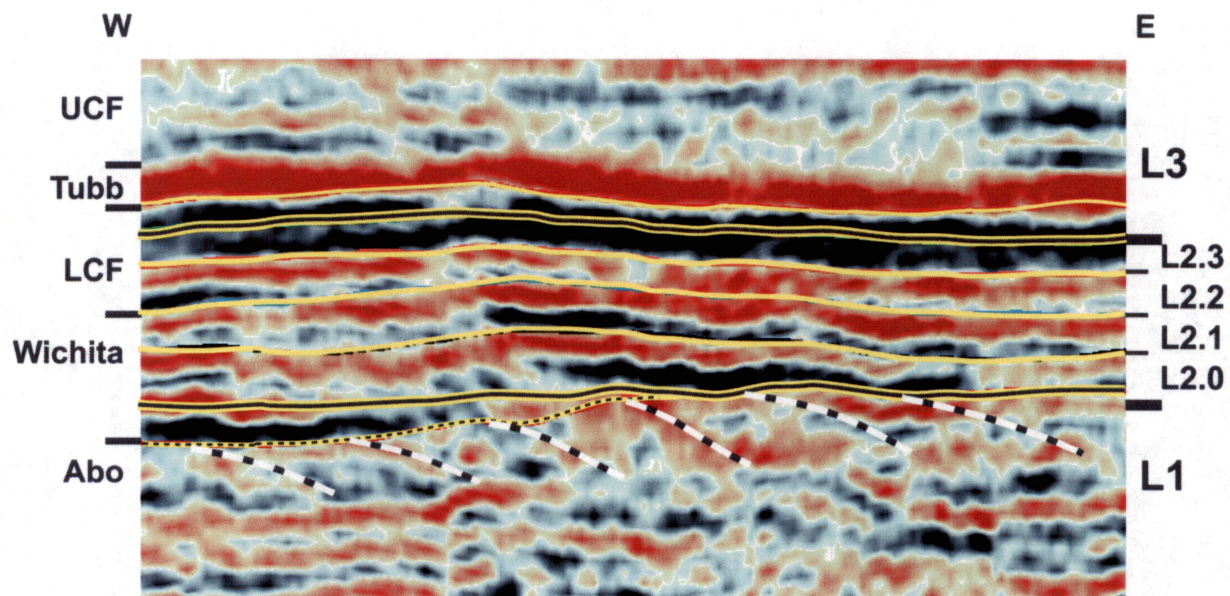


Figure 42. 3-D seismic section from Fullerton field showing general continuity and isopachous nature of Lower Clear Fork and Wichita reservoir intervals. Yellow lines are time lines; dotted line defines the top of Abo Formation.

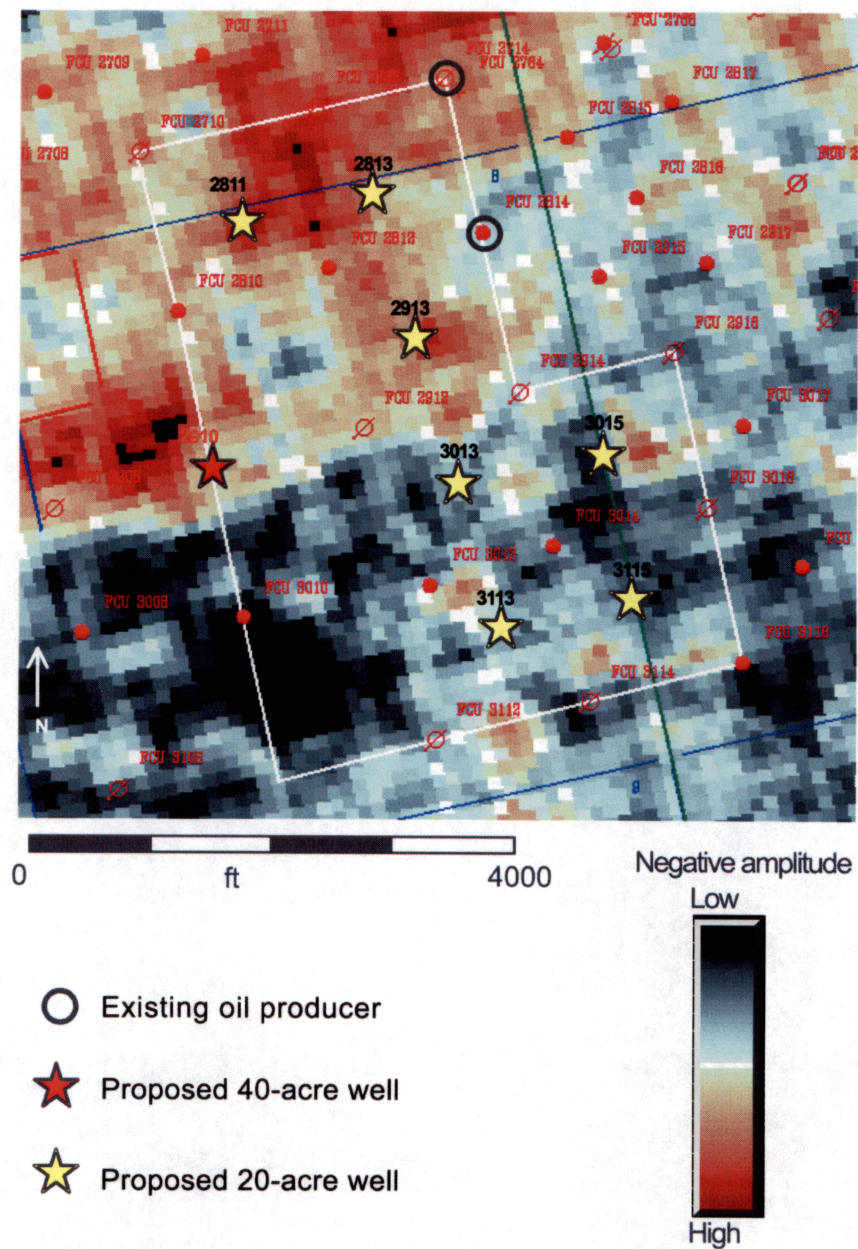


Figure 43. Map of negative amplitude data extracted from Fullerton 3-D data. The data show that proposed wells in the northern half of the area will encounter reservoir porosity, whereas those in the southern half will not.



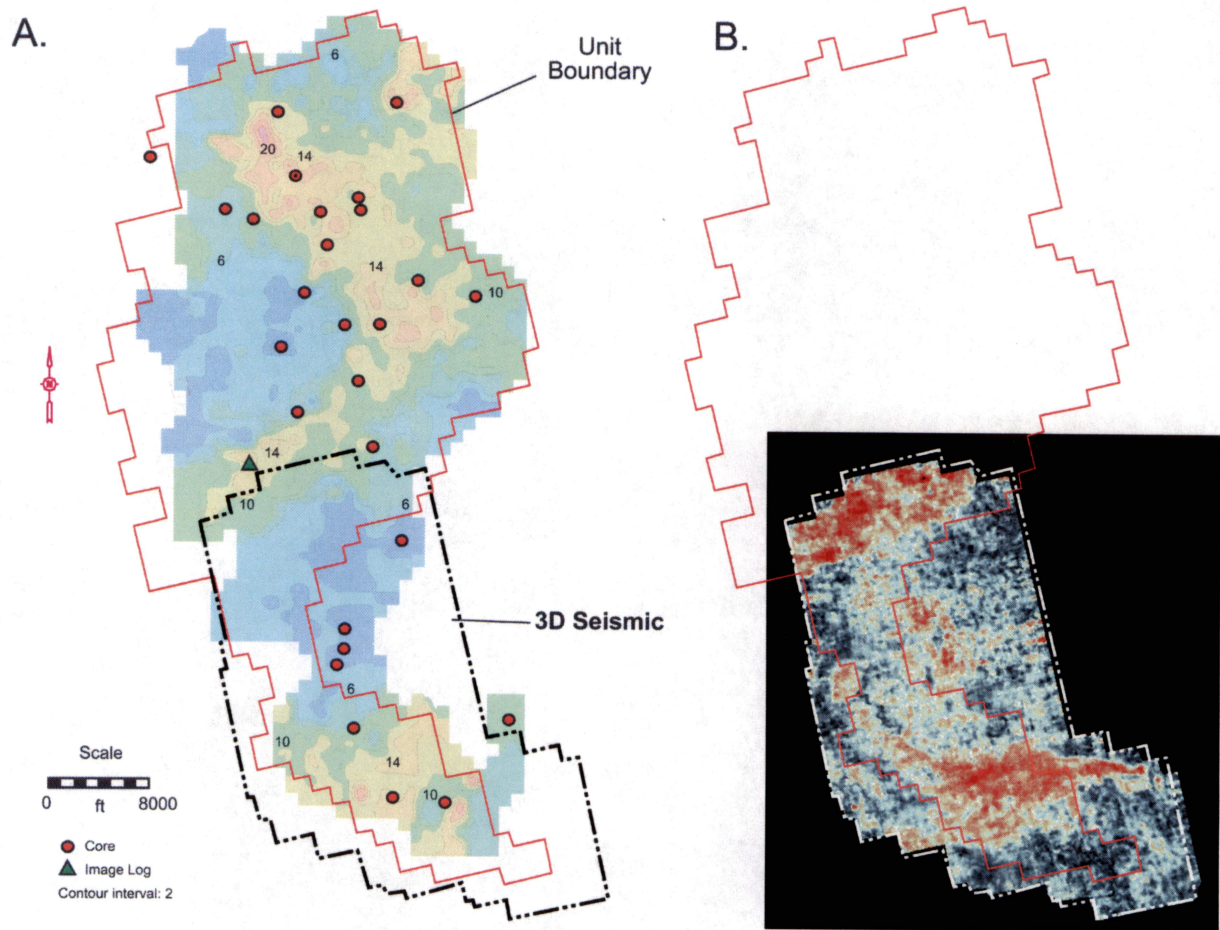


Figure 44. Porosity development in HFS 2.1. A. Map of porosity derived from well-log calculations. B. Map of negative amplitude data extracted from Fullerton 3-D seismic data. Note that the east-west-trending area of negative amplitude in the southern part of the field is not well imaged by wireline log data despite the close spacing of wells.

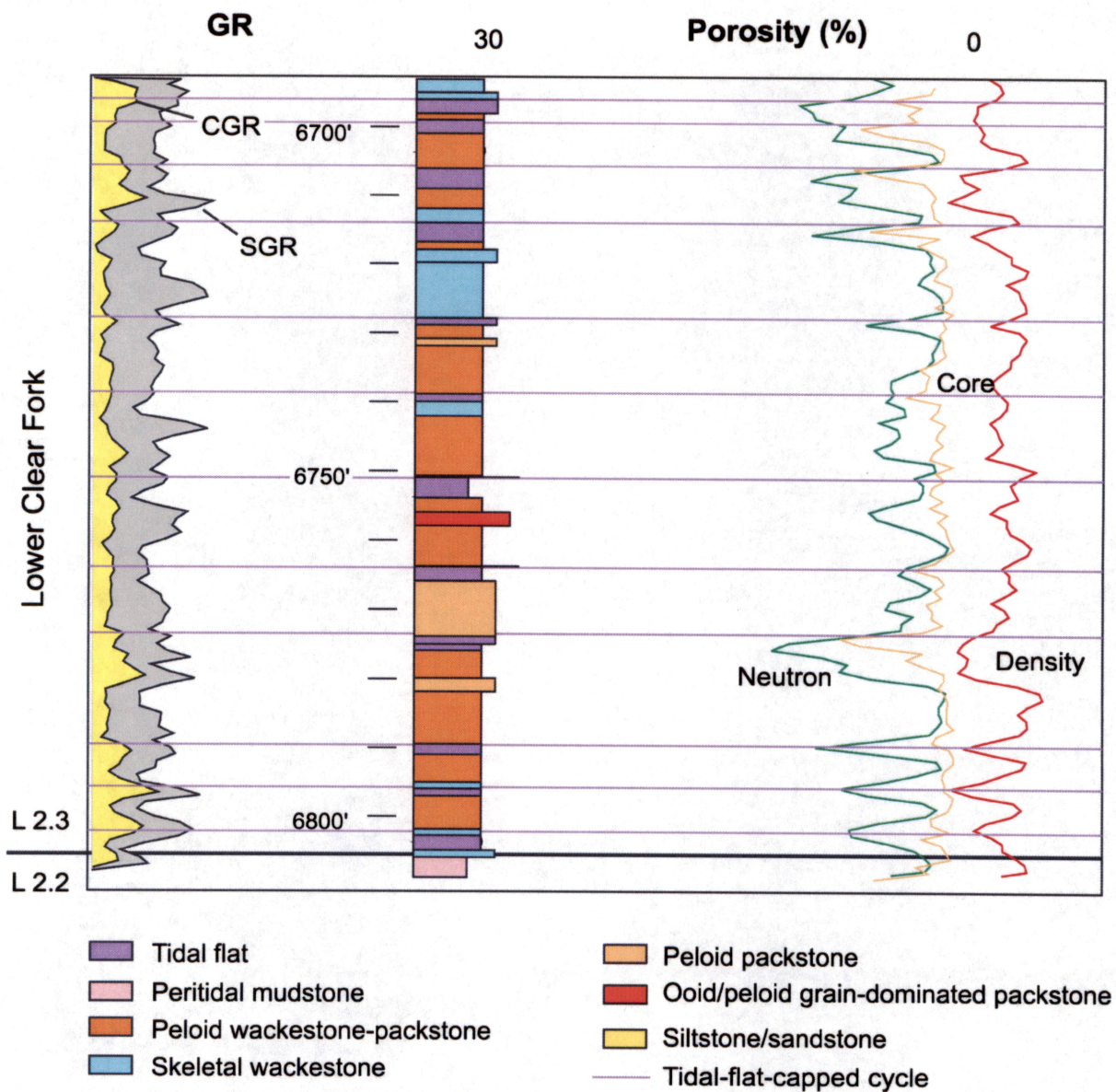


Figure 45. Comparison of core-defined facies and cyclicity with porosity logs in tidal-flat-capped cycles of HFS L 2.3. FCU 6122.



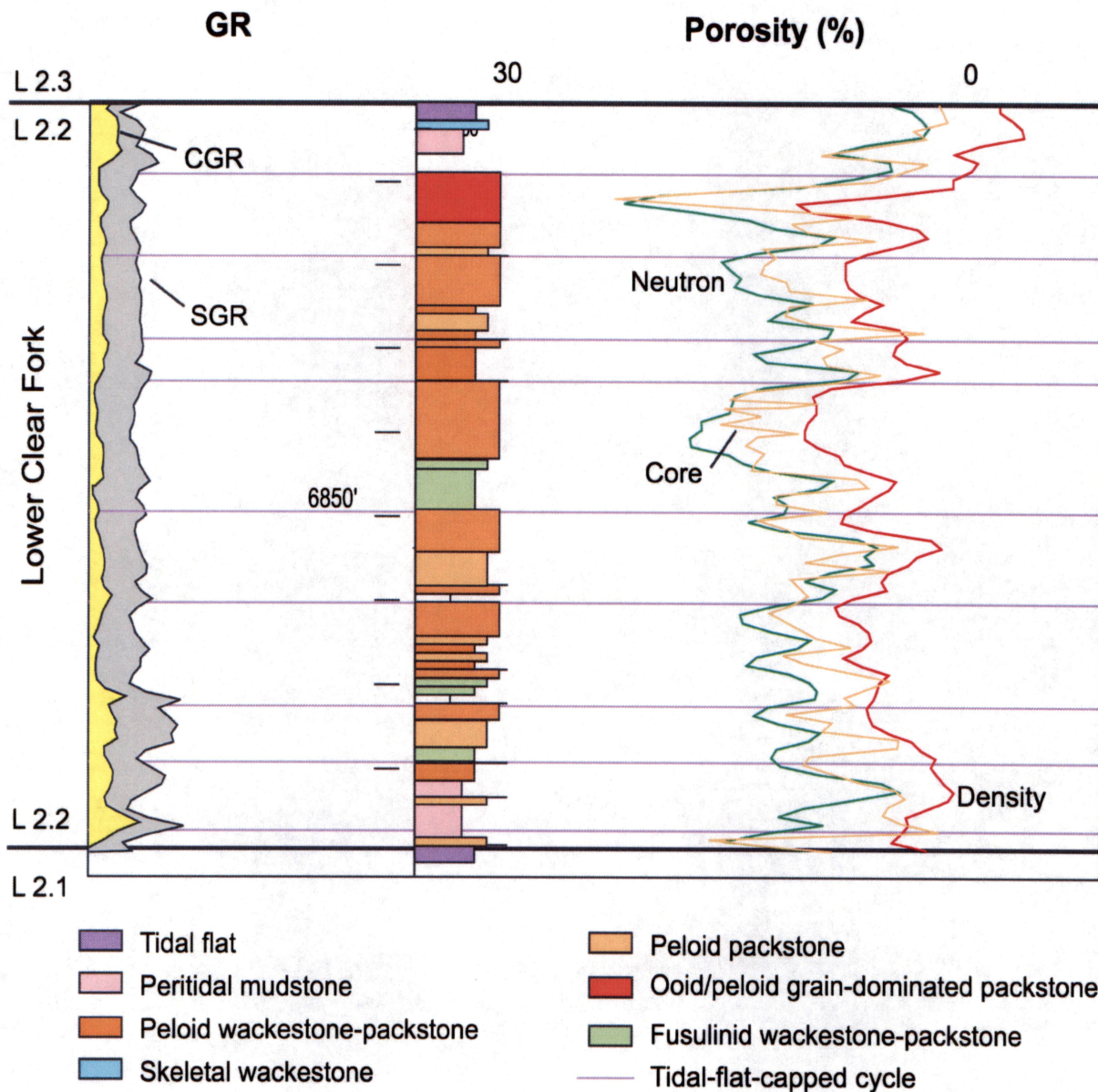


Figure 46. Comparison of core-defined facies and cyclicity with porosity logs in subtidal cycles of HFS L 2.2. FCU 6122.

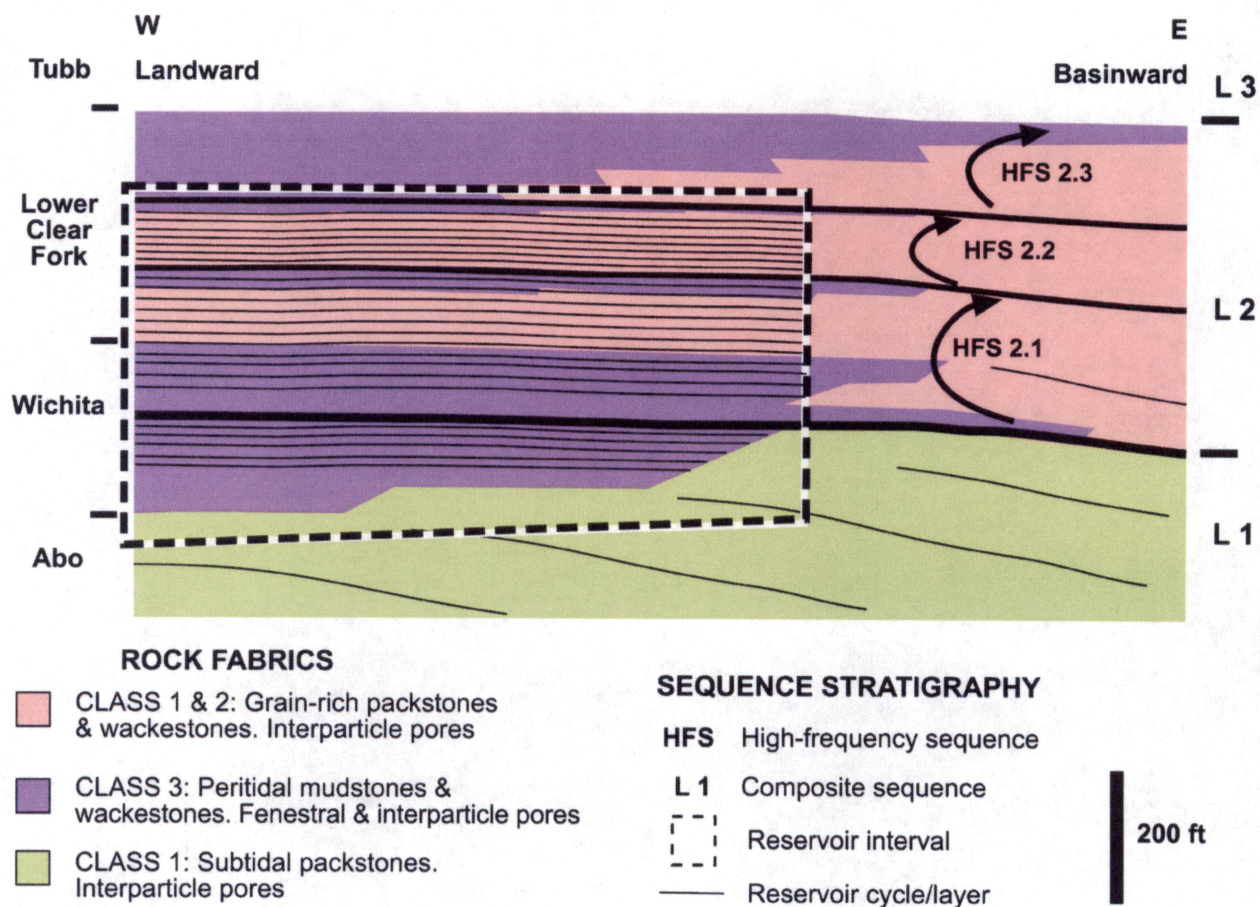


Figure 47. Schematic depiction of reservoir framework used for model construction at the Fullerton Clear Fork reservoir.



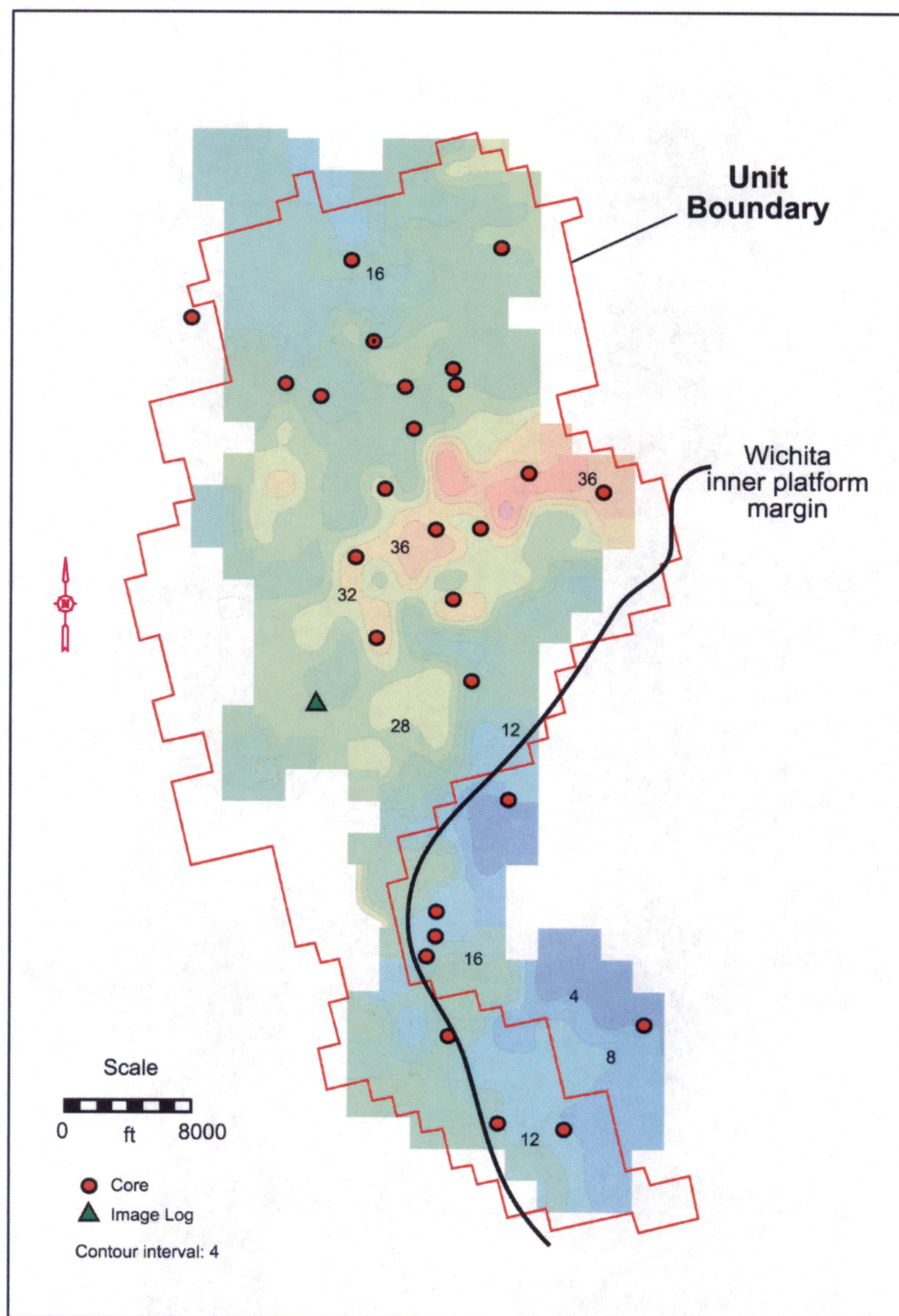


Figure 48. Map of total phi in the Wichita. Low values in the southeastern corner of the field are largely due to the facies change from Wichita tidal-flat facies to Abo facies in that area.

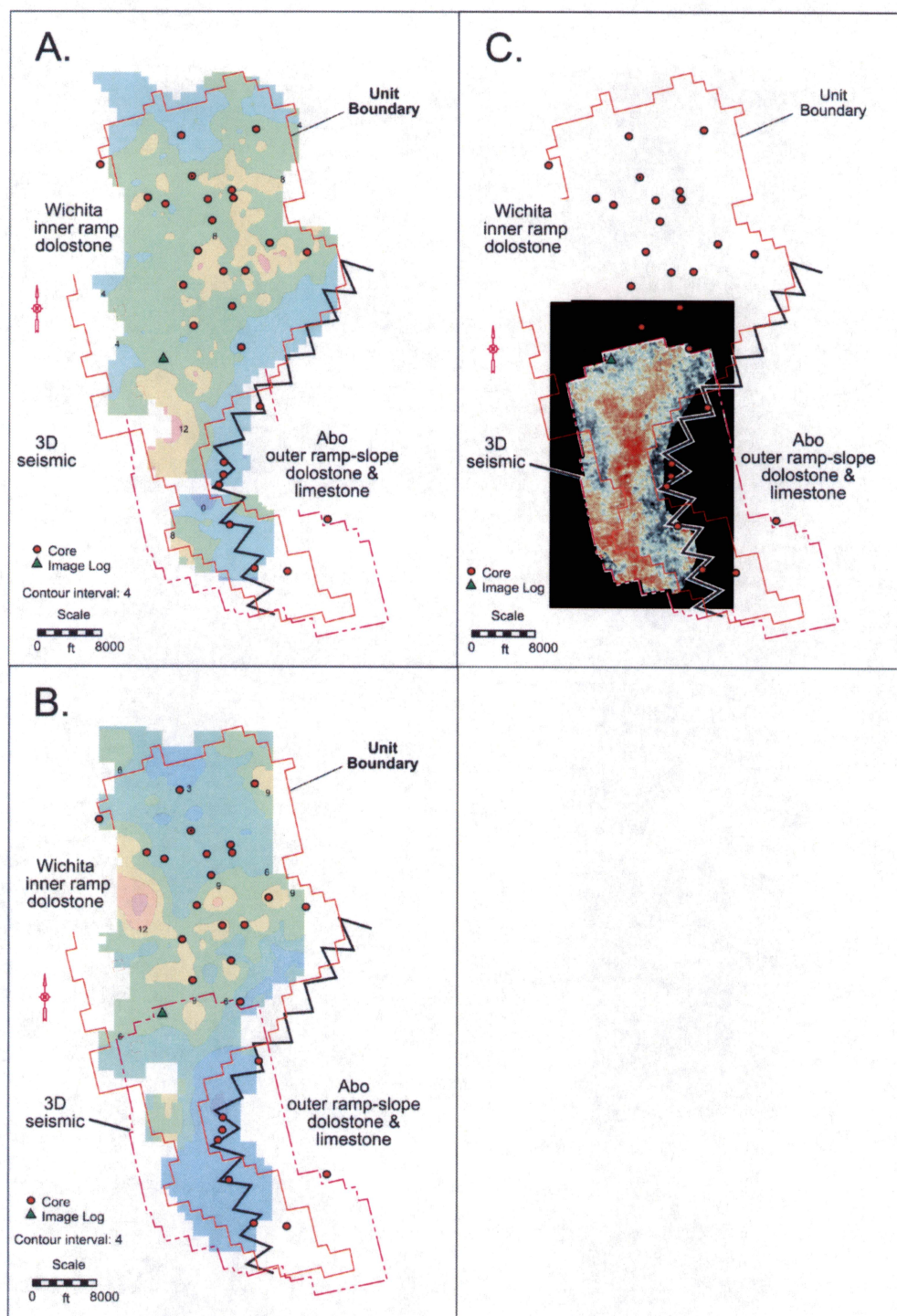


Figure 49. Maps of porosity distribution in the lower and upper parts of the lower Wichita (Sequence L 1). A. Phih map from wireline logs of the upper part of the lower Wichita (reservoir cycle/layers W8-W11). B. Phih map from wireline logs of the base of the lower Wichita (reservoir cycle/layer W12). C. Amplitude extraction from 3-D seismic volume for combined lower Wichita section. High negative amplitude equals high porosity. Zigzag line represents Wichita-Abo facies transition. Lower Wichita rocks are absent east of this line.



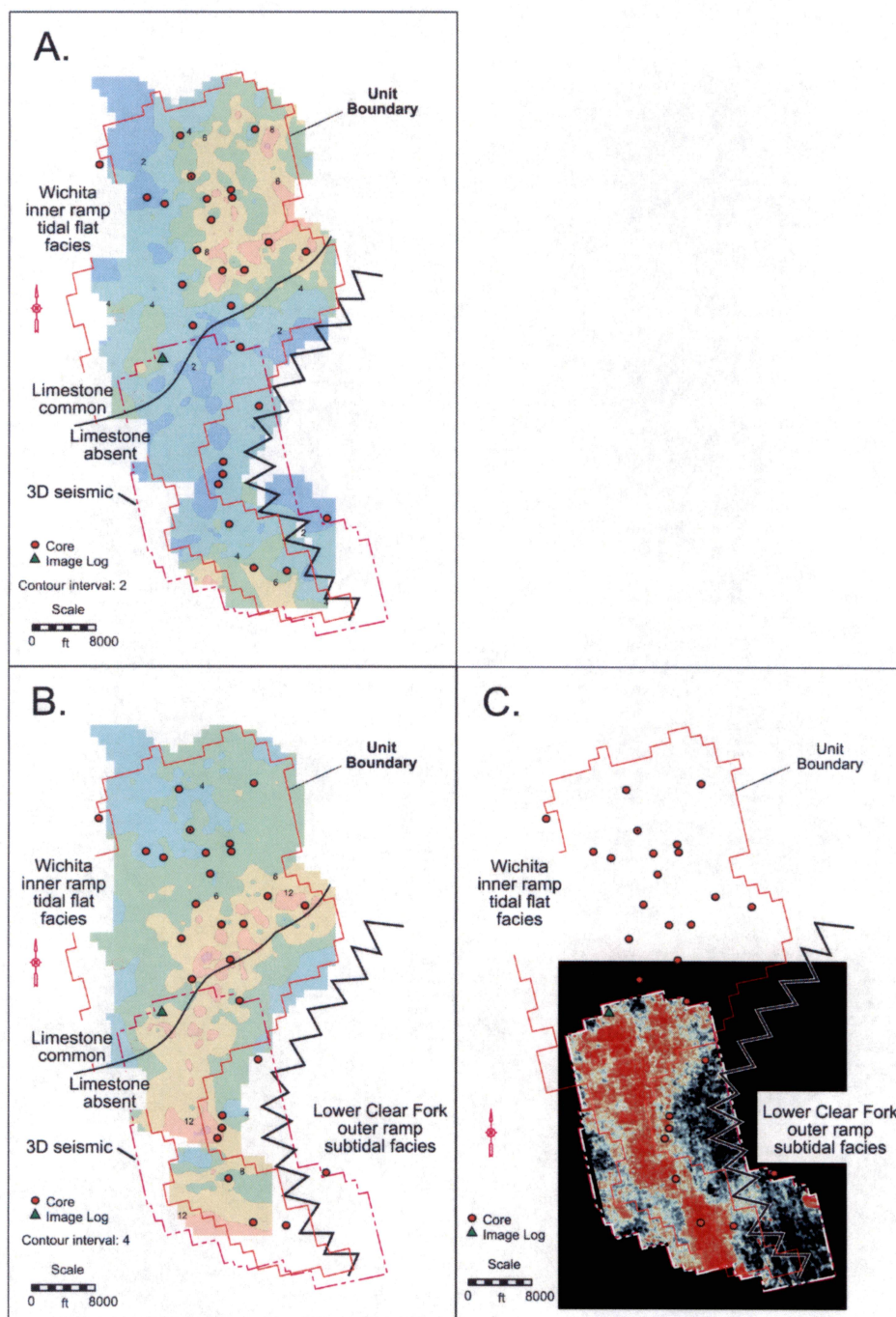


Figure 50. Maps of porosity distribution in the lower and upper parts of the upper Wichita (Sequence L 2.0). A. Phi<sub>h</sub> map from wireline logs of the upper part of the upper Wichita (reservoir cycle/ layers W1–W4). B. Phi<sub>h</sub> map from wireline logs of the base of the upper Wichita (reservoir cycle/ layers W4–W5). C. Amplitude extraction from 3-D seismic volume for combined upper Wichita section. High negative amplitude equals high porosity. Zigzag line represents Wichita–Lower Clear Fork facies transition. Upper Wichita rocks are absent east of this line. Note that porosity is concentrated along an arcuate belt that follows the outer edge of the Wichita inner platform tidal-flat complex.

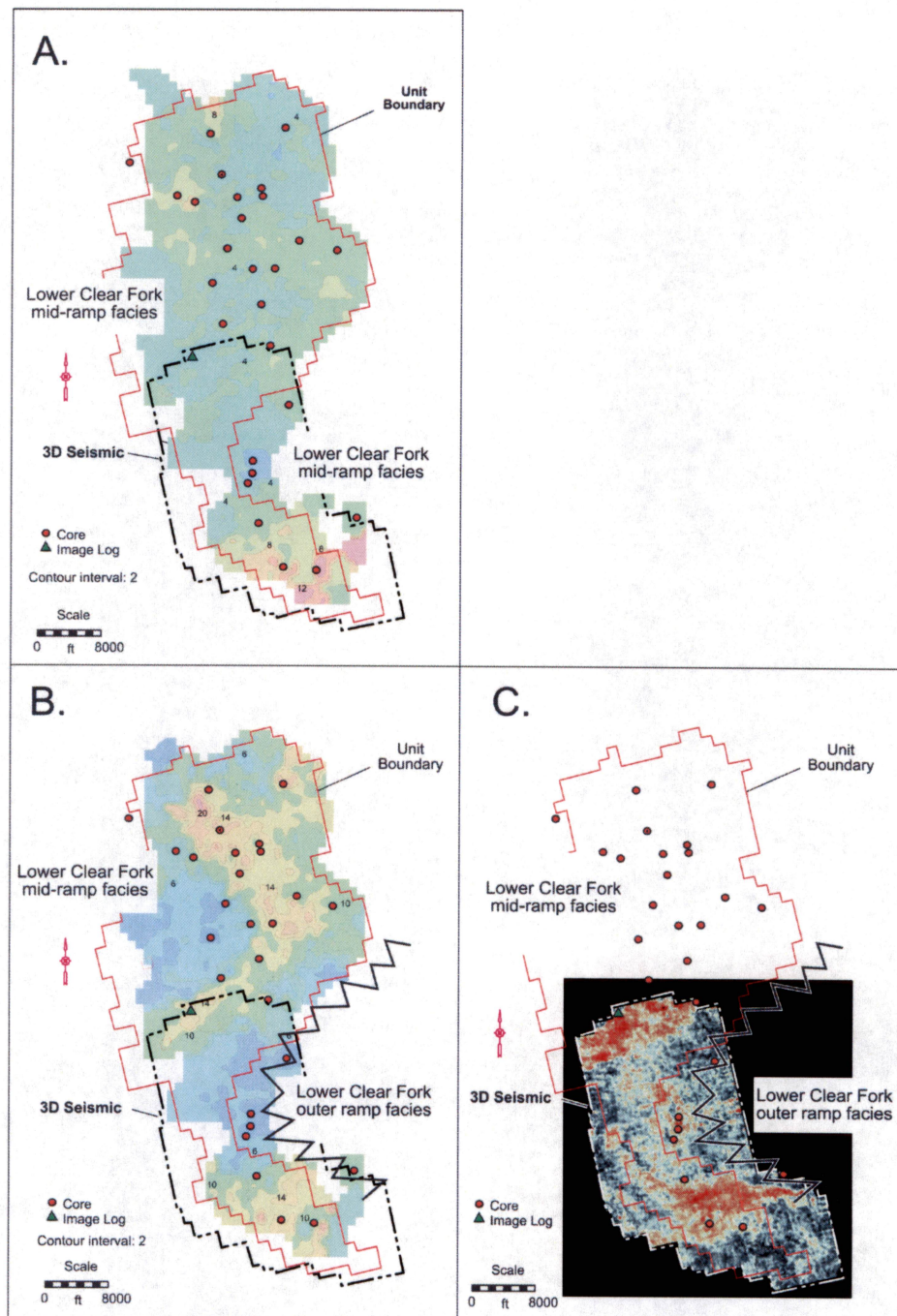


Figure 51. Maps of porosity distribution in the Lower Clear Fork. A. Pih map of HFS 2.2 from wireline logs. B. Pih map of HFS L 2.1. C. Amplitude extraction from 3-D seismic volume for HFS L 2.1 interval. High negative amplitude equals high porosity. Areas of high porosity in HFS L 2.1 and HFS L 2.2 correlate with areas of abundant limestone. Compare with figures 23 and 25.



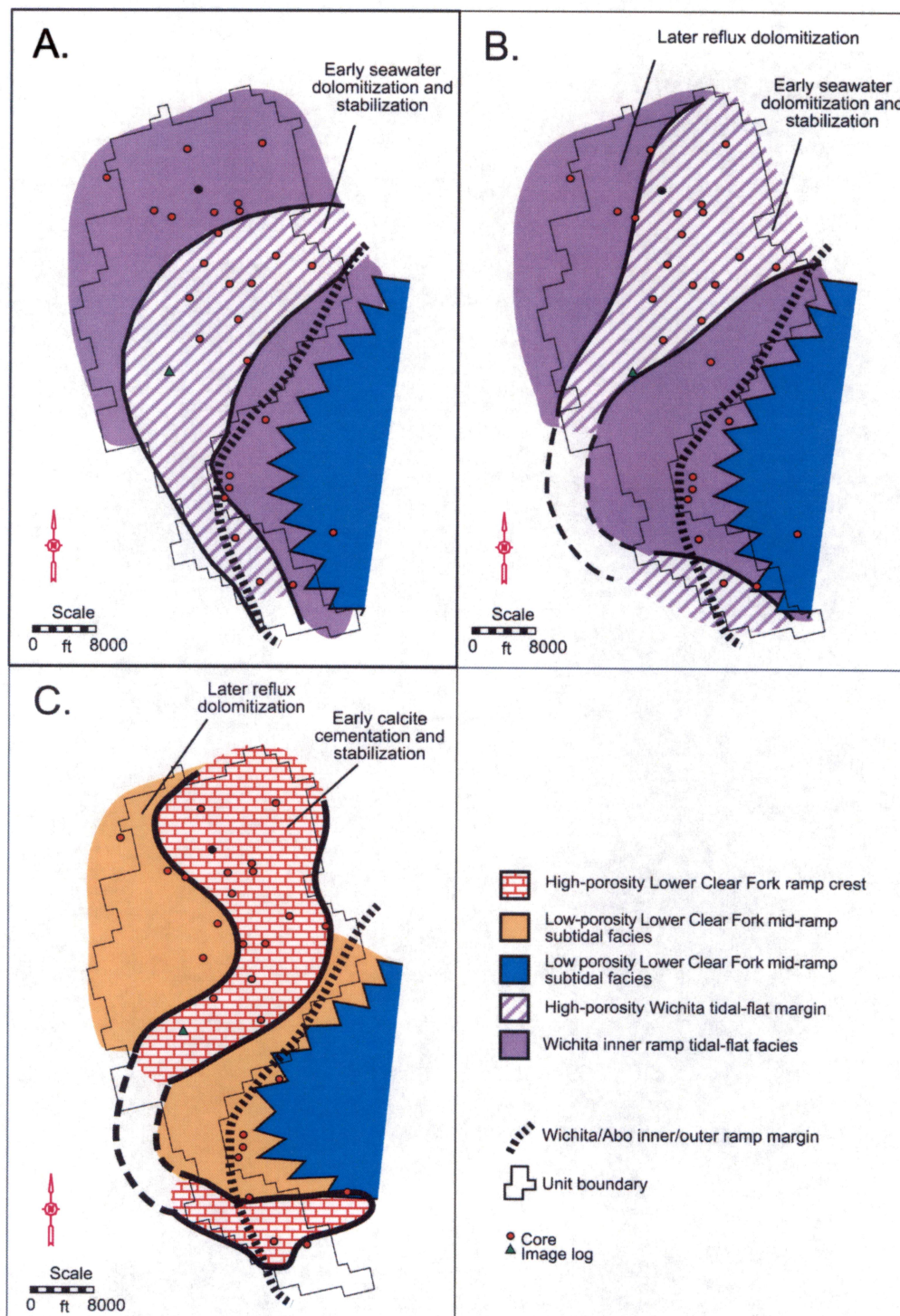


Figure 52. Models of porosity formation in the upper Wichita and the Lower Clear Fork (L2 sequence).

INTEGRATION OF ROCK FABRIC, PETROPHYSICAL CLASS,  
AND STRATIGRAPHY FOR PETROPHYSICAL QUANTIFICATION OF  
SEQUENCE-STRATIGRAPHIC FRAMEWORK,  
FULLERTON CLEAR FORK FIELD, TEXAS

Rebecca H. Jones and F. Jerry Lucia

Bureau of Economic Geology  
Scott W. Tinker, Director  
John A. and Katherine G. Jackson School of Geosciences  
The University of Texas at Austin  
Austin, Texas 78713-8924

ABSTRACT.....	125
INTRODUCTION .....	126
METHODS .....	128
RESULTS .....	129
Abo Formation .....	130
Wichita Formation .....	130
Lower Clear Fork Formation .....	131
Lower Clear Fork L2.0 .....	131
Lower Clear Fork L2.1 .....	132
Lower Clear Fork L2.2 .....	133
Lower Clear Fork L2.3 .....	134
DISCUSSION.....	135
Limitations Due to Petrophysical Data Distribution.....	135
CONCLUSIONS.....	137
ACKNOWLEDGMENTS .....	138
REFERENCES .....	139
APPENDIX I: ROCK-FABRIC INSTRUCTIONS: Classifying Carbonate Pore Space from Thin Sections.....	157

### Figures

1. Diagram showing fabrics composing petrophysical classes 1, 2, and 3 and a cross plot showing interparticle porosity vs. permeability, petrophysical class fields, and associated transforms .....	141
2. Photomicrographs of class 1 fabrics observed in this study .....	142
3. Photomicrographs of class 2 fabrics observed in this study .....	143
4. Photomicrographs of class 3 fabrics observed in this study .....	144
5. Location and boundaries of Fullerton field, Andrews County, Texas .....	145



6. Type log showing nomenclature used in this study and general vertical stacking of petrophysical classes.....	146
7. Porosity-permeability plot of old Abo interval core analysis from wells throughout the field with core described in this study .....	147
8. Photomicrographs of tidal-flat, class 3 fabrics observed in this study .....	148
9. Distribution of limestone, dolostone, and petrophysical classes in the Wichita.....	149
10. Wichita facies core analysis porosity-permeability plot and petrophysical class 3 transform used to calculate permeability .....	150
11. Plot and histogram for Lower Clear Fork L2.1 subtidal unit high-resolution samples from wells FCU 5927 and 6429 .....	151
12. Porosity-permeability plot of core analysis from wells with core displaying dominantly class 1 fabrics in the subtidal portion of high-frequency sequence L2.1 .....	152
13. Regions of different petrophysical classes and mineralogy in the subtidal portion of HFS L2.1 .....	153
14. Regions of different petrophysical classes and mineralogy in HFS L2.2.....	154
15. Porosity-permeability plot of Lower Clear Fork L2.2 showing that most samples plot in the class 1 field and photomicrograph example of poikilotopic anhydrite in a class 2 medium-crystalline dolostone .....	155
16. Typical preexisting core analysis data vs. core analysis data resulting from unbiased sampling and careful cleaning of plugs .....	156

# Integration of Rock Fabric, Petrophysical Class, and Stratigraphy for Petrophysical Quantification of Sequence-Stratigraphic Framework, Fullerton Clear Fork Field, Texas

Rebecca H. Jones and F. Jerry Lucia

## ABSTRACT

A major task in building a reservoir model is quantifying the geologic framework with petrophysical properties. Porosity and water saturation values can be obtained from wireline logs, but permeability is a rock property that cannot be obtained directly from logs. The traditional approach is to construct a single porosity-permeability transform to estimate permeability from porosity logs. In this study rock-fabric-specific porosity-permeability transforms are used together with the porosity log to estimate permeability. The numerous rock fabrics described from this field are grouped into three petrophysical classes, each having its unique transform, and the petrophysical classes are linked to stratigraphy through the study of high-resolution thin sections and core descriptions. The lowest stratigraphic unit studied in detail is the Wichita, which is composed dominantly of peritidal facies. It contains mostly fine-crystalline mud-dominated dolostones and mud-dominated limestones, all of which plot in the petrophysical class 3 field. Sequence L2.1 of the Lower Clear Fork contains an upper tidal-flat unit and a lower subtidal unit. The upper tidal-flat unit is composed of class 3 fine-crystalline mud-dominated fabrics similar to the Wichita. This unit extends over the entire field. The lower subtidal unit contains both limestone and dolostone. The dolostones are mostly medium-crystalline, subtidal grain-dominated dolopackstones and medium-crystalline mud-dominated dolostones that plot in the petrophysical class 2 field. Less common are intervals of oomoldic lime grainstone that also tend to plot in the petrophysical class 2 field on a porosity-permeability

cross plot. Grainstone is a class 1 rock fabric that plots in the class 2 field because total porosity—not interparticle porosity—is used. Interparticle porosity could not be calculated because of the lack of acoustic logs, and a class 2 transform was assigned to the limestones. In some areas old core analysis data suggest the presence of class 1 coarse-crystalline dolostones and anhydritic medium-crystalline dolostones. All other areas in the lower portion of sequence L2.1 are characterized by petrophysical class 2. The Lower Clear Fork sequence L2.2 is a class 2 medium-crystalline dolostone fabric that plots in the class 1 field because of the presence of large volumes of poikilotopic anhydrite. The sequence is characterized by a class 1 transform with the exception of a few areas of oomoldic limestone, which are characterized by a class 2 transform. The uppermost sequence in the Lower Clear Fork, L2.3, is composed of fine-crystalline dolostone class 3 peritidal facies and is characterized by a class 3 transform.

## INTRODUCTION

The theory and development of the rock-fabric approach for quantifying geologic models was first described by Bureau of Economic Geology researchers Kerans, Lucia, and Senger (1994), Lucia (1995, 1999), and Jennings and Lucia (2001). This approach has been used successfully in a number of studies characterizing other Permian Basin carbonate reservoirs, including the San Andres at Seminole field (Lucia et al., 1995; Wang et al., 1998); the Clear Fork at South Wasson field (Lucia and Jennings, 2002), and the Grayburg at South Cowden field (Lucia and Ruppel, 1996; Ruppel and Lucia, 1996; Lucia, 2000).

The goal of the rock-fabric approach is to better understand permeability and original water saturation distribution in carbonate reservoirs. However, unlike porosity and water saturation, permeability cannot be measured by wireline tools and therefore is not easily obtainable. Research at the Bureau of Economic Geology has shown that permeability and water



saturation are a function of rock fabric and interparticle porosity. The three basic rock fabrics are (1) grainstone or dolograins, (2) grain-dominated packstone or dolopackstone, and (3) mud-dominated fabrics composed of mud-dominated packstone, wackestone, and mudstone and modified by dolomite crystal size. These fabrics are grouped into three petrophysical classes and given rock-fabric-specific porosity-permeability transforms (fig. 1), assuming that only interparticle pore space is present. Petrophysical class 1 rock fabrics include grainstones, dolograins, and coarse-crystalline ( $>100\ \mu\text{m}$ ) dolostones (fig. 2); class 2 fabrics include grain-dominated packstones, grain-dominated dolopackstones, and medium-crystalline (20 to  $100\ \mu\text{m}$ ) dolostones (fig. 3); and class 3 fabrics include mud-dominated packstones, wackestones, and mudstones and their fine-crystalline ( $<20\ \mu\text{m}$ ) dolomitized counterparts (fig. 4).

Previous studies have shown that each petrophysical class has a respective porosity-permeability transform (fig. 1), which can be used to estimate permeability when interparticle porosity and petrophysical class can be determined from wireline logs. A complete suite of wireline logs is necessary to identify the rock-fabric petrophysical class. In the Fullerton Clear Fork field, however, there are few complete suites of wireline logs and the reservoir has been under waterflood for over 40 years. Therefore, this study was restricted to using gamma-ray logs and various types of porosity logs (Kane, this report). Consequently, separate-vug porosity, and thus interparticle porosity, could not be determined from logs, and relationships between total porosity and permeability had to be established. Likewise, petrophysical class could not be determined from porosity logs.

In this study, a new approach to determining petrophysical class was developed using the relationship between stratigraphy and petrophysical class. This approach is based on the concept

that petrophysical class is a product of rock fabrics and their dolomitization overprint and that this link between geologic description and petrophysical properties should result in a predictable relationship between petrophysical properties and stratigraphy. This report details the development of this relationship.

## METHODS

Initial rock-fabric descriptions were done in the flow simulation area located in the north-central part of the field, where data quality and quantity are greatest (fig. 5). Two cores were resampled throughout the productive interval; 384 plugs were drilled from FCU 5927 and 111 samples from FCU 6429. New plugs were cut from every foot of core and analyzed for porosity and permeability. Thin sections were made from a wafer sliced from the end of each plug. Later, matching thin sections and core analyses were obtained in a similar manner from 210 samples of a core from FCU 7630 (fig. 5). New thin sections (245) were obtained from several other cores in the north-central part of the field (FCU 6429, FCU 6229, FCU 6122) and in the southern part of the field (FCU 4828, Univ. Cons. IV-25) as a check on rock-fabric interpretations.

Existing petrophysical data sets and thin sections were used to fill in the areas between the control wells. Data from 787 existing thin sections from 14 wells and whole core analyses from 63 wells were used. Neutron/density and PEF logs from 108 wells were used to determine mineralogy for mapping lithology.

Thin sections were described at the Bureau of Economic Geology on a polarizing microscope. Visual mineralogy estimates were made of percent calcite, dolomite, and anhydrite. Trace amounts of pyrite and quartz were also observed. Dolostones were defined as containing 80% or more dolomite and limestones as containing less than 80% dolomite as a percentage of the carbonate fraction. Dolomite crystal size ( $\mu\text{m}$ ) was measured by selecting an average-sized

crystal and measuring the distance between its opposing crystal points. Fabrics were described using the Lucia classification (Lucia, 1995). These fabrics include grainstone, grain-dominated packstone, mud-dominated packstone, wackestone, and mudstone. Tidal-flat facies were described as grain dominated or mud dominated and brecciated. Separate-vug porosity was estimated and the presence of fractures noted. Point counts (300) were performed as necessary using a mechanical stage in areas of complex lithology or pore-type distribution to obtain more accurate estimates.

Appendix I contains detailed instructions for describing thin sections using the rock-fabric approach.

## RESULTS

Rock-fabric variations were observed on many scales in the high-resolution data sets acquired in the north-central part of the field. Within a typical Lower Clear Fork cycle, mud-dominated facies compose the cycle base and the grain-dominated facies compose the cycle top. However, the petrophysical class is commonly constant throughout the cycle because the mud-dominated fabrics have been converted to a class 2 medium crystal mud-dominated fabric similar to the class 2 grain-dominated dolopackstone. Wichita cycles are typically composed of mud-dominated fabrics capped by tidal-flat facies. These peritidal fabrics have been converted to class 3 fine-crystalline mud-dominated dolostones. This pattern has been observed for peritidal intervals in the Lower Clear Fork as well. Therefore, it was initially thought that petrophysical properties in the Wichita could be characterized using porosity and a class 3 transform, whereas the Lower Clear Fork could be characterized using porosity and a class 2 transform. Figure 6 depicts the generalized stacking of petrophysical classes in a 1-D vertical profile for the Wichita and Lower Clear Fork Formations. However, several interesting variations were uncovered by

the detailed study, as shown by the characterization of sequence L2.2 as class 1 (fig. 6). Other lateral variations will be discussed in the following sections.

### Abo Formation

The Abo Formation was not extensively studied because it is not part of the main reservoir. However, there are sufficient cores and core analysis data in the field to suggest that this formation can be characterized as a class 1 coarse-crystalline dolostone. No new core analysis or thin sections were made of the Abo, but there is marked consistency for the old data to plot in the class 1 field (fig. 7). Although a more detailed study of the Abo would most likely reveal complications, a petrophysical class 1 transform was assigned to the Abo Formation throughout the field for estimating permeability and initial water saturation.

### Wichita Formation

The Wichita Formation consists of peritidal deposits that represent an updip, proximal facies equivalent of both the Abo outer platform succession and the lower portion of the Lower Clear Fork. As described in Ruppel and Jones (this report) core and outcrop data suggest that the Wichita composes parts of two depositional sequences: the highstand leg of sequence L1 and the transgressive leg of Leonardian sequence 2 (L2). The lower Wichita represents the updip, tidal-flat facies tract equivalent of the downdip, outer platform facies tract of the Abo in sequence L1, whereas the upper Wichita represents the updip tidal-flat facies equivalent of the basal Lower Clear Fork subtidal facies in high-frequency sequence L2.0, the earliest component of sequence L2.

The Wichita consists of mud-dominated fabrics including mudstones, wackestones, mud-dominated packstones, and tidal-flat fabrics. Typical tidal-flat features include pisolites, fenestrae, fine laminations, and desiccation cracks (fig. 8). Fenestrae are commonly lined with dolomite crystals and



filled with anhydrite or, less commonly, calcite. Fractures are locally present and typically filled with anhydrite or calcite. Very low porosity (<3%) limestones are interbedded with porous dolostones in the north-central part of the field (fig. 9) and may act locally as baffles to fluid flow. The rest of the Wichita contains primarily fine-crystalline dolostones. Both the limestones and the dolostones are dominantly petrophysical class 3, owing to the mud content and fine crystal size (fig. 10). Some class 2 grain-dominated dolopackstones and medium-crystalline mud-dominated dolostones are locally present but are uncommon in most of the field. Therefore, the formation was assigned petrophysical class 3, and a class 3 transform was used to estimate permeability and initial water saturation.

### Lower Clear Fork Formation

The Lower Clear Fork sequences L2.0, L2.1, and L2.2 are composed primarily of subtidal facies with minor tidal-flat facies. The subtidal facies contain skeletal debris, including fusulinids, peloidal material, and ooids. Rock fabrics include wackestone, mud-dominated packstone, grain-dominated packstone, and grainstone. Both limestones and dolostones are present. Limestones in the Lower Clear Fork are grain dominated (figs. 2a and 3a) and often more porous than the dolostones, with most porosity values ranging from 5 to 15%, and some as high as 30%. The petrophysical classes are dominantly class 1 and 2, owing to the more grain-rich textures of the limestones and the medium and coarse dolomite crystal size in the dolostones.

#### *Lower Clear Fork L2.0*

In most of the field area, high-frequency sequence (HFS) 2.0 consists of amalgamated tidal-flat deposits of the upper Wichita, which are assigned to petrophysical class 3. However, subtidal Lower Clear Fork deposits of L 2.0 were deposited during the latter part of this HFS at the margins (downdip) of the field, as evidenced by core description of the most distal

southeastern well, but are not penetrated by other wells in the field. There is very little data from this facies, and it was assigned a petrophysical class of 2 because the limited data suggest that it is a medium-crystalline dolostone.

### *Lower Clear Fork L2.1*

As described in Ruppel and Jones (this report), L 2.1 consists of a basal section of transgressive to early highstand subtidal platform facies and an upper section of highstand tidal-flat facies. In the lower subtidal interval, cycles shallow upward from lower energy wackestones and mud-dominated packstones to higher energy grain-dominated packstones and grainstones. The class 3 mud-dominated fabrics have been converted to a class 2 medium-crystalline dolostone similar to the class 2 grain-dominated dolopackstone. (fig. 11). Lime grainstones and grain-dominated packstones are interbedded with dolostones in some areas. Although the limestones are class 1 and 2 fabrics, respectively, they plot in the class 2 and 3 field on the porosity-permeability cross plot, most falling in the class 2 field, as shown by a histogram illustrated in figure 11. The limestones plot in the class 2 and 3 field because they contain considerable amounts of moldic porosity (a type of separate vug), and total porosity, not interparticle porosity, is used in the cross plot. Ideally, moldic porosity would be subtracted from total porosity and a class 1 transform and interparticle porosity would be used to estimate permeability. However, without acoustic logs, estimates of moldic porosity could not be made. In addition, the lime grainstones are interbedded with dolostones and cannot be mapped separately. Therefore, the moldic grain-dominated limestones are assumed to be class 2 because most of the data fall in the class 2 field. Accordingly, the subtidal portion of HFS L2.1 was characterized by a class 2 transform.

Class 1 dolostone fabrics are interpreted as dominant in two areas of the field on the basis of old core data (fig. 12). The class 1 dolostones appear to be coarse-crystalline dolostones and anhydritic medium-crystalline dolostones. The effect of patchy anhydrite on petrophysical class will be discussed more fully in the section HFS L2.2. The distribution of lithology and petrophysical class is shown in figure 13.

The upper highstand leg of HFS L2.1 consists of peritidal deposit fabrics, including mudstones, wackestones, and some mud-dominated packstones, many of which display exposure features, similar to the Wichita peritidal section. Dolostones are mud-dominated and fine-crystalline class 3 fabrics (fig. 6), and petrophysical class 3 is used to characterize this unit throughout the field.

#### *Lower Clear Fork L2.2*

HFS L 2.2 is composed dominantly of dolostone. Limestone is dominant in some areas of the field: in the south and in a small area in the northwestern part of the field (fig. 14). Most samples studied are class 2 grain-dominated dolopackstones and medium-crystalline mud-dominated fabrics. However, many samples plot in the class 1 field rather than the class 2 field as expected (fig. 15a). The samples that plot in the class 1 field do not appear to have any consistent stratigraphic position. Most of these medium-crystalline dolostones contain  $\geq 10\%$  poikilotopic anhydrite (fig. 15b), and their petrophysical class 1 behavior can be explained by the patchy distribution of anhydrite as discussed below. These rocks are consistently present throughout the field (except where limestone is present) and are best fit by a class 1 transform for estimating permeability and initial water saturation.

The shift of medium-crystalline class 2 dolostones into the class 1 field coincides with an increase in poikilotopic anhydrite, as explained by the fact that discrete patches of pore-filling

anhydrite will decrease porosity without decreasing pore-throat radius. Because permeability is controlled by the pore-throat radius, this reduction in porosity does not result in a corresponding decrease in permeability. This effect was first observed in the South Wasson Clear Fork reservoir by Lucia and Jennings (2002) and was discussed by Lucia et al. (2004).

Limestone is interbedded with dolostone over most of the southern part of the field and locally in the northwest (fig. 14). HFS L2.2 in these areas is composed of a mix of low-porosity medium-crystalline mud-dominated dolostones (fusulinid wackestones) and high-porosity grain-dominated limestones (grain-dominated packstones and grainstones). The grainstones tend to contain mostly separate-vug porosity, and the grain-dominated packstones tend to have mixed separate-vug and interparticle porosity. These moldic limestones typically plot in the petrophysical class 2 and 3 field, as illustrated in figure 11. As a result, a class 2 transform was used in these areas to estimate permeability and initial water saturation.

### *Lower Clear Fork L2.3*

Tidal-flat-capped restricted subtidal cycles compose the uppermost Lower Clear Fork high-frequency sequence (L 2.3) throughout most of the field area. Tidal flat caps are typically fine-crystalline mud-dominated fabrics with fenestrae, and the underlying cycle-base subtidal rocks are dominantly fine-crystalline mud-dominated dolostones. Whereas these cycle-capping tidal-flat facies are porous and nearly continuous across the field, they are very thin and contain little if any reservoir permeability. Both the thin tidal-flat caps and the fine-crystalline subtidal dolostones are petrophysical class 3. A possible exception to this classification occurs along the outer margins of the field where grain-rich peloidal packstones of the middle ramp become more common. A detailed study of this facies found a predominance of class 3 fabrics. Thus, a class 3 transform was used for L2.3 permeability and initial water saturation calculations throughout the field.



## DISCUSSION

### Limitations Due to Petrophysical Data Distribution

The detailed rock-fabric data available in the three wells studied in detail were extrapolated throughout the field using preexisting data sets. These detailed data sets are necessary in order to judge the quality of preexisting data sets and to determine the usefulness of the data. Preexisting data sets are variable in their quality, quantity, and distribution throughout the different stratigraphic intervals and must be used judiciously. Figure 16 shows the difference between the new data obtained in this study and preexisting whole core analysis on a porosity-permeability plot. The low-porosity, highly variable permeability data in the old analyses were eliminated because the data are most likely the result of biased samples or poor analysis procedures.

In addition to basic data quality issues, existing thin sections were often too widely spaced or biased toward a particular feature to yield an adequate description of the vertical variation in rock fabrics and petrophysical classes. More thorough sampling of many of the cores would have been useful. For example, vertical variations between class 3 and 2 dolostone fabrics occur on a scale smaller than that at which most cores are sampled, and these variations have been smoothed over in order to arrive at a usable approach. In particular, the rich variability in limestone fabrics has been overlooked and averaged out into an oversimplified petrophysical characterization. The impact of both data limitations and rock-fabric smoothing is discussed in the following section by stratigraphic unit.

The Abo subtidal facies (L1) is poorly known because of the lack of well penetration. Our class 1 rock-fabric assignment for this interval is based on the porosity-permeability plot of all available core analysis data (Fig. 7) from wells with core and confirmed by thin sections

examined in this study. However, there is considerable room within the data for areas and intervals that contain class 2 and 3 fabrics.

In the Wichita (L1 and L2), most fabrics are class 3, and the entire interval was modeled as class 3. However, thin sections and core descriptions indicate local and laterally discontinuous deposition of class 2 dolostone fabrics, particularly during the initial flooding of the platform during early L2 transgression. We were unable to establish any continuity of these fabrics across the field, which eliminated the possibility of including them in the model. Where present, their permeability is probably underestimated because class 3, rather than class 2, was applied. In addition, core descriptions show intervals of collapse breccia, suggesting the possibility of a touching-vug pore system composed of fractures and vugs that have not been included in this rock-fabric model. Indeed, the flow simulation required an increase in permeability by a factor of 15 to match injection volumes in the lower Wichita.

In the Lower Clear Fork, major changes in petrophysical class are mapped in both L2.1 and L2.2. In both HFS L2.1 and L2.2, distinct regions of petrophysical class 2 and class 1 dolostones are mapped. Regions of interbedded limestone and dolostone were mapped using new and existing thin sections, core analysis, grain density information, and wireline logs. The limestones have different rock fabrics from the dolostones. In most cases, the limestones are highly porous, are grain dominated, and contain separate-vug (often oomoldic) porosity. The interbedded dolostones are typically lower porosity, are more mud dominated, and have fine to medium dolomite crystals. As described in the results section, both the limestones and dolostones plot in the class 2 and 3 fields, with a majority of points in the class 2 field. Because most of the data plot in the class 2 field, a class 2 was assigned to the areas of interbedded limestone and dolostone. A more accurate petrophysical model would have resulted if dolostones

and limestones could have been mapped separately. However, the lack of adequate logs precluded mapping lithology at this scale.

## CONCLUSIONS

At Fullerton field, we have linked rock fabrics and petrophysical-class transforms, depositional facies, diagenetic overprints, and stratigraphic position. Three basic porosity-permeability transforms are used: class 1, 2, and 3. Dolomitized tidal-flat facies are fine-crystalline dolostones and mud-dominated limestones that fall in the class 3 field. Subtidal facies in the Lower Clear Fork tend to be medium- to coarse-crystalline dolostones occasionally containing large amounts of poikilotopic anhydrite. Limestones tend to be class 1 and 2 grain-dominated fabrics having large volumes of separate vugs causing them to plot in the class 2 and 3 fields. This link between rock fabric, petrophysical class, and petrophysical properties allows the use of the three basic transforms and results in a reasonable petrophysical model. The use of multiple transforms keyed to stratigraphy represents a big improvement over single-transform techniques, which would have drastically overestimated permeability in some intervals and underestimated permeability in others.

Changes in petrophysical classes and thereby porosity-permeability transforms are the most significant between intervals composed primarily of subtidal facies and intervals composed primarily of peritidal facies. Core analysis demonstrates at least 12% porosity is required in the Wichita to provide 1 md of permeability, whereas only ~8% porosity is required to provide the same permeability in the Lower Clear Fork, owing to the significant differences in rock fabric and petrophysical class between these formations.

Finer scale changes in petrophysical class are present within and between cycles, within and between high-frequency sequences, between systems tracts, and between regions of the field.

The ability to incorporate subtle changes in petrophysical class at the field scale is highly dependent upon petrophysical data quality and quantity and degree of homogeneity in geologic and petrophysical parameters across the field. Refinements of our rock-fabric model would certainly be possible with additional high-resolution data. However, the results we achieved utilizing high-resolution data acquired in this study, in conjunction with preexisting data in a sequence-stratigraphic context, are very satisfactory, as measured by the excellent match between rock-fabric-modeled permeability and core-analysis-derived permeability throughout the reservoir (Lucia, Kane, and Jones, this report)

#### ACKNOWLEDGMENTS

This research was funded by ExxonMobil Production Company, The University of Texas System, and the U.S. Department of Energy under contract DE-FC26-01BC15351. The Bureau of Economic Geology acknowledges support of this research by Landmark Graphics Corporation via the Landmark University Grant Program.



## REFERENCES

- Jennings, J. W., Jr., and Lucia, F. J., 2001, Predicting permeability from well logs in carbonates with a link to geology for interwell permeability mapping: Proceedings 2001 SPE Annual Technical Conference and Exhibition, Society of Petroleum Engineers, SPE 71336, p.1–16.
- Kerans, Charles, Lucia, F. J., and Senger, R. K., 1994, Integrated characterization of carbonate ramp reservoirs using Permian San Andres Formation outcrop analogs: American Association of Petroleum Geologists Bulletin, v. 78, no. 2, p. 181–216.
- Lucia, F. J., 1995, Rock-fabric/petrophysical classification of carbonate pore space for reservoir characterization: American Association of Petroleum Geologists Bulletin, v. 79, no. 9, p. 1275–1300.
- Lucia, F. J., 1999, Carbonate reservoir characterization: Berlin, Springer-Verlag, 226 p.
- Lucia, F. J., 2000, Petrophysical characterization and distribution of remaining mobile oil: South Cowden Grayburg reservoir, Ector County, Texas: The University of Texas at Austin, Bureau of Economic Geology, Report of Investigations No. 260, 54 p.
- Lucia, F. J., and Jennings, J. W., Jr., 2002, Calculation and distribution of petrophysical properties in the South Wasson Clear Fork field, *in* Lucia, F. J., ed., Integrated outcrop and subsurface studies of the interwell environment of carbonate reservoirs: Clear Fork (Leonardian-age) reservoirs, West Texas and New Mexico: The University of Texas at Austin, Bureau of Economic Geology, Final Technical Report prepared for U.S. Department of Energy under Contract No. DE-AC26-98BC15105, p. 95–142, <http://www.osti.gov/dublincore/ecd/servlets/purl/811895-4EHgbz/native/811895.pdf>.
- Lucia, F. J., Jones, R. H., and Jennings, J. W., 2004, Poikilotopic anhydrite enhances reservoir quality (abs.): American Association of Petroleum Geologists Annual Convention Abstracts Volume, v. 13, p. A88.
- Lucia, F. J., Kerans, C., and Wang, F. P., 1995, Fluid-flow characterization of dolomitized carbonate-ramp reservoirs: San Andres Formation (Permian) of Seminole field and Algerita Escarpment, Permian Basin, Texas and New Mexico, *in* Stoudt, E. L., and Harris, P. M., eds., Hydrocarbon reservoir characterization: geologic framework and flow unit modeling: SEPM (Society for Sedimentary Geology), SEPM Short Course No. 34, p.129–153.
- Lucia, F. J., and Ruppel, S. C., 1996, Characterization of diagenetically altered carbonate reservoirs, South Cowden Grayburg reservoir, West Texas: Proceedings, 1996 SPE Annual Technical Conference and Exhibition, Society of Petroleum Engineers, SPE 36650, p. 883–893.

- Ruppel, S. C., and Lucia, F. J., 1996, Diagenetic control of permeability development in a highly cyclic, shallow-water carbonate reservoir: South Cowden Grayburg field, Ector County, Texas: West Texas Geological Society Fall Symposium, p. 7–22.
- Wang, F. P., Lucia, F. J., and Kerans, C., 1998, Modeling dolomitized carbonate-ramp reservoirs: A case study of the Seminole San Andres Unit—Part I, Petrophysical and geologic characterizations: *Geophysics*, v. 63, no. 6, p. 1866–1875.

## PETROPHYSICAL CLASSES

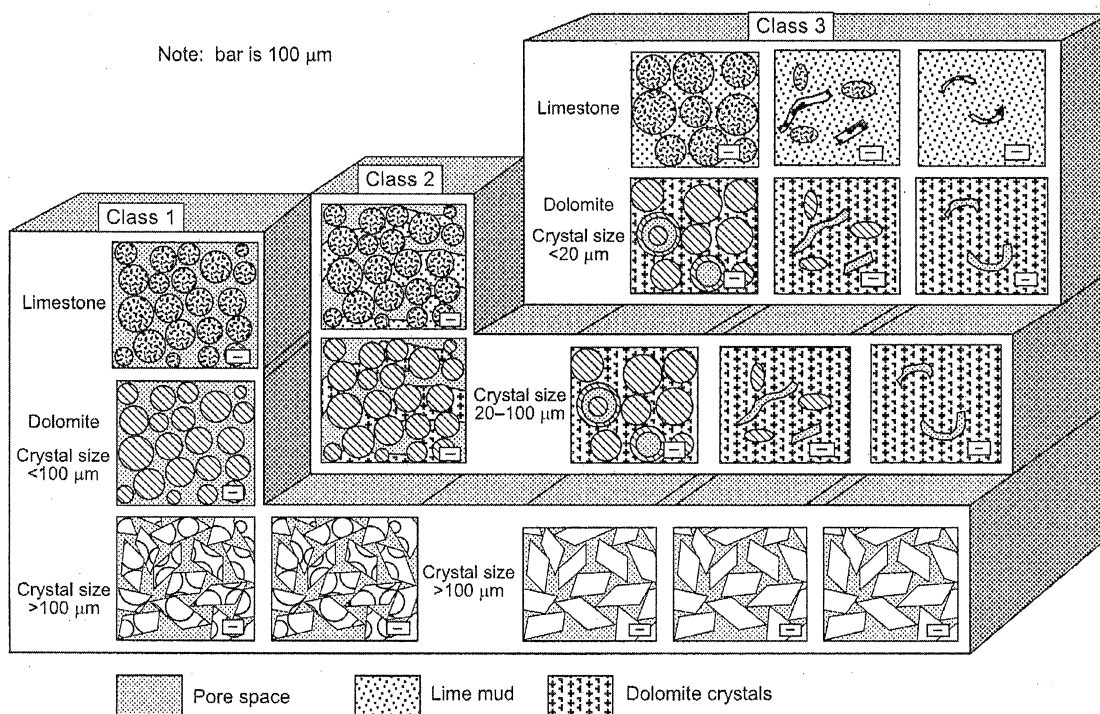
### GRAIN-DOMINATED FABRIC

GRAINSTONE

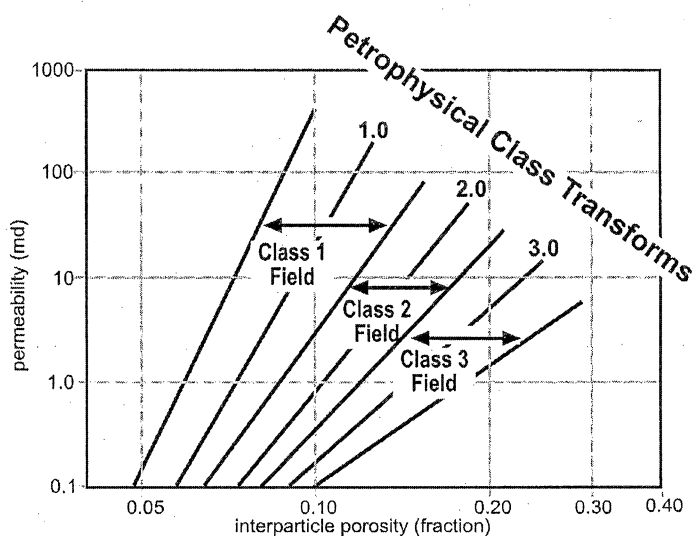
PACKSTONE

### MUD-DOMINATED FABRIC

PACKSTONE WACKESTONE MUDSTONE



QA 15772c



QAd2746c

Figure 1. Diagram showing fabrics composing petrophysical classes 1, 2, and 3 and a cross plot showing interparticle porosity vs. permeability, petrophysical class fields, and associated transforms.



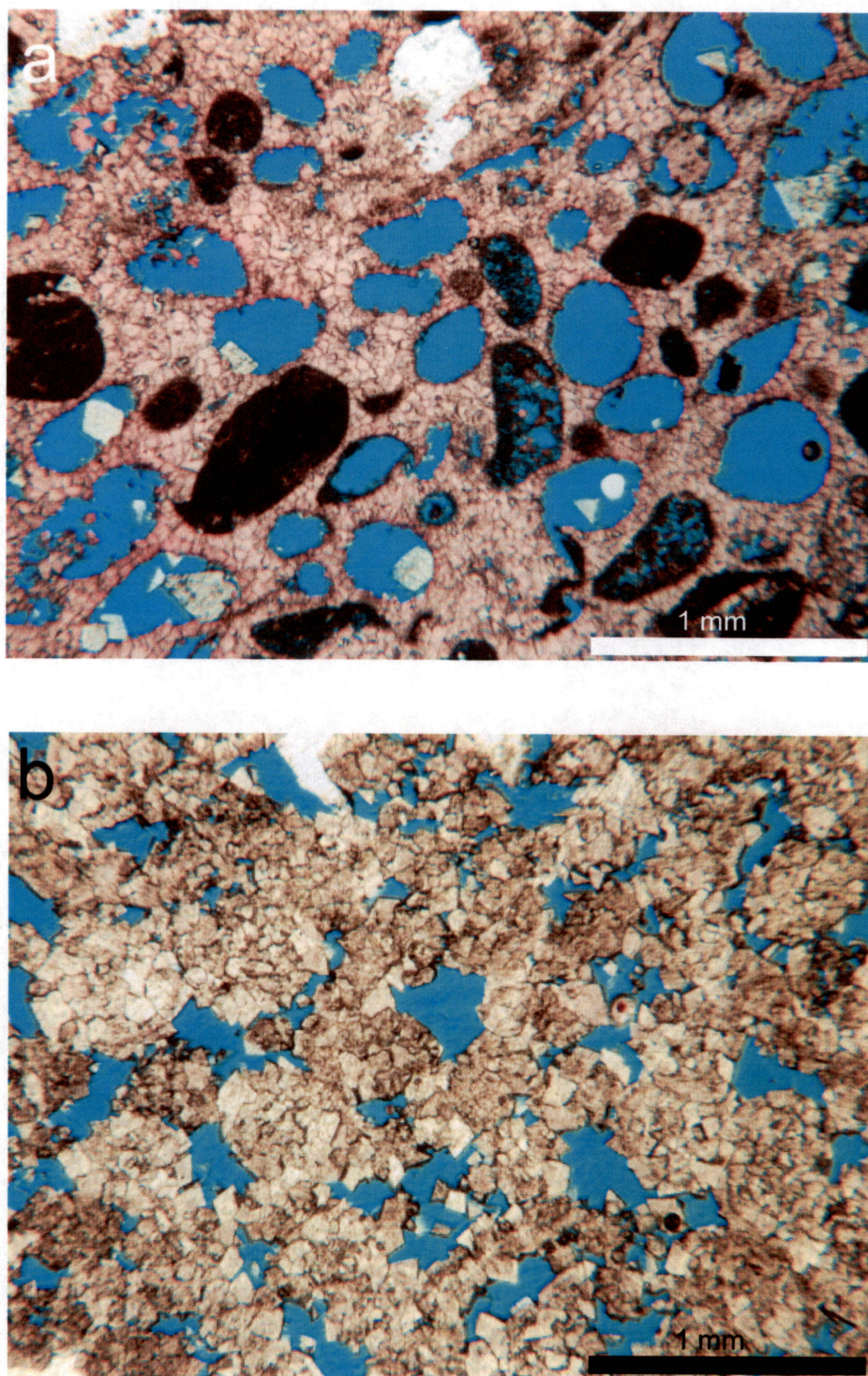


Figure 2. Photomicrographs of class 1 fabrics observed in this study: (a) Lime grainstone with separate-vug pore space: FCU 5927, 6913',  $\phi = 22.0\%$ ,  $k = 2.69$  md. (b) Coarse-crystalline dolograins: FCU 7630, 6997',  $\phi = 11.7\%$ ,  $k = 112.56$  md, dolomite crystal size  $120\ \mu\text{m}$ .



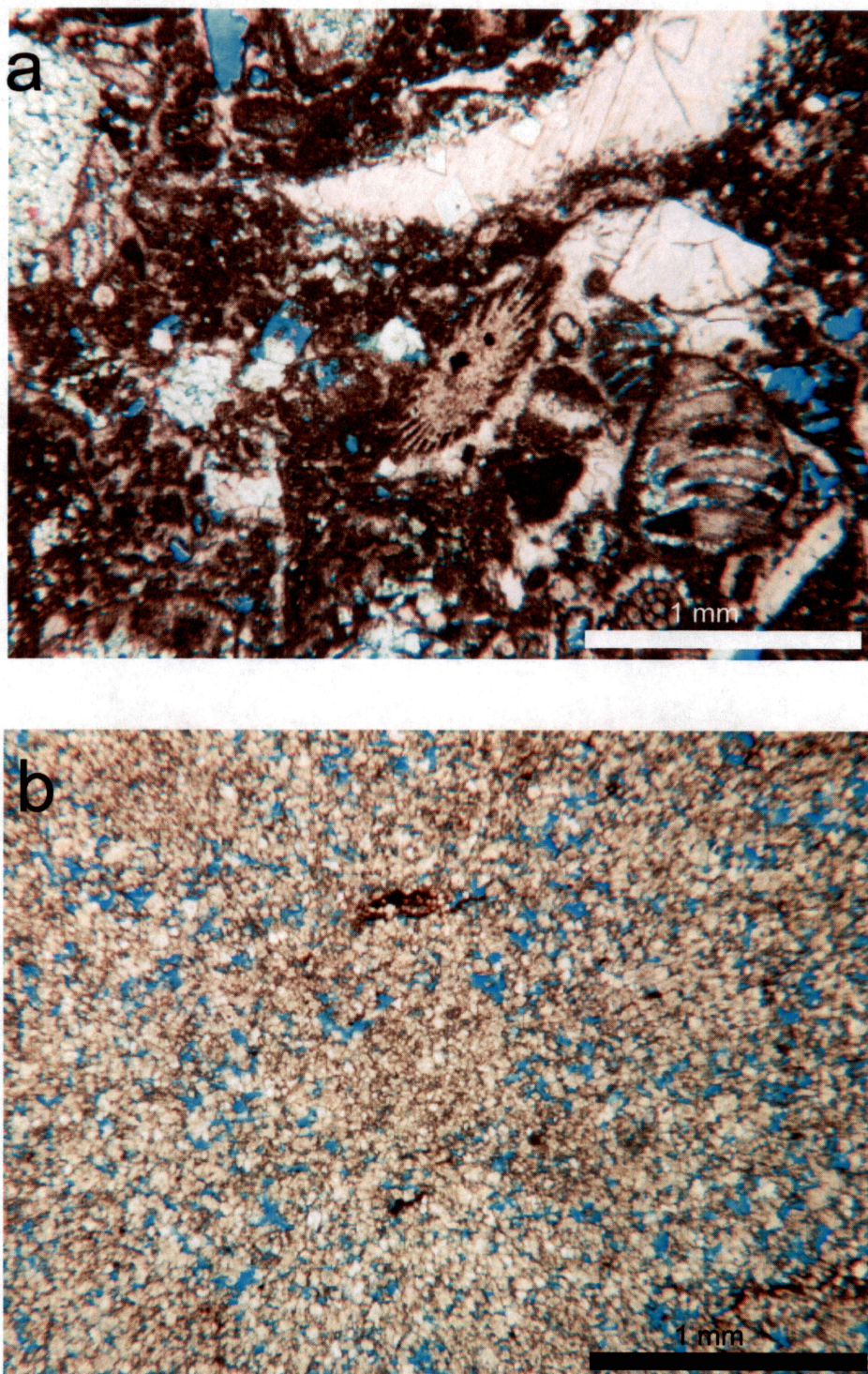


Figure 3. Photomicrographs of class 2 fabrics observed in this study: (a) Grain-dominated packstone with separate-vug pore space: FCU 5927, 6987',  $\phi = 8.8\%$ ,  $k = 0.04$  md. (b) Medium-crystalline grain-dominated dolopackstone: FCU 6429, 6914',  $\phi = 18.1\%$ ,  $k = 27.2$  md, dolomite crystal size  $55\ \mu\text{m}$ .



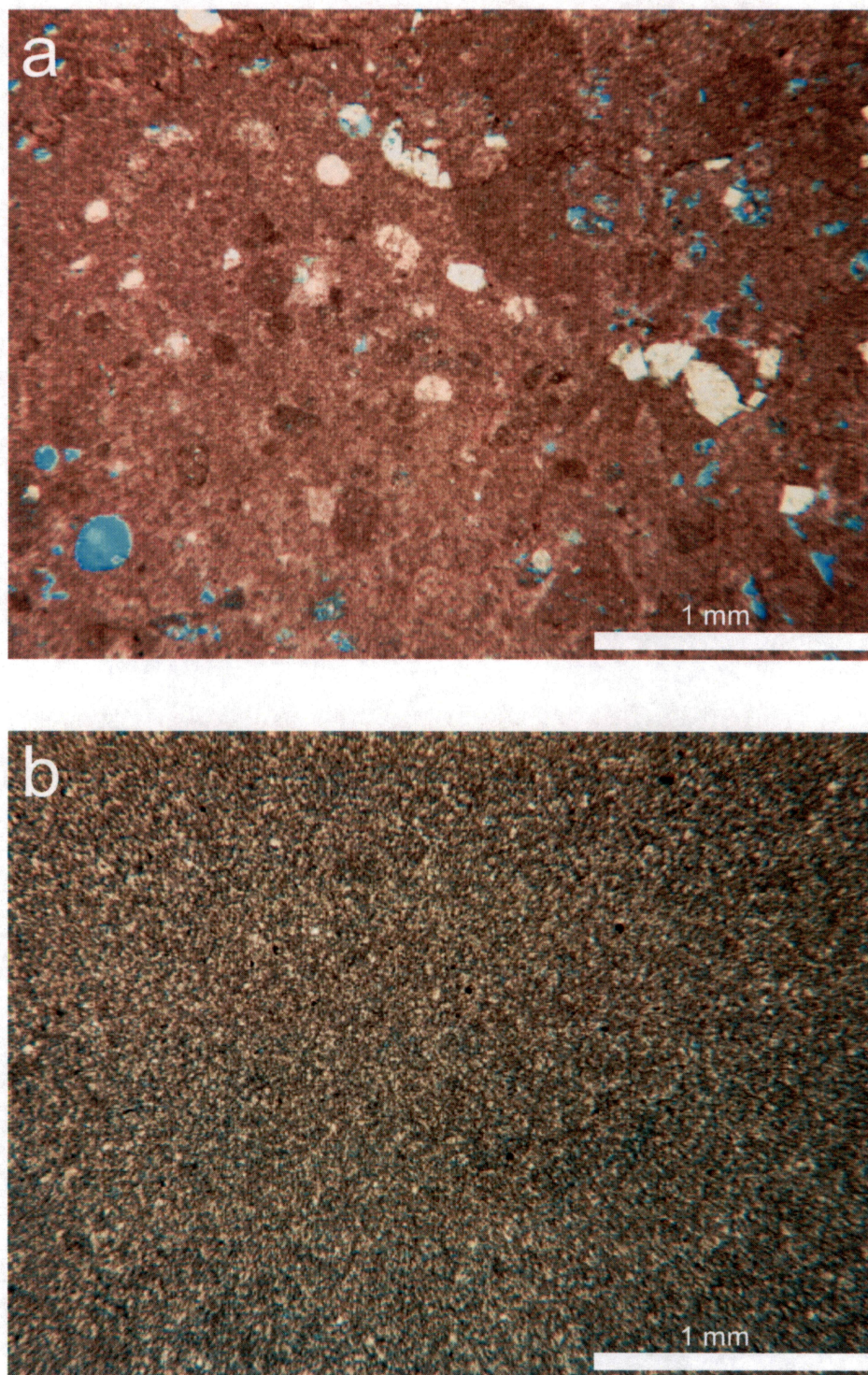
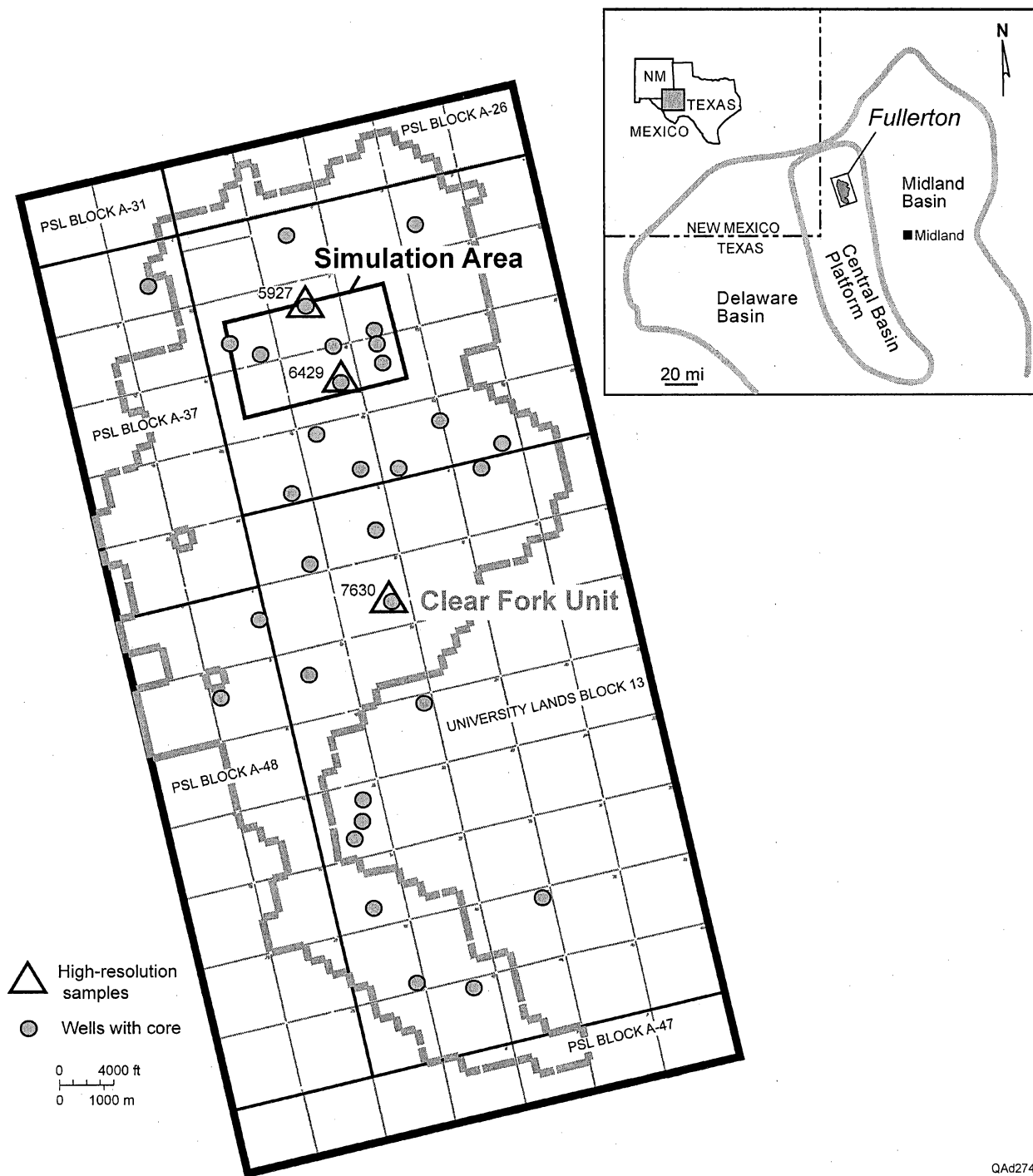
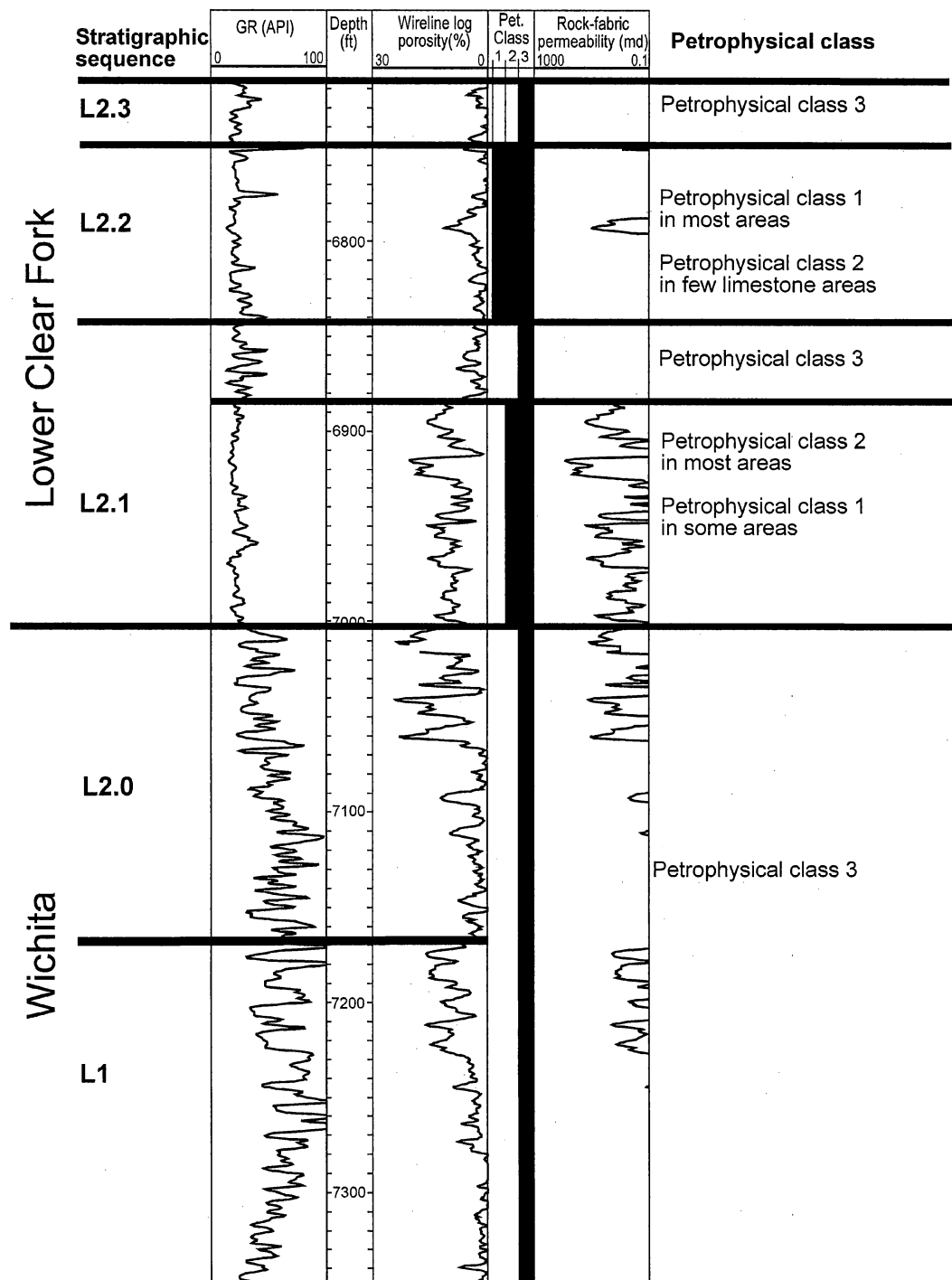


Figure 4. Photomicrographs of class 3 fabrics observed in this study: (a) Wackestone: FCU 5927, 6903',  $\phi = 11.2\%$ ,  $k = 0.74$  md. (b) Fine-crystalline dolomudstone with microporosity: FCU 5927, 7009',  $\phi = 15.7\%$  porosity,  $k = 0.86$  md, dolomite crystal size  $<10$   $\mu\text{m}$ .



QAd2744c

Figure 5. Location and boundaries of Fullerton field, Andrews County, Texas. Boundaries include the Clear Fork Unit and the flow simulation area of this study. Also shown are the location of cored wells and detailed study cores.



QAd2754c

Figure 6. Type log showing nomenclature used in this study and general vertical stacking of petrophysical classes. Formations and Leonardian stratigraphy displayed on the left side of logs. Wireline logs are from FCU 5927 and are gamma-ray, wireline-log porosity, and rock-fabric-calculated permeability.



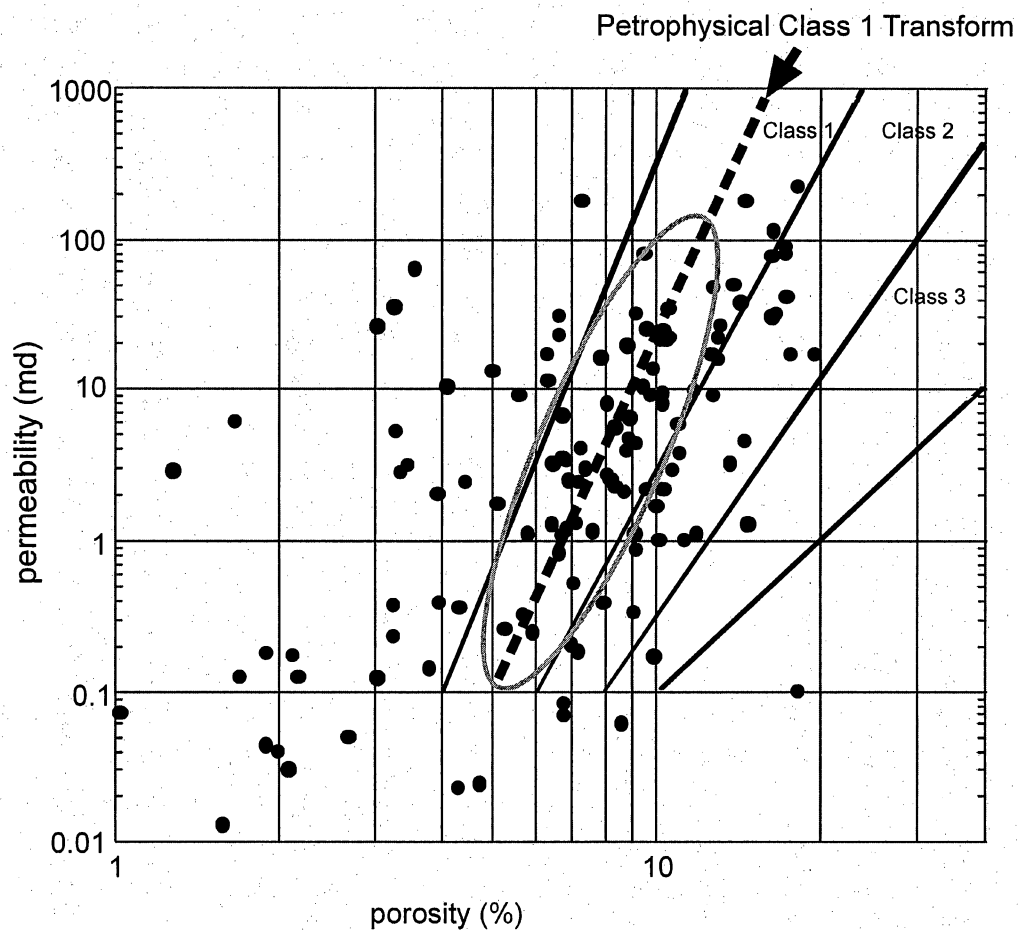


Figure 7. Porosity-permeability plot of old Abo interval core analysis from wells throughout the field with core described in this study.

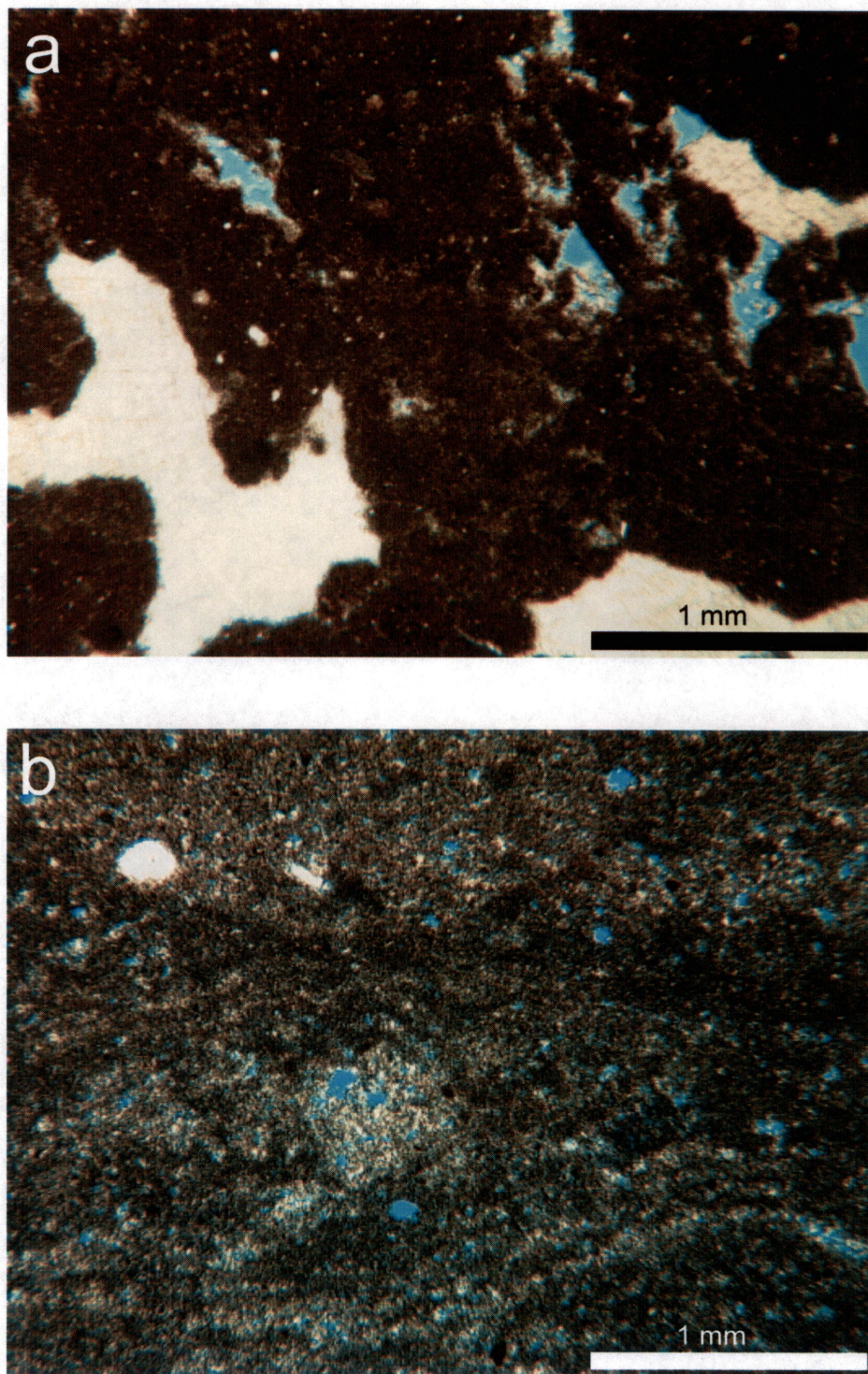


Figure 8. Photomicrographs of tidal-flat, class 3 fabrics observed in this study: (a) Tidal-flat facies with fenestral pores nearly completely filled with anhydrite (white): FCU 5927, 6999',  $\phi = 10.2\%$ ,  $k = 0.08$  md. (b) Tidal-flat facies with separate-vug porosity and microporosity: FCU 5927, 7001',  $\phi = 17.7\%$ ,  $k = 1.26$  md, dolomite crystal size  $<10$   $\mu\text{m}$ .

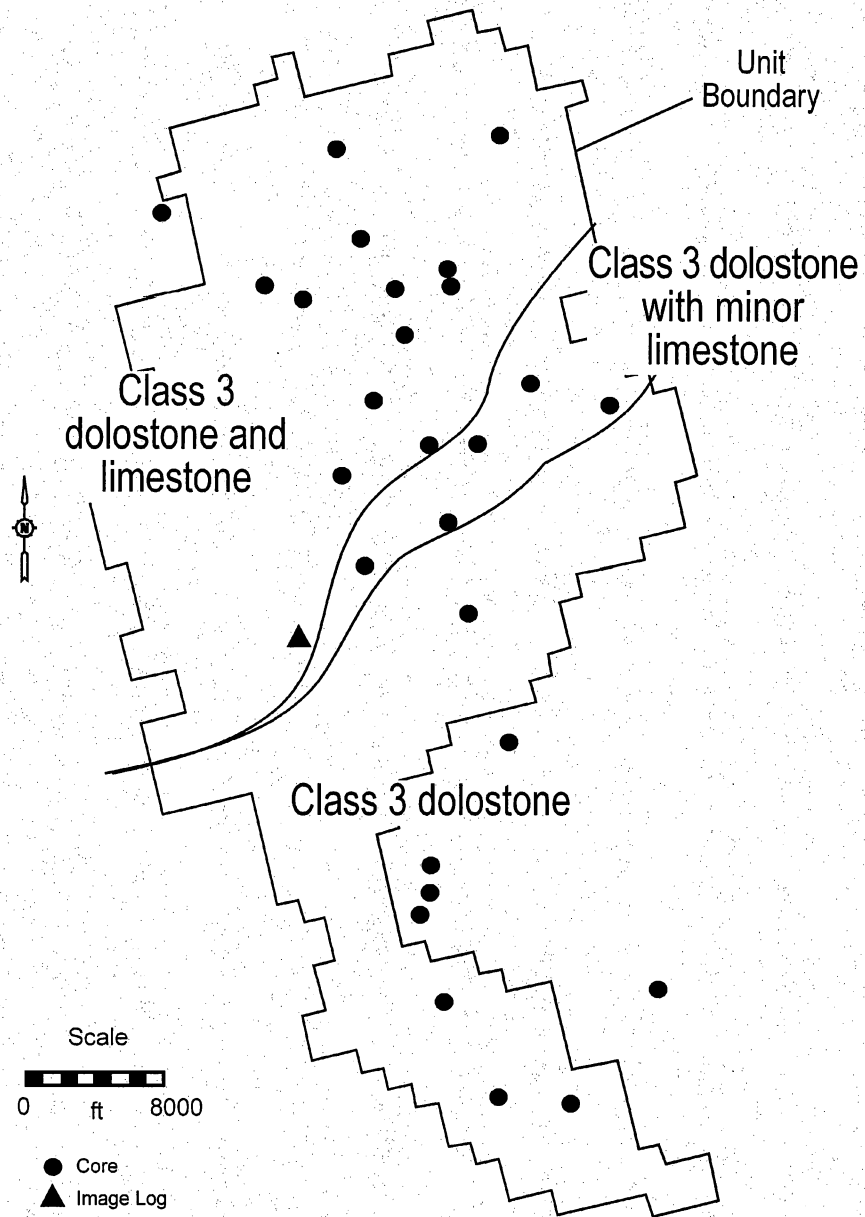


Figure 9. Distribution of limestone, dolostone, and petrophysical classes in the Wichita.



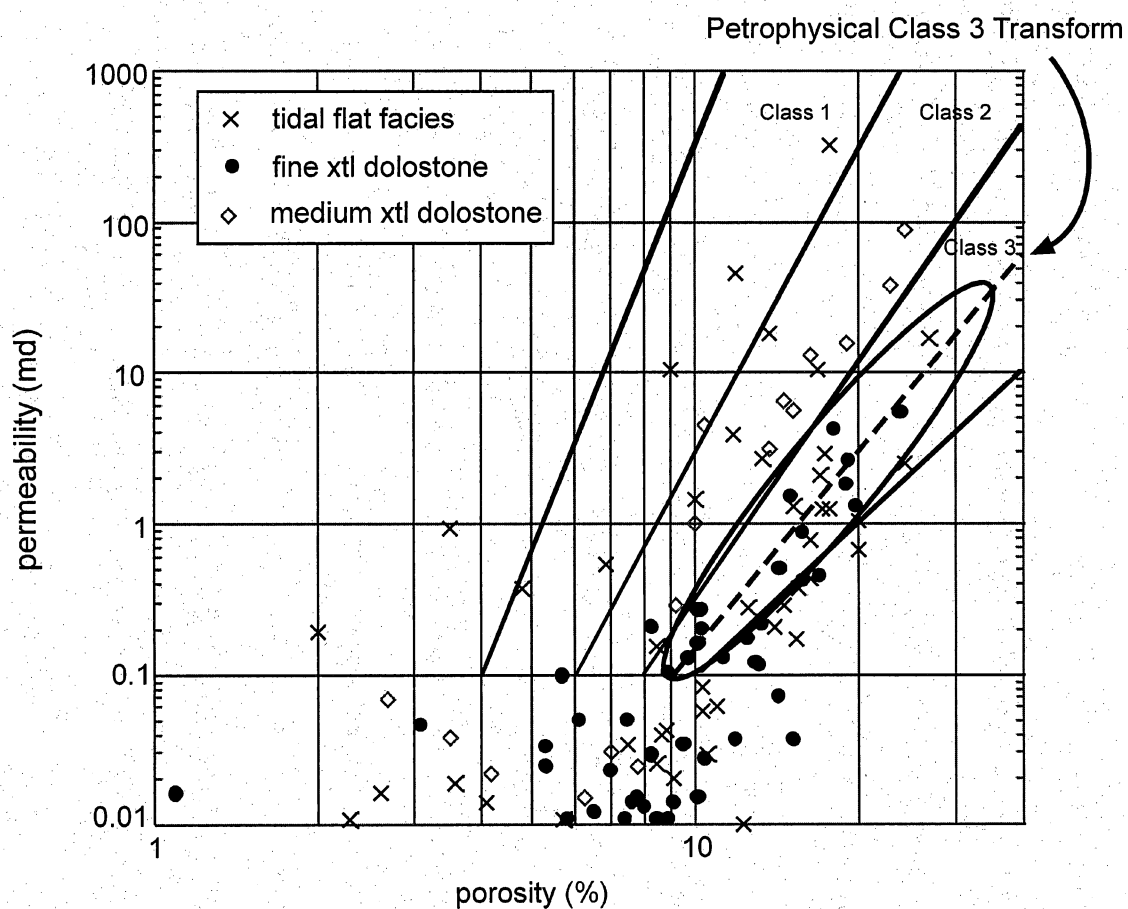


Figure 10. Wichita facies core analysis porosity-permeability plot and petrophysical class 3 transform (heavy dashed line) used to calculate permeability. Ellipse shows that the majority of data plots in the class 3 field.



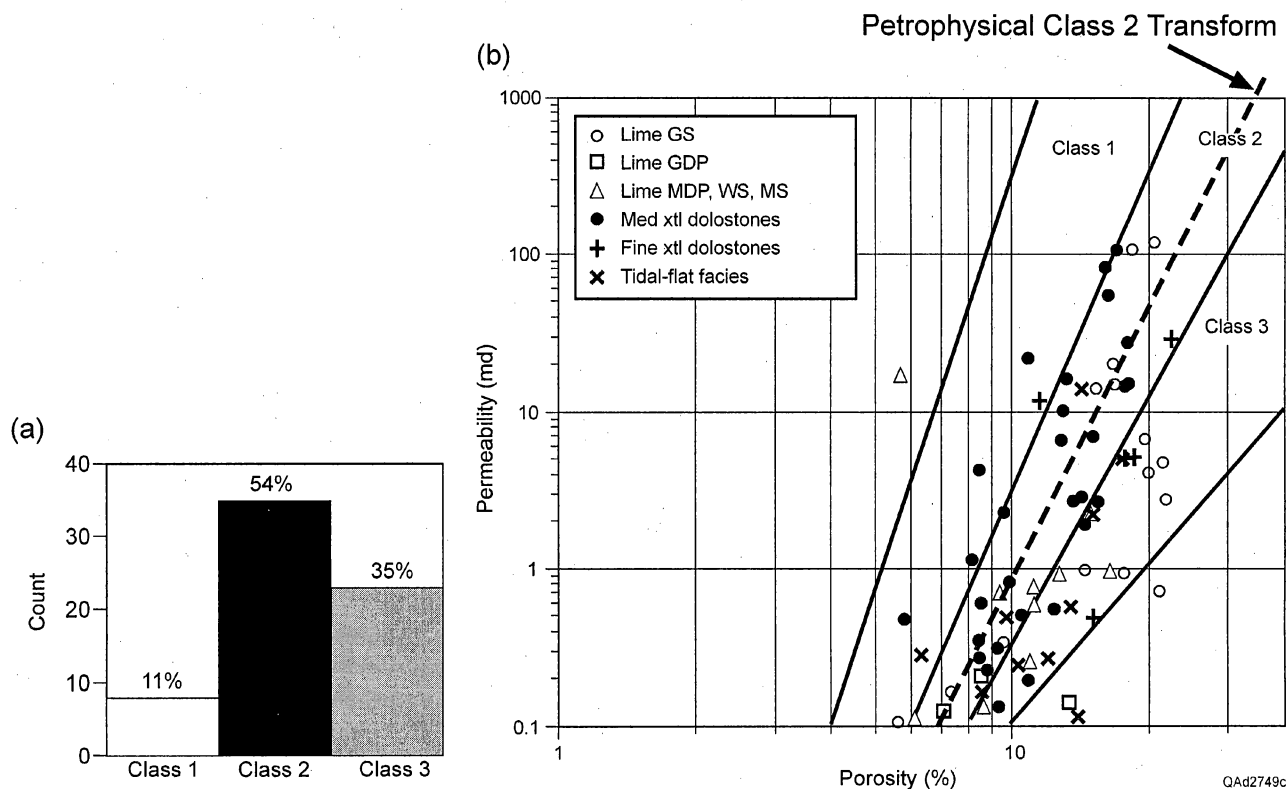


Figure 11. Plot and histogram for Lower Clear Fork L2.1 subtidal unit high-resolution samples from wells FCU 5927 and 6429. (a) Total core porosity vs. permeability plot of these rock fabrics showing that class 2 dolostones and the higher permeability class 1 moldic limestones both plot in the class 2 field. The petrophysical class 2 transform was used for permeability calculations. (b) Histogram showing sample populations from this plot showing that more than 50% of the samples plot in the class 2 field. Those that plot in the class 3 field are moldic grain-dominated limestones and class 3 limestones and dolostones.

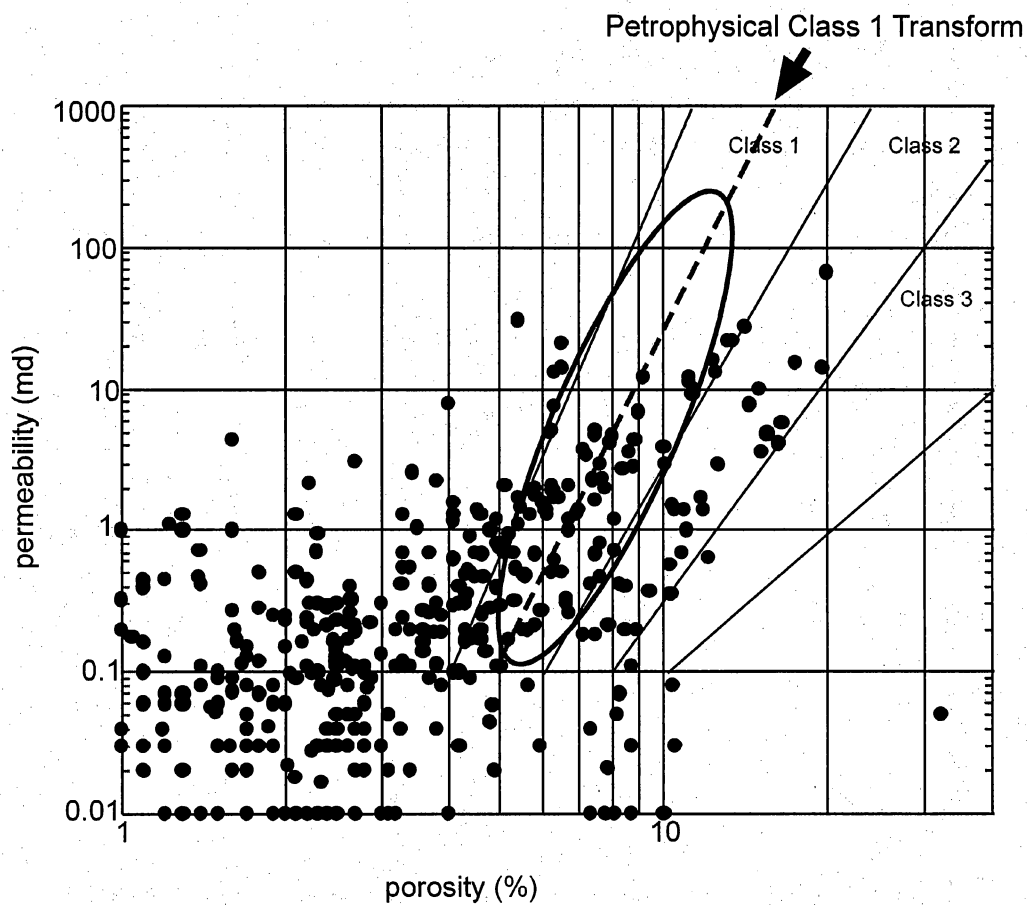


Figure 12. Porosity-permeability plot of core analysis from wells with core displaying dominantly class 1 fabrics in the subtidal portion of high-frequency sequence L2.1.

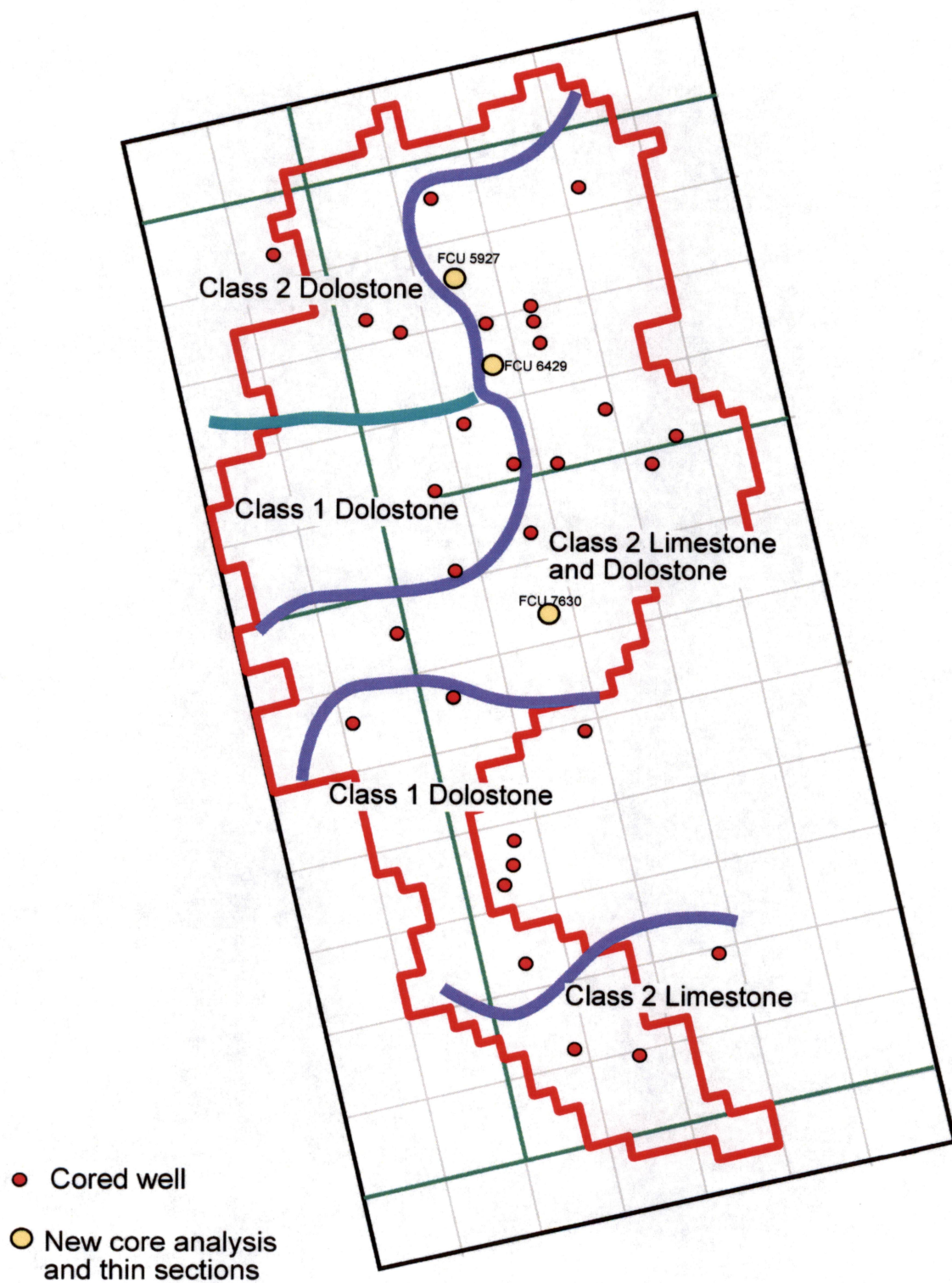


Figure 13. Regions of different petrophysical classes and mineralogy in the subtidal portion of HFS L2.1.

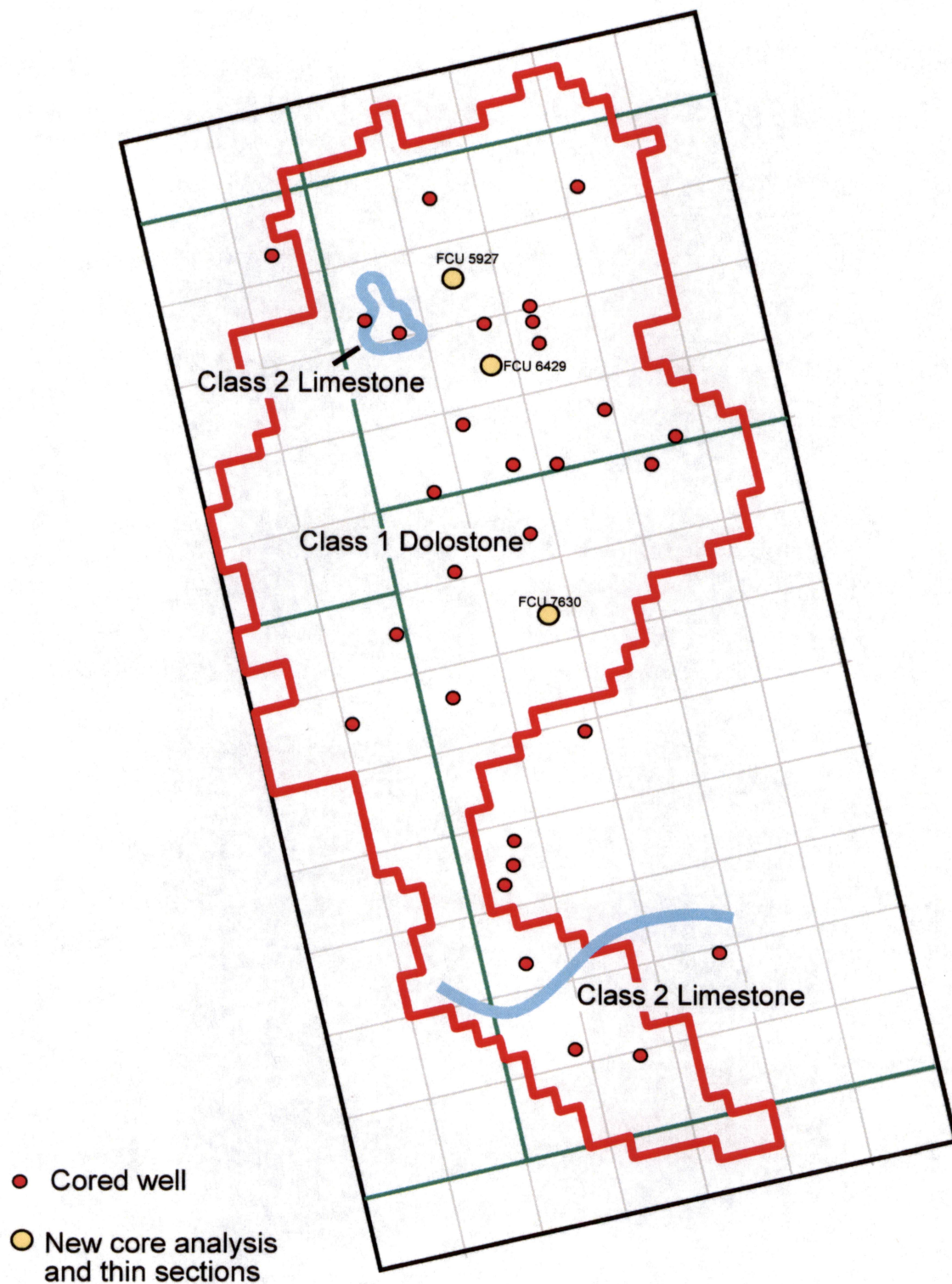
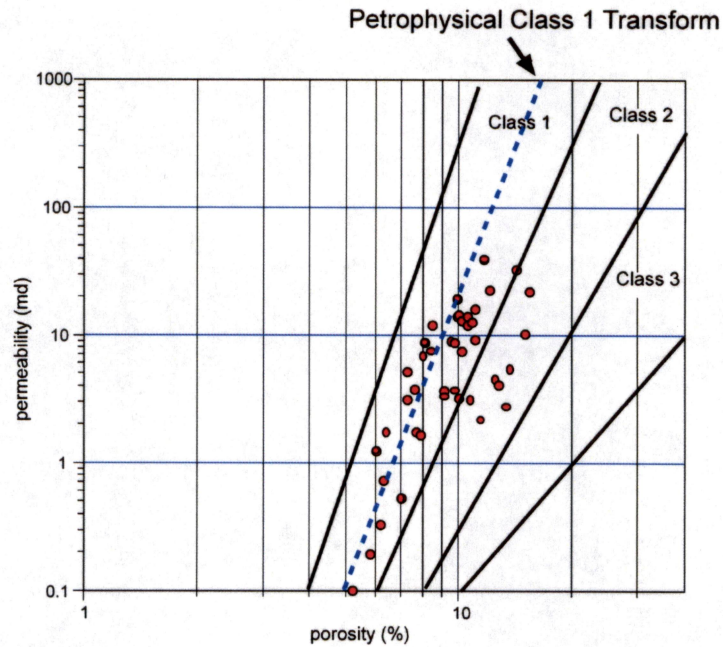


Figure 14. Regions of different petrophysical classes and mineralogy in HFS L2.2.



(a)



(b)

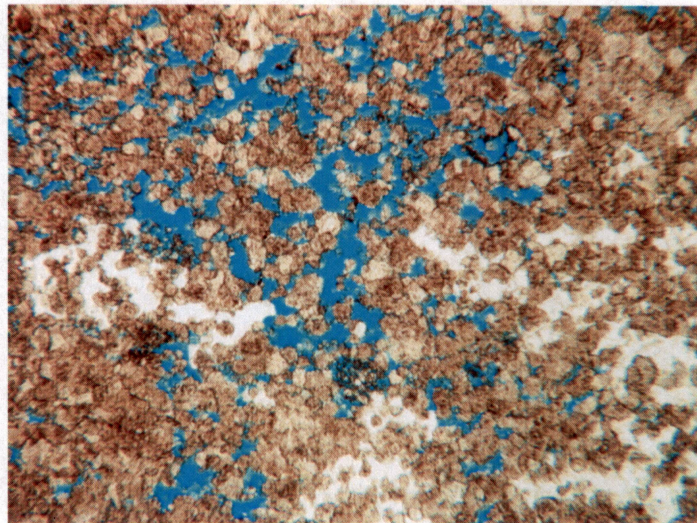


Figure 15. (a) Porosity-permeability plot of Lower Clear Fork L2.2 showing that most samples plot in the class 1 field although they are mostly class 2 medium-crystalline dolostones. (b) Photomicrograph example of poikilotopic anhydrite in a class 2 medium-crystalline dolostone having  $\phi = 8.1\%$ ,  $k = 9.02$  md, and 30% anhydrite. The presence of a large volume of anhydrite shifts the sample into the class 1 field.

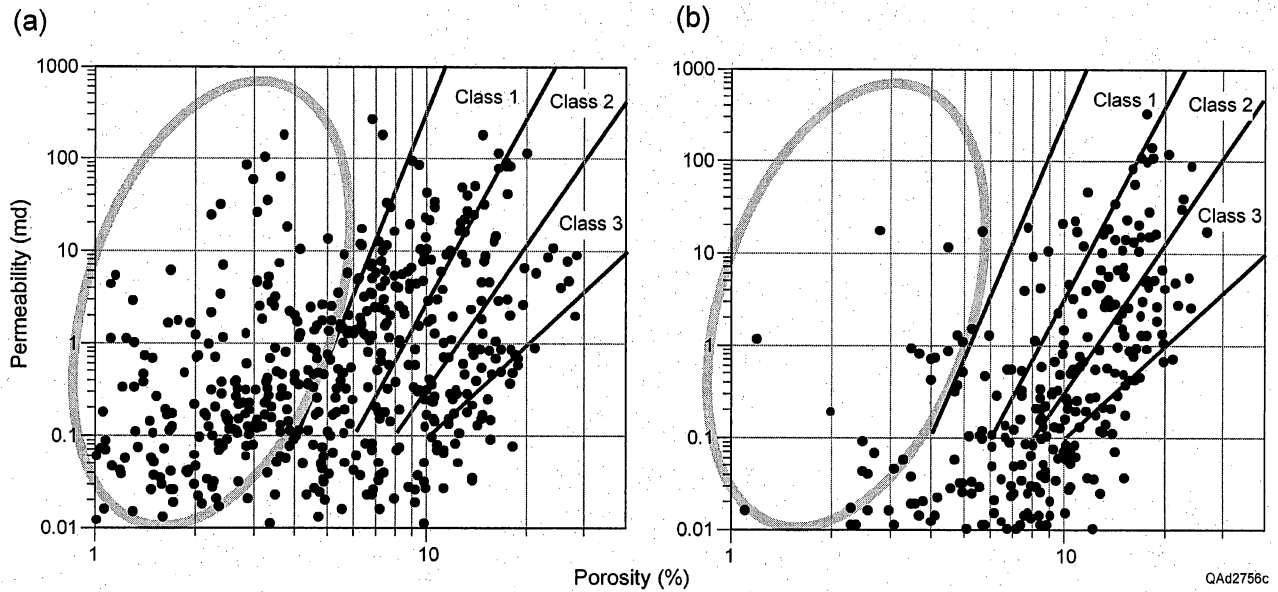


Figure 16. Typical preexisting core analysis data (a) vs. core analysis data resulting from unbiased sampling and careful cleaning of plugs (b). Note the large low-porosity data cloud denoted by the gray ellipse in (a) is not present in (b). Data in (a) are from FCU 6921 (just south of flow simulation area); data in (b) are the new samples of FCU 5927 and 6429 obtained for this study.

## **APPENDIX I: ROCK-FABRIC INSTRUCTIONS**

### **Classifying Carbonate Pore Space from Thin Sections**

#### **Procedure**

The following comments outline the general procedure for describing pore space for petrophysical characterization.

#### **1. Identify grains.**

Easily done in most limestones and fine crystalline dolostones, more difficult but usually possible in medium crystalline dolostone, and often highly interpretive in large crystalline dolostone.

#### **2. Look between grains and at grain sorting (figs. 1, 2).**

##### **Limestones**

If intergrain volume contains only pore space (no mud-size material) or pore filling minerals (Calcite, dolomite, sulfate) and is well sorted, the rock is a grainstone: petrophysical class 1

If intergrain volume contains pore space or pore filling minerals, mud-sized sediment, and if the grains are poorly sorted, the rock is a grain-dominated packstone: petrophysical class 2.

If intergrain volume contains only mud-sized sediment and no intergrain porosity, the rock is a mud-dominated fabric: petrophysical class 3. If the fabric is grain supported it is classified as a mud-dominated packstone, if not grain supported and more than about 10 percent grains, wackestone, and if less than 10 percent grains, mudstone.

The boundary between grain-dominated and mud-dominated packstone is gradational, and some judgment is required in selecting the correct classification.

##### **Dolostones**

The above comments can be applied to fine crystalline dolostones and medium crystalline grain-dominated fabrics without modification. However, the dolomite crystal size is important in large crystalline dolostones and in medium crystalline mud-dominated fabrics. All large crystalline dolostones are petrophysical class 1 without regard to precursor fabric, and medium crystalline mud-dominated dolostones are class 2, not class 3.

### **3. Look within grains or crystals (fig. 3).**

Pore space located within grains of crystals is referred to as intraparticle pore space, a type of separate-vug porosity.

The size of the intraparticle pore space has a large effect on the petrophysical properties. If the separate-vug porosity is clearly visible (moldic, intrafossil, etc.), the pores will be oil saturated. However, if the intraparticle pore space is microporosity (faintly visible), the pores may be filled with oil and capillary held water.

### **4. Look for pore space significantly larger (>2X) than the particle (grains or crystals) size (fig. 3).**

Pores that are significantly larger than the particle size may be separate vugs or touching vugs, and it is difficult to tell the difference in thin section. If the large vugs are fabric selective they are probably separate vugs. However, if they are connected by microfractures they may form a touching-vug pore system. If the large vugs are not fabric selective, they may form an interconnected pore system.

## **Documentation**

The following comments outline the procedures for completing the attached thin-section description form (fig. 4).

### **Lithology**

Dolomite crystal size is most important because it controls pore size in mud-dominated dolostones.

Types of anhydrite include poikilotopic, pore filling, and nodular. This may have important implications as to pore-size distribution. Gypsum is important in log analysis.

### **Texture**

Enter the rock-fabric name. Grainstone, grain-dominated packstone, mud-dominated, mud-dominated packstone, wackestone, mudstone. Alternatively, show percent mud vs grains graphically. May indicate grain types by name or by symbol.



## **Petrophysical Fabric**

Estimation of interparticle porosity (Ippor). Interparticle porosity is estimated by subtracting vuggy porosity from core analysis porosity, if available. May be estimated from thin sections if core analysis is not available.

Size of particles, grains or crystals, is given in microns. If the fabric is a grain-dominated packstone, the size of the particles and the interparticle fabric (mud of crystals) is given as a fraction.

Separate-vug porosity (Svug) from thin section description. Types in include grain molds, intrafossil, intragrain microporosity, etc.

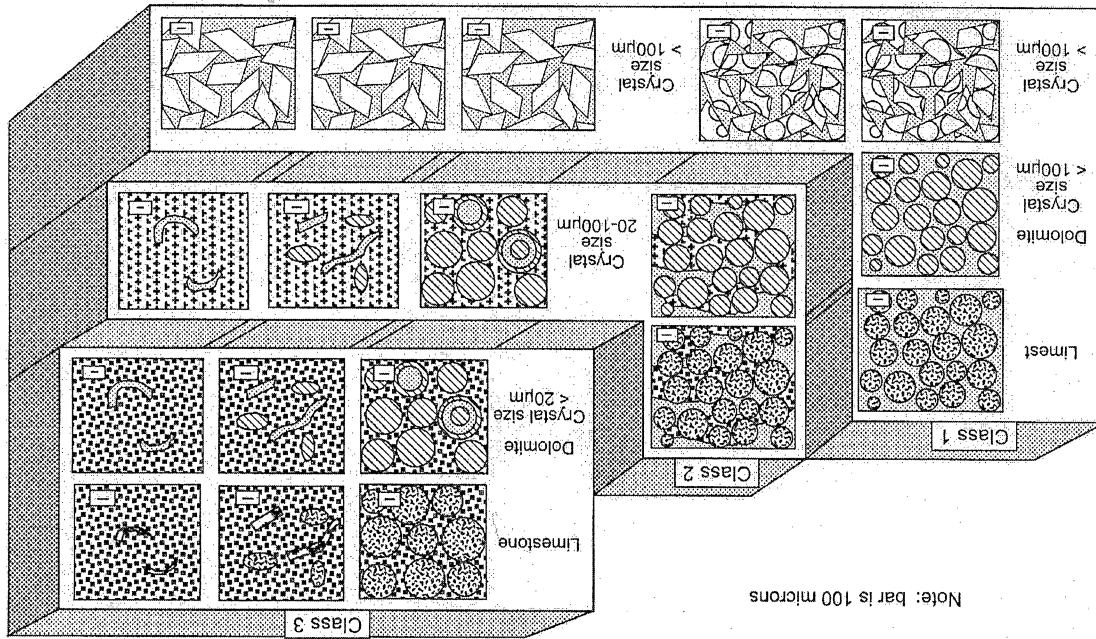
The presence of touching vugs (Tvug) should be indicated by type (fracture, vug, etc.).

One of three petrophysical classes is normally recorded. However, because there is a range of classes from 0.5 to 4, any value within this range is acceptable. See attachment for explanation of class range to rock fabrics.

## **Core Analysis**

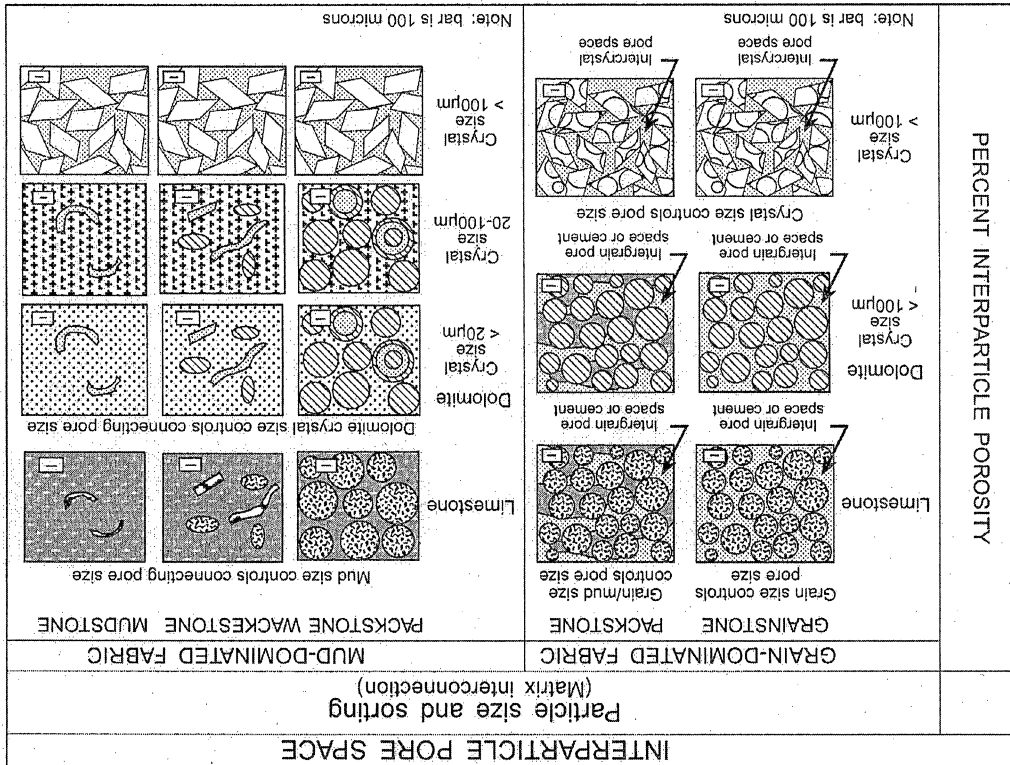
The data entered here is normally from the thin-section sample. If not, it should be so noted.

Figure 2



GRAIN-DOMINATED FABRIC  
PACKSTONE  
GRAINSTONE  
MUD-DOMINATED FABRIC  
PACKSTONE WACKSTONE MUDSTONE

Figure 1



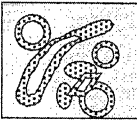
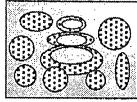
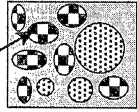
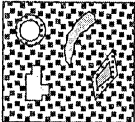
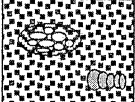
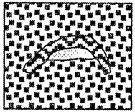
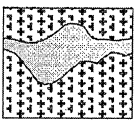
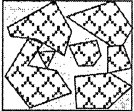
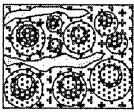
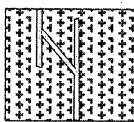
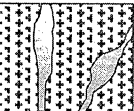
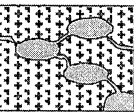
VUGGY PORE SPACE				
SEPARATE-VUG PORES (VUG-TO-MATRIX-TO-VUG CONNECTION)			TOUCHING-VUG PORES (VUG-TO-VUG CONNECTION)	
PERCENT SEPARATE-VUG POROSITY	GRAIN-DOMINATED FABRIC	MUD-DOMINATED FABRIC	GRAIN- AND MUD-DOMINATED FABRICS	
	EXAMPLE TYPES	EXAMPLE TYPES	EXAMPLE TYPES	
	<p>Moldic pores</p>  <p>Intrafossil pores</p>  <p>Intragrain microporosity</p> 	<p>Moldic pores</p>  <p>Intrafossil pores</p>  <p>Shelter pores</p> 	<p>Cavernous</p>  <p>Breccia</p>  <p>Fenestral</p> 	<p>Fractures</p>  <p>Solution enlarged fractures</p>  <p>Microfractures connecting moldic pores</p> 

Figure 3

[illegible][illegible]

COMMENTS \_\_\_\_\_